EXPLORING THE EFFECTS OF ELECTRICAL STIMULATION FOR USE WITH OSSEOINTEGRATED IMPLANTS

by

Brad Michael Isaacson

A dissertation submitted to the faculty of
The University of Utah
in partial fulfillment of the requirements for the degree of

Doctor of Philosophy

Department of Bioengineering

The University of Utah

May 2011

STATEMENT OF DISSERTATION APPROVAL

The dissertation of **Brad Michael Isaacson**

has been approved by the following supervisory committee members:

Roy Bloebaum	, Chair	**January 11, 2011** Date Approved
James Peter Beck	, Member	**January 10, 2011** Date Approved
Larry Meyer	, Member	**January 10, 2011** Date Approved
Joseph Webster	, Member	**January 10, 2011** Date Approved
Rob MacLeod	, Member	**January 10, 2011** Date Approved
Robert Hitchcock	, Member	**January 10, 2011** Date Approved

and by **Patrick Tresco** , Chair of the Department of **Bioengineering**

and by Charles A. Wight, Dean of The Graduate School.

ABSTRACT

Military personnel with amputations face unique challenges due to their short residual limbs and high incidences of multiple limb loss sustained after blast injuries. However, transcutaneous osseointegrated implant (TOI) technology may provide an alternative for individuals with poor socket tolerance by allowing a structural and functional connection between living bone and the surface of a load bearing implant. While TOI has improved activity levels in European patients with limb loss, a lengthy rehabilitation period has limited the expansion of this technology, and may be accelerated with electrical stimulation. The unique advantage of electrically induced TOI is that the exposed exoprosthetic attachment may function as a cathode for regulating electrical current while also serving as the means of prosthetic limb attachment to the host bone. Using this design principle, the goal of this dissertation was to investigate the potential of electrical stimulation for enhancing the rate and magnitude of skeletal fixation at the periprosthetic interface using the implant as a cathode.

Although previous studies have examined electrical stimulation for healing atrophic nonunions, inconsistent results have required new predictive measures. Therefore, finite element analysis (FEA) was used as a prerequisite for estimating electric field and current density magnitudes prior to *in vivo* experimentation. Retrospective computed tomography scans from 11 service members (28.3 ± 5.0 years) demonstrated the feasibility of electrically induced TOI, but variability in residual limb anatomy and

the presence of heterotopic ossification confirmed the necessity for patient-specific modeling.

Electrically induced osseointegration was also evaluated *in vivo* in skeletally mature rabbits after establishing design principles based on *in vitro* cell culturing and FEA. Data from the animal experiment indicated that there were no statistical differences for the appositional bone index (ABI), mineral apposition rate and porosity between the electrically stimulated implants and the unstimulated control implants (UCI). Higher mechanical push-out forces were observed for the UCI group at 6 weeks ($p=0.034$). In some cases, qualitative backscattered electron images and ABI did indicate that direct current may hold promise for improving suboptimal implant "fit and fill," as bone ongrowth around the cathode was observed despite not having direct contact with the endosteum.

In loving memory of Norman Young

and to the four wonderful women in my life: Megan, Rae, Rose and Jackie

TABLE OF CONTENTS

SYMBOLS

OIF	Operation Iraqi Freedom
OEF	Operation Enduring Freedom
FEA	Finite Element Analysis
TOI	Transcutaneous Osseointegrated Implants
IED	Improvised Explosive Device
RPG	Rocket Propelled Grenade
ABI	Appositional Bone Index
SEM	Scanning Electron Microscopy
BSE	Backscattered Electron Imaging
MAR	Mineral Apposition Rate
HO	Heterotopic Ossification
OA	Osteoarthritis
Ra	Average Surface Roughness
ESI	Electrically Stimulated Implants
UCI	Unstimulated Control Implants
H&E	Hematoxylin and Eosin
PMMA	Polymethylacrylate
SCBS	Sodium Cacodylate Buffer Solution

ACKNOWLEDGMENTS

It is impossible for me to imagine completion of my dissertation without the support of my colleagues, friends and family. I would like to first and foremost acknowledge my PhD committee members for their guidance, patience and assistance throughout my graduate career. Rob MacLeod, Robert Hitchcock, Peter Beck, Joseph Webster, Larry Meyer, Mark Van Dyke and Rob Bloebaum have molded me into the scientist I am today and I am extremely grateful for their time. My advisor, Roy Bloebaum, has also been an incredible mentor, friend, father figure, fitness coach and fly fishing partner and I will always remember to "keep thinking butch." Thank you for taking a risk on a young east coast kid who didn't hesitate to ask: "What's an osteoblast?"

I appreciate the support of my colleagues at the Bone and Joint Research Laboratory who have endured many lunchtime rants, games of scrabble and for giving me advice when I needed it. I am thankful for having such wonderful, passionate friends in the lab: Dustin Williams, Sujee Jeyapalina, Tyler Epperson, Teri Rosenbaum Chou, Kassie Woodbury, Amy Tanner, Amber Van Sickle and Gwenevere Shaw. I will sincerely miss your company. I would also like to express my gratitude to Amalia Brown and Lucille Brunker who have been exceptional undergraduate students and friends to me. I could not imagine completing my experiments without your dedication and support.

Special thanks are necessary for those individuals responsible for providing funding support and technical assistance throughout my graduate career. I would like to thank the Department of Veterans Affairs and Dan Tripodi and Moj Eram from the University of Utah Technology Commercialization Office for supporting my PhD experiments. I am thankful for the assistance provided by the Scientific Computing and Imagining Institute, namely Jeroen Stinstra, Darrell Swenson and Kedar Aras. I am also indebted to Brooke Kawaguchi, Landon Bodily, John McShee and Kerry Matz for their technical assistance with experiments and manuscript preparation.

Finally, I would like to thank my family and friends, without whom this would not be possible. H.T Johnson, Chris Johnston, Saralee Manwaring, Janis Deitrick, Jason Yeager, Dan Martin and Tom Brody, thanks for giving me the nights I will never remember with the friends I'll never forget. To the love of my life, Megan Witherspoon, thank you for your support and continuing to inspire me each day. Mom, Gary, Bub, the Hosseini family, the Young family, the Ehrlich family, the Witherspoon family, the Damon-Lezon family and my adopted family, the Bloebaums, thank you for your love, guidance and, at times, financial support to keep me afloat throughout graduate school.

CHAPTER 1

PROSTHETIC COMPLICATIONS AND THE DEMAND FOR OSSEOINTEGRATION

1.1 Limb Loss Data

The early ability to stabilize and transport injured servicemen and women from Operation Enduring Freedom (OEF) and Operation Iraqi Freedom (OIF) to specialized military centers in the continental United States has resulted in an approximate 92% survival rate, higher than any other major military conflict.[1] As a result, service members have returned from theatre with multiple amputations and have required extensive rehabilitation in medical centers within the Department of Defense and the Department of Veterans Affairs. Approximately 2% of injured military personnel returning from OEF and OIF have sustained limb loss.[2] Military databases have indicated that as of April 2010, military medical centers have treated combatants with 992 major limb amputations (822 from OIF and 170 from OEF) and 341 minor amputations (317 from OIF and 24 from OEF) (Personal communication, Colonel Paul Pasquina). The relative youth and high fitness level of service members prior to limb loss have made them an ideal population for aggressive rehabilitation,[3] but have also exposed the limitations of existing

prosthetic technologies. Congressional research service reports have indicated that the amputation-to-death ratio in OIF has been 1:4 compared to 1:54 in World War II (Table 1). Military personnel with amputations may face unique challenges due to their short residual limbs,[2] unplanned amputations,[4] high incidences of multiple limb loss and comorbidities.[5]

1.2 Options Available for Upper and Lower Limb Amputees

Historically, military conflicts and the associated trauma-related amputations have led to increased attention and advances in prosthetics.[6] Numerous improvements over the past 10-20 years in prosthetic design and components have allowed individuals with amputations to achieve functional goals not previously possible. These advances have included improvements in the actual components of the prosthesis as well as artificial limb attachment systems and prosthetic control mechanisms.[7] Newer socket designs utilizing lightweight carbon composites and flexible inner liners have provided better accommodation for fluctuations in residual limb volume.[7] Various materials including silicone and copolymer gels have provided an interface between the residual limb and the prosthetic socket to provide cushioning, stability and shear reduction to the skin.[7] Customized options for the suspension of the prosthesis to the residual limb have included various forms of suction and vacuum suspension.

Developments in lower limb prosthetics have led to microprocessor-controlled knee and foot devices capable of monitoring gait in real-time and making automatic adjustments based on changes in terrain and angular velocity of the prosthetic component.[7] Newer foot and ankle prosthetic components have energy storage and return

capabilities during ambulation because of the elastic response properties intrinsic to the materials.[7,8] Additionally, targeted muscle reinnervation techniques, which specifically relocate nerves severed in an amputation to alternative muscles to improve control of a myoelectric prosthesis, have been implemented in individuals with upper limb loss.[8]

1.3 Problems Associated with Traditional Socket Prostheses

1.3.1 Physical Problems with Current Prosthetic Technology

Nonphysiological loading and stress shielding of limb bones has remained a concern following limb loss, with cortical erosion noted to occur as early as 6 days postamputation.[9] Carol Barber reported in a study conducted on the immediate and delayed healing in amputated limbs that osteoporosis occurred in the diaphysis of long bones and appeared to have a "moth-eaten texture."[10] Socket-type prostheses have also been known to exacerbate muscle and skeletal atrophy following an extremity amputation, since the forces exerted on these biological tissues do not approach the minimal effective strain threshold required for tissue growth and maintenance.[11,12]

In the case of unilateral lower extremity limb loss, the unamputated limb often carries a higher load than the affected limb and subsequently has an increased likelihood of developing osteoarthritis (OA) (Figure 1).[13] The potential for pathological joint disorders such as OA has been reported to be based on residual limb length, as high proximal amputations have been known to create pelvis instability[14] and may be more difficult to transfer loads to a socket-type prosthesis.[15] Magnetic resonance imaging of high transfemoral amputations have also demonstrated pronounced muscle atrophy

within the amputated limb for both the cleaved and intact muscles (range: 40-60% atrophy and 0-30% atrophy, respectively).[15]

The relationship between limb loss and pathological bone disorders may also be pronounced in patients with high body mass and lower extremity amputations, as a 1-pound increase in weight has been known to result in a fourfold increase in compressive force on the knee.[16] Kulkarni et al. corroborated these biological principles as male war veterans with major lower limb amputations had a threefold increased risk of OA on the unaffected limb for those with above-knee compared to below-knee amputations.[17] As such, prosthetic users may develop asymmetric gait patterns to compensate for this discomfort, with a longer stance occurring on the unaffected limb and longer swing on the amputated limb during ambulation.[18]

While socket prosthesis may improve functionality for patients with limb loss, these devices have been reported to be difficult to attach to short residual limbs, and may have problems with proper fit due to weight fluctuations, muscular atrophy, pressure necrosis and ulceration.[19-22] The high frequency of skin-related socket complications have resulted from mechanical breakdown at the skin-socket interface, since skin thickness at an extremity amputation site has been known to be considerably thinner than the palms and soles which are especially equipped for high load bearing regimens.[23] Physical limitations with socket-devices have included heat/sweating in the prosthetic socket,[24,25] skin irritation[21,26,27] and the inability to walk on challenging terrain.[25] Previous studies investigating skin breakdown in below-knee amputees revealed that one-third of patients (26/86) suffered from unhealed wounds or damaged skin,[28] and 40% of lower extremity amputees (337/828) had at least one skin problem on the lower limb.[29]

The anatomical location of an amputation has also been known to significantly affect the acceptance of a socket-type prosthesis.[30] More specifically, in upper extremity amputees, Moore et al. noted that greater than 50% of prosthetic operators stop using their assistive device because of discomfort and poor functionality.[31] Loeb also documented that upper extremity amputees may be much more limited than lower extremity amputees because of the additional degrees of motion the shoulder has than that of the knee and also the absence of cues from mechanical locomotion.[30]

1.3.2 Financial Burden of Prosthetics

Aside from the physically demanding requirements for upper and lower extremity prosthetic users, high financial costs may pose a problem, especially for individuals not in the military. According to the Amputee Coalition of America (ACA), a standard below-the-knee prosthesis that allows a user to stand and walk on level ground costs between $5,000 and $7,000 and a device that allows the user to become a "community walker" capable of going up and down stairs and traversing uneven terrain costs approximately $10,000.[32] These costs may even be underreported as Sanders et al. has noted that within the first 2 years following an amputation, several socket changes may be necessary to accommodate the rapid changes in stump volume.[33]

High fluctuations in residual limb volumes often require frequent modifications to prosthetic limbs. Smith et al. reported in a study on the functional outcome of traumatic below-knee amputees that it required on average 1.5 years of continuous prosthetic use before an individual felt comfortable using a socket, with most users requiring 4-5 prosthetic devices by 5 years postoperation.[34] One study conducted by Lerner-Frankiel et

al. noted that only 10% of amputees (1/10) were capable of crossing a crosswalk in the allotted time, with most individuals unable to walk for 600 meters continuously,[35] the distance required to be an "independent community ambulatory."[35] As such, the lifetime health-care cost for patients who have sustained one limb loss may be as high as $510,000.[36]

An independent Department of Veterans Affairs study conducted by Sherman observed that all 45 war veterans in his study population had complications with their prosthetic socket stemming from poor prosthetic fit to superficial infections.[37] Most importantly, Sherman explicitly noted that there have been significant unsolved issues with current prosthetic options which must be addressed.[37] As such, several research groups have developed a novel alternative which allows a prosthetic device to be directly attached to the human skeleton, termed transcutaneous osseointegrated implants (TOI).[38]

1.4 Osseointegrated Implant Technology

The term osseointegration has been used to describe a structural and functional connection between living bone and the surface of a load bearing implant.[39] With osseointegration, a metal device is surgically inserted directly into the bone of the residual limb and may serve as an attachment system for connecting and suspending a prosthesis to the residual limb (Figure 2).[40] This procedure may reduce skin irritation,[41-43] enhance osseoperception[38,44,45] and better serve individuals with limited residual limb length.[40,46]

There are currently three osseointegration centers conducting clinical trials for patients who advocate for TOI — a Swedish group, led by Dr. Rickard Brånemark, who

has set up osseointegration centers in Europe, Asia, South America and Australia; a German group which consists of an osseointegration center in Lübeck, Germany led by Dr. Horst Aschoff; and an English group, led by Gordon Blunn, Catherine Pendegrass and Norbert Kang. European clinical trials for patients with TOI have demonstrated increased patient activity levels and gait performance when compared to traditional socket prostheses,[47-49] but differences in implant design, operative procedures and rehabilitation regimens have existed between the osseointegration centers.

According to the orthopaedic literature, the Brånemark group has treated 100 patients between May 1990 - June 2008 and reported an 18% failure rate.[50] However, the majority of failure cases in this subset have been known to occur prior to the introduction of a 2-phase surgical and rehabilitation protocol known as OPRA (Osseointegrated Prostheses for the Rehabilitation of Amputees). In the first stage, an intraosseous implant is inserted into the bone with a predefined healing period to allow for adequate osseointegration without any initial implant pre-loading. This period has been reported to last 6 months for femoral implants and 3 months for implants of the digits.[51] In the second stage of the Brånemark protocol, a soft tissue revision is made to insert the transcutaneous component (abutment) and is followed by a controlled loading and rehabilitation protocol after the 6th postsurgical week.[50,51] More recently, a 2-year follow-up by Hagberg et al. noted that 94% (17/18) of the amputees with osseointegrated implants (and who used the OPRA protocol) were still functioning operators and reported a higher quality of life compared with socket-type prostheses.[52]

Since 1999, a similar osseointegration procedure has been adopted by the Aschoff group in Lübeck, Germany.[53] Personal communication with Dr. Aschoff has indicated

that approximately 30 surgeries have been conducted to date, but his results have not been published in the orthopaedic literature. The German technique for osseointegration has remained similar to the Brånemark group in that the procedure requires two surgical stages, but Aschoff does not restrict load bearing after inserting the implant abutment. In most cases, the second stage will be conducted 4 to 6 weeks after the first implantation, with rehabilitation regimens designed to gradually increase weight-bearing between 4 to 6 weeks after the second surgery.

The intraosseous transcutaneous amputation prosthesis (ITAP) developed by Blunn, Pendegrass and Kang, at the University of London,[54] was designed to mimic the surface pore structure of the deer antler on the TOI, maximize soft tissue attachment and prevent superficial infections at the skin-implant interface.[41,42] Early clinical trials for patients who have lost fingers, thumbs or upper limbs—including two people injured in the July 7th bombing in London— have indicated good success rates (personal communication, Dr. Catherine Pendegrass), but clinical and follow-up data have not been published to date. One novel feature developed by Blunn, Pendegrass and Kang has been a one-stage operative technique, which has been a significant disadvantage of both the Brånemark and Aschoff design principles.

Although only currently available in Europe and Australia, TOI may assist service members in the United States in the near future following FDA approval.[7,39] Animal studies developed by Roy Bloebaum, Peter Beck and Kent Bachus have demonstrated success of TOI in a single stage ovine model.[55,56] Data from this model have indicated that durable skeletal attachment and immediate weight-bearing may be attained with TOI in properly designed implants with adequate "fit and fill."[55,56] Gait analysis has

confirmed the beneficial impact of this designed TOI protocol, as 84% of preoperative loads occurred on the animals' amputated limb by 3 months postoperation.[57]

1.5 Limitations of Osseointegration

While osseointegration technology has shown promise for individuals who may not qualify or reject socket technology, protracted rehabilitation periods developed by the Brånemark and Aschoff groups have limited the expansion of TOI. One challenge with using natural biological skeletal fixation has been allowing the bone to heal and osseointegrate with the implant surface, thereby attaining a strong skeletal interlock, a prerequisite for long-term implant function and stability.[58,59] To prevent mechanical loosening at the bone-implant construct, the OPRA program, developed by Brånemark, has been designed with extensive periods of restricted load bearing (12-18 months from the first operation to full weight bearing) to allow for sufficient bone attachment and to prevent overloading at the bone-implant interface (Figure 3).[25,60-68] Limiting the force on the periprosthetic bone following insertion of a TOI has been based on the principle that stress must be exerted gradually to promote firm skeletal attachment, since under- or over- loading may compromise the integrity of the host bone before osseointegration may occur. However, previous literature has indicated that immediate implant loading may not compromise the integrity of the bone-implant interface or prevent osseointegration if micromotion has been controlled in properly designed implants.[59,61-63,67-71]

1.6 Rationale for Study Design

The aim of this present study was to investigate the ability of electrical stimulation to improve the quality and quantity of skeletal fixation of osseointegrated implants. Current TOI rehabilitation protocols require prolonged periods of restrictive load-bearing to prevent over-loading at the bone-implant interface.[25,60-68] However, electrical stimulation has been proposed as a therapeutic alternative given the high success rates reported for electrically induced fracture healing[72] and the osteoinductive abilities of direct current (DC).[40]

A unique design concept of electrically induced TOI is that the implant will exit the residual limb functioning as an exoprosthetic attachment, but may also be easily modified to be a functional cathode.[46] By using the orthopaedic implant as an electrode in a DC configuration, an electrical current at the bone-implant construct may be directly measured and avoid problems with approximating current pathways through the body (Figure 4). While electrically induced osseointegration has been evaluated once previously in a unicortical model,[73] no animal or human studies have used intramedullary implants for direct enhancement of TOI with detailed histological and mechanical testing. TOI has been considered to be an optimal electrical design since the implant may be fit with implantable sensors in the future[74] to help monitor electric field magnitudes and provide real-time feedback to the prosthetic user and physician.

To evaluate electrically induced osseointegration, a methodical scientific approach was developed which utilized finite element analysis (FEA), *in vitro* cell culturing and an *in vivo* small animal model. This scientific outline was created so that each research initiative would be predictive and may be validated using the *in vivo* rabbit

model. In this dissertation, Chapter 2 criticizes the peer-reviewed electrical stimulation literature, addresses the classic pitfalls of previous experiments and provides a background on the bioelectric phenomenon of bone as it applies to piezoelectricity, fracture healing and overall changes in bone metabolism. Chapter 3 introduces FEA for predicting current densities and electric fields in the residual limbs of wounded service members to determine the feasibility of electrically induced TOI. Developing accurate three-dimensional reconstructions was necessary for ensuring that the electric metrics selected for animal and clinical use would theoretically induce osteoinduction, but not cause tissue degradation. Chapter 4 expands the principles in Chapters 3 and used FEA in higher order volume conductor models with a larger patient population and included heterotopic ossification, an ectopic bone growth known to be prevalent with service members injured by improvised explosive devices (IEDs). Chapter 5 uses the electric metrics developed in Chapters 3 and 4 and investigates the effect of DC on osteoblasts to ensure current density levels would not cause a decrease in cell viability prior to *in vivo* experimentation. Chapter 6 reduces electrically induced osseointegration to practice by employing these biological principles in a small animal *in vivo* model. Lastly, Chapter 7 summarizes these experiments, evaluates the predictability of the scientific model and provides insight for future investigations.

Table 1: 2010 Congressional Research Service report detailing injuries, amputations and deaths of American service members for previous military conflicts.

	Deaths	Wounded	Amputated	Amputations: Deaths
OIF	4,301	31,430	1,112	1:3.9
OEF	714	3,162	112	1:6.4
Vietnam War	58,220	153,303	5,283	1:11.0
Korea War	36,574	103,284	1,477	1:24.8
World War II	405,399	670,846	7,489	1:54.1
World War I	116,516	204,022	2,610	1:44.6

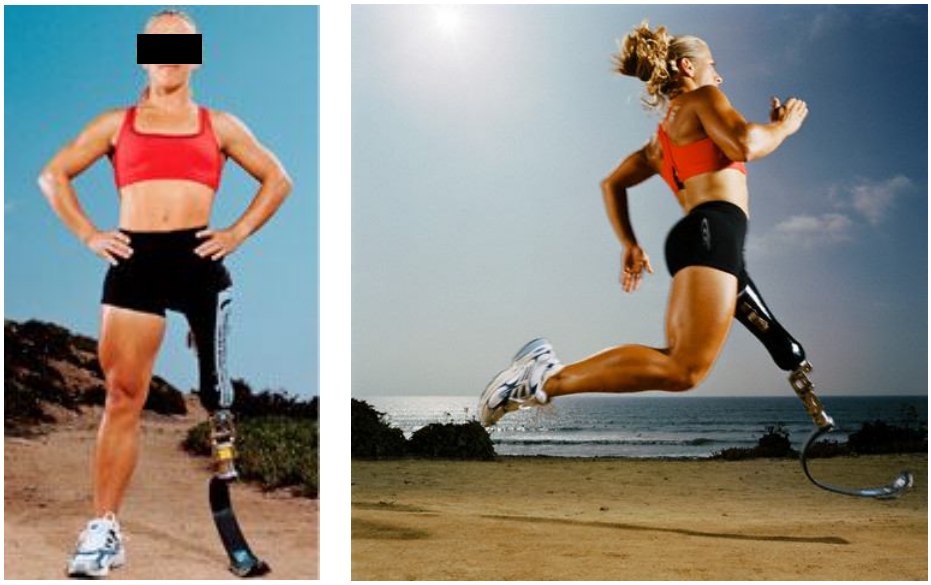

Figure 1: The female athlete featured above has a pronounced discrepancy in the size of her lower limbs due to stress shielding and atrophy from her prosthetic socket. This dissimilar loading pattern, often occurring in unilateral lower extremity amputees, may lead to OA in the unaffected limb and osteoporosis in the amputated limb.

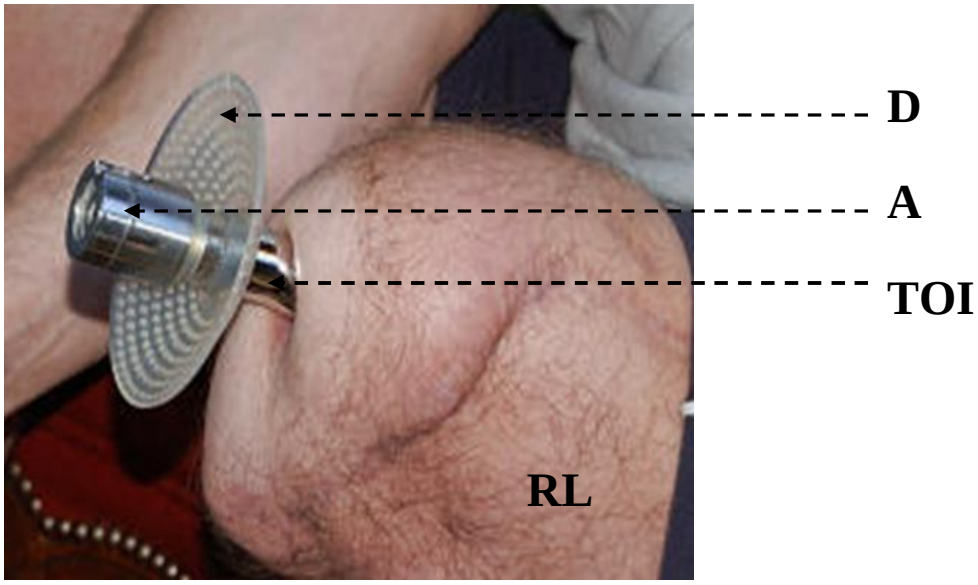

Figure 2: A magnified image of an amputees' residual limb (RL) and TOI. In this procedure, an orthopaedic implant is inserted in the medullary canal and permits direct skeletal attachment with the host bone. An exoprosthetic device may connect to the TOI abutment (A) and allows for quick donning and doffing. Additionally, the TOI may be adapted with a disk (D) to prevent bacterial penetration at the skin-implant interface.

Figure 3: A transfemoral patient with a TOI demonstrating the OPRA rehabilitation regimen developed by Brånemark. Slow incremental load-bearing has been advocated to ensure direct skeletal attachment and a durable bone-implant interface prior to dynamic loading.

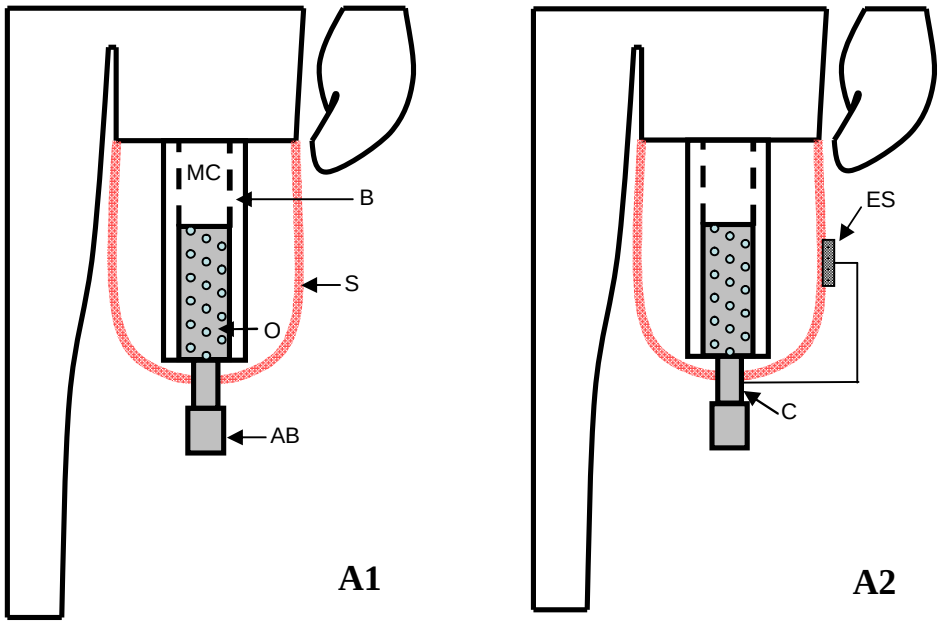

Figure 4: Schematic diagram illustrating osseointegration technology in a unilateral amputee (A1). Using the Brånemark approach, a patient with a lower extremity limb loss would require a two-stage surgical procedure. In the first stage an osseointegrated implant (O) would be inserted into the medullary canal (MC) of the bone (B) to allow for skeletal fixation. In the second stage an abutment (AB) would be connected via a transcutanous opening in the skin (S) and function as an exoprosthetic. However, electrical stimulation (ES) may accelerate skeletal attachment and allow the osseointegration implant to function as the cathode (C), thereby accelerating rehabilitation times (A2).

CHAPTER 2

REVIEW AND CRITICISM OF PEER-REVIEWED ELECTRICAL STIMULATION RESEARCH

It has long been recognized that the human body is an electrically dynamic system which tightly regulates bone growth and development.[75] Endogenous electrical currents have been recorded from fetal development to fracture healing and may affect the quality and quantity of bone deposition.[75] In order to develop electrically induced osseointegration and explore the potential for using an exoprosthetic as a functional cathode and TOI, a critical assessment of the peer-reviewed literature was required. This chapter investigates the bioelectric phenomenon as it applies to bone and the classic misunderstandings which have limited the expansion of exogenous electrical stimulation.

2.1 Endogenous Currents in the Human Body

The ability for humans and animals to generate endogenous electric signals, termed "animal electricity," was first documented in 1792 by Luigi Galvini when he noticed that an accidental spark discharge caused frog muscle fibers to contract.[76] Since that initial observance, it has been generally accepted that all organisms are

electrodynamic systems, with large but stable gradients.[77] It has been reported that all living beings from bacteria to mammals are sensitive to electromagnetic fields,[78] and this has been known to affect cell division rates,[79] tissue growth[77] and wound repair.[77] The phenomenon that electrical signals govern tissue healing has been well recognized in the peer-reviewed literature as tissues which generate endogenous electrical signals have a higher capacity to regenerate.

When a tissue has been damaged, injury potentials create steady electric fields which exist locally for days after the insult. These potential differences result largely from ion flux though leaky cell membranes, have been described as direct current-like, decay with time and have been estimated to be between 1-2 V/cm at the surface of damaged skin.[80] Although wound healing has been known to be a dynamic response, occuring in concert with cells, cytokines and enzymes, bioelectric research has indicated that electrical gradients generated by injured tissue may be an integral part in the regeneration process.[81]

Endogenous electrical currents aid in cellular growth and play an intricate role in animal and human development. Measurements recorded during embryonic growth have demonstrated that substantial endogenous currents exist as early as fetal development.[81] These electrical signals function as a natural control system, ensuring proper cellular expression[82] and facilitating cell migration and orientation, known as galvanotaxis and galvanotropism.[80,83-85] These governing electrical responses are also present in all animals, but have been reported to be uniquely dependent on the species type. In the case of newts, who have the ability to fully regenerate injured extremities, large electrical currents have been recorded during the limb regeneration process.[82]

Observations that endogenous electrical currents affect tissue growth and repair has spurred interest in exogenous electrical stimulation for accelerating bone healing and remodeling in the field of orthopaedics. However, exogenous electrical stimulation has been clouded with uncontrolled variations in experimental design[86] and the utility of these devices still remain a controversial topic in the peer-reviewed literature.[81,86] Therefore, it was the purpose of this chapter review to (1) assess the bioelectric potential of bone, (2) investigate the use of exogenous electrical stimulation for bone healing and (3) identify classic problems in order to improve the current understanding of this topic prior to implementing electrically induced TOI in the clinical environment.

2.2 Bone: The Transducer

Bone is a highly organized anisotropic tissue,[87] which serves as a reservoir for calcium and phosphate,[88] a site for hematopoiesis[88] and provides the structural support required for movement.[88] Bone remodeling is a tightly coupled dynamic system.[89] It is coordinated by cells,[90] hormones[91] and enzymes,[89] and is strongly influenced by age,[92] activity level[93] and mechanical loading.[12,94] Physical forces exerted on bone alter bone architecture and has been a well established principle known as Wolff's law.[95] The functional adaptation of osseous tissue, studied mostly in the proximal femur, has demonstrated the unique ability of bone to alter its trabecular orientation as a result of loading conditions.[96] A basic understanding of solid mechanics notes that stresses and strains are related by Hooke's law. However, bone biologists, such as Harold Frost, have preferred to describe the transformation of bone as a strain-driven event.[12] It has been

hypothesized by Frost that a minimal effective strain is required to maintain bone architecture[12] and physiologic bone strains rarely exceed 3% *in vivo*.[97]

The principle that mechanical deformations of bone alter endogenous electrical signaling, and subsequent control of bone cell activity, has been well regarded in the peer-reviewed literature.[98] However, it was not until the 1980s that the electromechanical properties of bone were postulated as a biophysical basis for Wolff's Law.[98,99] While it has been noted that mechanically deformed or actively remodeling bone always produces electrical current *in vivo*,[100] and is electronegative with respect to the resting environment,[101-104] bone formation and electrical stimulation were not initially considered to be an integrated system. Experiments conducted on the mechanical and electrical interactions of bone remodeling have indicated that successful bone growth results from a combination of both competent mechanical strain stimuli and endogenous electrical currents.[105] Correlations between bone formation rates and bioelectric potentials have been demonstrated by the ability of rabbit tibias to spontaneously generate potential differences up to 6 mV *in vivo*.[106] However, the belief that electrical signaling affected bone growth did not occur until stress-generated potentials, known as piezoelectricity, emerged in the peer-reviewed literature.

2.2.1 Piezoelectricity

The realization that biological tissue had the ability to generate electrical signals was derived from Eiichi Fukada and Iwao Yasuda's work on piezoelectricity in the 1950s.[100,102,107,108] Bone specimens, harvested from human and ox femurs, demonstrated that stress-generated potentials were created by the shear forces of collagen[107] and the

deformation of fluid filled channels (Haversian and Volkmann) that exist in bone (Figure 5).[109] It has been generally regarded that while hydroxyapatite (HA) is vital for bone strength,[110] HA was not the basis for stress-generated potentials. While the amount of electricity generated by bone was less upon removal of HA,[111] piezoelectricity has been regarded as a collagen-dominated phenomenon.[112] Fukada and Yasuda noted that when bone was submerged in acid for 3 weeks to remove the apatite crystals between the collagen fibers, electrical gradients were still produced.[107]

Generation of electric potentials, as described by Bassett and Becker, reaffirmed that mechanical deformation caused electrical stimuli and subsequently controlled osteogenic growth.[113] In this investigation, the amplitude of electrical potentials was dependent on the rate and magnitude of bone loading, while polarity was determined by the direction of the deformed bone.[113] *In vivo* experimental recordings from the human tibia while walking has indicated a piezoelectric response as high as 300 mV.[100] The specific loading pattern of bone has been documented as an important piezeoelectric parameter since potential differences in bone have been known to be caused by charge displacement during the deformation period.[114]

The piezoelectric effect of bone has been known to be strongly influenced by the state of the biological tissue. Because 10-15% of bone may be remodeling at any given instant,[90,115] there has been evidence to support natural variations in piezoelectricity over time.[116] The structural and chemical composition of bone may vary based on age, gender, anatomical location, nutritional factors and hydration, and may subsequently affect the electrical properties of bone.[98] Hydration of the host bone has been known to play a unique role in piezoelectricity, given that water distribution through the pores in bone and

extracellular space naturally decreases over time and with progressive mineralization.[117] Investigational studies evaluating the effect of dry and wet tendon and bone have demonstrated that piezoelectric coefficients decrease with increasing water content due to absorption of free water.[118] It may be postulated that a fluctuation in the amount of water attached to collagen, as well as mobile water within the Haversian and Volkmann canals, affect bone's mechanical properties and electrical metrics.[117]

The clear coupling between mechanical forces and endogenous currents required for maintaining skeletal architecture has been clearly demonstrated since the 1950s. However, the use of exogenous electrical stimulation for expediting osseous growth dates back to the early 1840s.[119,120] While electrical stimulation was used sporadically in the early 19th and 20th centuries, lack of reproducibility almost rendered this technology extinct. In fact, in 1910, the Carnegie Foundation condemned the use of electrical stimulation and relegated electrotherapy to a scientifically unsupportable position, causing it to fade almost completely from medical practice.[72] However, in the past 160 years, through rigorous *in vitro* and *in vivo* experimentation, the mechanisms of electrically induced bone growth have become more apparent.

2.2.2 Cellular Interaction to Electrical Stimulation

The formation of bone by mechanical and electrical transduction is facilitated by up regulation and down regulation of important signaling molecules at the cellular level. The propagation of these highly specialized signals may be facilitated by both chemical and electrical cues.[121] However, problems in accurately delineating the electromagnetic mechanisms have not only been complicated by molecular and cellular complexities, but

also the complexities inherent in properly defining the electric, magnetic and pulsed combination of these energy fields.[86] The electric fields generated from both mechanical stimuli and external electrical devices exert forces on ions through the cellular membrane and interstial fluid.[78] Because the influx and efflux of ions pass through the cell membrane more rapidly with electrical stimulation, it has been postulated that the cell membrane is the primary site of electromagnetic field interactions. Transduction of weak electrical signals, at receptor sites, facilitates transmission of signals to the cell interior and coupling proteins.[122] In fact, cell processes such as ion-binding, defined as the passage of ions though the cell membrane, have been known to alter the membrane double-layer and produce changes in cellular function.[116] The tightly regulated cell membrane has been noted to be uniquely affected by electrical stimulation since osteoblasts are asymmetric and secrete extracellular matrix on one side of their cell.[123] Enzymatic activity of osteoblasts has been reported to be higher on the cell membrane adjacent to an electrode site.[124] These exogenous electrical signals cause a high voltage drop across the cellular membrane, but only a negligible drop in the surrounding electrical matrix. Cellular homeostasis has been known to change when cell polarization and ion displacement occur along the cellular membrane.[125]

The transduction coupling membrane model, proposed by W.R. Adey, postulated that electrical stimulation was effected at the cellular level by (1) humoral stimulation of molecules at receptor sites that alter calcium binding, (2) transmission of the signal which initiates receptor sites in the cell interior and (3) intracellular responses that occur from the transmembrane signal.[122] The ability for calcium to freely enter and exit the cell membrane may be the primary means for electrical stimulation function and cellular

transmission. Calcium ions (Ca^{2+}) are ubiquitous in the body and help regulate many important physiological functions. The parathyroid hormone (PTH), which is affected by serum Ca^{2+} levels, directly alters bone resorption by acting as a potent stimuli for osteoclasts.[126] When PTH is released, it acts upon adenyl cyclase which in turn regulates cyclic AMP (cAMP) and prevents the body from forming new bone.[127] However, increases in pressure, or the induction of electrical stimulation, inhibits membrane-associated cAMP and in turn increases cellular uptake of calcium.[127,128] Electrical and mechanical perturbations of the epiphyseal cartilage have been known to alter cAMP levels by early cell signaling and affect bone remodeling (Figure 6).[127]

Research with capacitive pulsed electrical stimulation of osteoblasts have revealed that 0 to 13 V/cm electric fields decreased cAMP and increase DNA synthesis by 40%.[125] However, calcium ion activity in osteoblasts has been known to be dependent on the frequency and duration of these waveforms and has led to variability in electrical stimulation efficacy.[129] Electric field exposure by McLeod et al. demonstrated that 1 mV/cm exposure with 30 hertz increased intracellular calcium by 20% within 20 minutes. However, a 60 hertz exposure decreased intracellular calcium by 25% over the same experimental time period, indicating a frequency dependency in calcium transduction.

Brighton et al. experimented with several electrical configurations (capacitive coupling, inductive coupling and combined electromagnetic fields), and concluded that the molecular mechanisms of electrical stimulation converged on common pathways in the cascade of healing. With all of their experimented electrical systems, an increase in intracellular calcium led to amplification of calmodulin and cell proliferation.[130] However, Brighton et al. demonstrated that the preliminary steps for electrical stimulation differed

based on the specific electrical modality. The initial event with capacitive coupling was Ca^{2+} translocation through cell-membrane voltage-gated calcium channels, whereas inductive coupling and combined electromagnetic fields initiated by releasing Ca^{2+} from intracellular stores.[130]

The ability to alter cellular migration and orientation, resulting from ion fluctuations through the cellular membrane, has been one of the therapeutic advantages of electrically induced osteogenesis. When electrodes are implanted in the human body, passive influx of Ca^{2+} on the anodal side increases the local intracellular Ca^{2+} concentration, whereas passive efflux and/or intracellular redistribution decreases the local intracellular Ca^{2+} concentration on the cathodal side. These changes give rise to push-pull effects and lead to cell migration towards a cathode.[83] This phenomenon has been known to occur because osteoblasts, like many other cells, have a negative membrane potential and exposure to DC, which causes cellular movement also known as galvanotaxis.[80,84,131] In this process, the membrane side towards the anode is hyperpolarized and attracts Ca^{2+}, while the side of the cell contracts propelling it toward the cathode direction (Figure 7).[83] Cellular realignment and relocation from electric fields has played a major role in experiments of bone regeneration[127] and osteoinduction.[132]

Osteoinduction is a fundamental process for osteogenesis and has been reported for all forms of bone healing.[132] Immature mesenchymal cells differentiate into preosteoblasts and help repair or remodel bone, especially in fracture healing situations.[132] However, as noted above, proper implementation of electrical stimulation also has the ability to alter cell migratory patterns and may assist with skeletal fixation around a cathode site. The mesenchymal stem cells, which arrive at the cathode following

galvanotaxis and galvanotropism, may derive into osteoblasts and secrete osteocalcin, osteonectin and type I collagen into the extracellular matrix environment.[90] The ability to alter mesenchymal stem cell function may be of utmost importance for future prevention and treatment of pathological bone disorders (osteopenia and osteoporosis) due to the reduced capacity to heal with age,[133] which may be improved with electrically induced bone remodeling.

2.2.3 Bone: The Electrical Connective Tissue

Although the effect of electrical stimulation may be the result of alterations in molecular and cellular mechanisms, the majority of research on electrically induced osteogenesis has focused on the entire continuum of bone at the tissue level. As stated previously, injury potentials which result from tissue damage help establish endogenous electrical currents for wound healing.[80] Injured musculoskeletal tissues in the early process of healing (termed the lag phase) display electrical and electromagnetic currents which are very disorganized.[134] In the case of normal long bones, the metaphyseal region has been reported as electronegative while the midshaft approaches isopolarity. However, when a bone has been fractured, the metaphysis becomes even more electronegative and the entire shaft of the bone site becomes negative with respect to the resting environment (Figure 8). The change in long bone electronegativity has been known to exist until fracture healing has occurred and returns the diaphysis to its previous isopolar state.[135]

The known architectural change in bone due to age and loading conditions, has provided an electric relationship with Wolff's law and has been known to contribute to the fluctuations in electric metric recordings *in vivo*. For instance, the resistivity of rabbit

femurs has been reported to range from 8 to 500 kΩ/cm.[98,136] One explanation for the wide variability in bone resistance, aside from bone orientation, has been due to the state of the specimen (living vs. dead) and the volume of blood inside the bone specimen. As noted by Liboff et al., the resistance of tissue drastically changes between living and dead specimens[136] and bone tested without a blood supply will significantly affect the recorded measurements.

Bone is the most variable resistive medium in the body,[137] and vascular integrity has been of utmost importance when empirically determining bioelectric metrics. The blood supply in bone travels longitudinally though Haversian canals, which have an average diameter of 20-50 μm.[138] Haversian canals comprise approximately 5-10% of the cross sectional area of human cortical bone,[90] but change with age.[139] Fluctuations in the volume of blood within the vascular cavities will affect the resistance of bone, since the electric metrics of blood depend on blood volume, hematocrit, flow and temperature.[140]

2.3 Application of Bioelectricity in Orthopaedics

In orthopaedics, the use of electric and electromagnetic fields has focused primarily on promoting healing of bony nonunions.[141] For clinical applications in fracture healing, there have been three commonly used modalities: inductive coupling, capacitive coupling and direct current. It has been generally recognized that capacitive and inductive coupling are noninvasive techniques, since electrical devices used externally do not require surgical intervention.[109] However, it has been reported that invasive and noninvasive setups have similar success rates.[109] In order to improve understanding of the currently available electrical stimulation tools for healing bone defects, Table 2 provides

a brief overview of inductive coupling, capacitive coupling and direct current. It is interesting to note that even as of 1976, clinical indications favoring one technique versus another were still not well defined.[101]

The use of controlled electrical stimulation results in electrochemical reactions at the electrode sites. With faradic exchange of electrons, reduction-oxidizing (Redox) reactions generate hydrogen and hydroxide ions which alter localized pH. A slightly alkaline environment has been known to occur at the cathode during fracture healing applications and has been more favorable for bone growth.[114,142-144] Investigational studies on tissue pH and oxygen tension, in healing bone defects, have indicated that changes in oxygen tension are a normal part of bone formation. Gradients exist at the epiphyseal plate during growth with the lowest oxygen tension occurring at the cartilaginous junction[145] having a localized alkaline pH of 7.70.[146] It has not been determined whether the low oxygen tension at the cathode site has been the result of increased oxygen consumption or decreased oxygen supply to the area. Heppenstall et al. postulated that the physiological reason may be that low oxygen tension acts as a stimulus for mesenchymal stem cells and assists with osteoinduction.[145]

The surgical implantation of a direct current fracture healing device ultimately results in fibrous encapsulation at the anode site and creates variations in electrical resistance which cannot be accurately approximated analytically. While the thickness of the fibrous sheaths have been reported to be independent of electrical stimulation usage,[147] resistance at the electrode sites initially decreased due to inflammation and leaky cell membranes, but increased over time from the fibrous encapsulation of the

implanted electrodes. Increased resistance of an internal electrical stimulation device may dissipate power and has been a common problem with chronic electrical stimulation.[148]

2.3.1 Electrically Induced Fracture Healing

While bone is a fairly predictable tissue in respect to its healing abilities,[149] inadequate mobilization, disruption of vasculature and scar tissue formation may all contribute to atrophic nonunions.[150] For those who experienced delayed healing or non-unions, few therapeutic alternatives aside from surgical intervention were available for bone healing until the mid-20th century when electrical stimulation emerged as a tool for expediting osseous growth.[134] As noted by Tomaz Cieszynski, during the consolidation of a fracture callus, there is a beneficial effect exerted by the redistribution of electric charges in the patient's body.[151] Recent surveys done by Canadian orthopaedic surgeons corroborate this principle stating that 45% of the polled population currently use electrical stimulation devices for complicated tibial shaft fractures.[152] Despite the reported 100,000 nonunions healed as of 1990 with electrical stimulation,[72] skepticism still exists within the scientific community largely in part from lack of homogeneity with trial design and dosage.[153] The variability in electrically induced fracture healing has resulted from the extent of direct and indirect trauma[154] and fracture gap size.[72] It has been generally regarded that the fracture gap size cannot exceed half the diameter of the bone for effective electrical stimulation treatment,[72] otherwise surgical intervention will be required.

2.4 Problems with Clinical Use of Electrical Stimulation

The increased understanding of molecular, cellular and tissue interactions with electrical stimulation has created high commercialization opportunities and is a 500 billion dollar market in the United States.[134] However, over eager product development has significantly limited the acceptance of electrical stimulation. Before the first randomized control study of inductive coupling was performed, more than 11,000 devices had been sold worldwide for treatment of nonunions.[155] A meta-analysis performed by Akai et al. demonstrated the inconsistencies reported for electrically induced osteogenesis by combining results of 12 bone studies and 16 soft tissue trials. They discovered that 37% of patient data was unknown, 35% of bone results were qualitative, 35% of studies did not reveal limitations and 12% of statistics were not well defined.[153] Observations by Akai et al. also demonstrated that bone was treated from 1 month to 36 months while soft tissue injuries were treated for 1 day to 12 months with high patient drop out rates.[153]

Discontinued use of electrical stimulation has resulted previously from incorrect assumptions on electrical current being the dominating factor affecting bone growth. Clinical usage of electrical stimulation exponentially increased for fracture healing in the early 1970s because of clinical trials conducted by Carl Brighton and Zachary Friedenberg.[135] However, these investigators inaccurately attributed the 73% success rate of electrically induced bone formation in one study to be the result of electrical current.[156] Brighton and Friedenberg noted that 5-20 μA progressively increased quantities of bone while current levels greater than 20 μA gradually gave rise to cellular necrosis.[157] The misconception that current (5-20 μA), not current density, was vital for controlling bone

growth was frequently reported throughout the peer-reviewed literature[116,135,156-160] and occurred because of the false misconception that spatial position of electrodes did not affect bone growth.[158] It was not until the early 1980s that current density and the subsequent electric field were considered to be the governing factor affecting the efficacy of exogenous human and animal electrical stimulation.[161] Investigation studies conducted by Hassler et al. noted that bone degradation occurred when the calculated average current density exceeded 625 $\mu A/in^2$.[140]

Tissue degradation from excessively high current densities has been frequently documented in clinical reports and histological studies. At current densities of 5 mA/cm^2 or greater, blood vessel damage has been known to occur since hydroxide ions generated by electrochemical reactions cannot be adequately buffered.[162] The quantity of tissue destruction created by fluctuations in pH is directly related to charge density.[162] While slight increases in pH favor bone deposition, substantial pH changes may damage the host bone.[163] When tissue integrity has been compromised from excessive heat generation at the cathode, tissue destruction has been reported as fibrinoid necrosis involving the cortical endosteum with many empty lacunae.[164] Reports by Ishida et al. corroborated this occurrence since osteonecrosis resulted in marrow cell necrosis and empty lacunae devoid of osteocytes.[165]

Severe patient complications from excessively high electrical current densities have occurred because of the focus on maintaining only a low electric current. This problem has been replete in the peer-reviewed literature.[166] Despite maintaining low levels of electrical current, which were proposed to be osteogenic, researchers and clinicians have failed to realize that the distance of electrode placements have not been

uniform on a patient-to-patient basis. Most notably, when tibial fractures were treated with electrical stimulation by Torben Jorgensen, one patient refused to continue treatment because of heat and pain in the affected limb.[166] In separate trials, tissue reactions at the electrode site also developed into superficial infection sites and required removal of cathode components.[156]

Electrical complications which have occurred because of unnecessary attention paid to electrical current, not current density, have been reported with animal models as well. The animal model most frequently used for electrical stimulation studies has been the New Zealand white rabbit. Studies evaluating the effect of the direct current on bone noted that 70 μA of current (expected current density unknown) applied between two electrodes, in close apposition, produced noticeable bone retardation.[167] Confounding variables have added to the ambiguity with the current density versus current argument since Tomasz Cieszynski also used New Zealand rabbits, but included both genders. His animal population also had high weight fluctuations (1.15-3.45 kg) and electrical currents ranging from 0.66-4.00 mA, which drastically altered the localized field strengths.

It is therefore important that investigators know that the electrical metrics (electric field and current density) established for electrical stimulation must ensure tissue integrity by confirming the buffering capability of the body to adapt to the hydroxide ions generated.[162] Failure to maintain electric fields below 10 V/cm have resulted in cellular damage from joule heating effects[131] and current densities exceeding 1-2 mA/cm^2 have created localized tissue injury from heat generation,[46,162,168] most noted from histological evaluation of the anode site postmortem.[158,164,169] Maintaining current densities below the standard of practice continues to be of utmost importance since fluctuations may occur *in*

vivo due to variations in ion concentrations, temperature, hydration, and have been difficult variables to predict *in vivo*.

2.5 Conclusions

The dynamic response of bone cells to alterations in localized mechanical stresses and electric fields has been vital for increasing secretion of growth factors,[170] intracellular calcium,[130] cell proliferation[130] and bone remodeling.[157,160,171] As noted previously, the structural integrity of bone is maintained by anatomical forces which are electrical in nature.[90] However, despite the vast expansion seen with electrical stimulation devices for fracture healing applications, clinical cases still continue to be conducted using 5-20 μA as the required threshold without regard to current densities.[172]

Additionally, because bone is a composite material continually changing over time, developing standard electrical metrics for electrically induced osteogenesis may not be feasible. As stated by Marino et al., there is little hope of understanding the interaction with electric fields and tissue on the basis of fundamental biophysical principles.[173] This occurs largely since the dielectric constant and conductivity of tissue remains not well characterized and it has been very difficult to measure field strengths inside living organisms *in vivo*.[173] While experimental calculations provide a range of expected field strengths, current densities may only be crudely estimated without finite element analysis (FEA).[136] Determining electric fields *in vivo* has also been ambiguous because tissue conductivity fluctuates based on fiber orientation.[174] Therefore, in order to improve the current understanding of electrical stimulation, more concentrated efforts must be made

to evaluate current density and the subsequent electric field magnitudes prior to implementing electrically induced TOI.

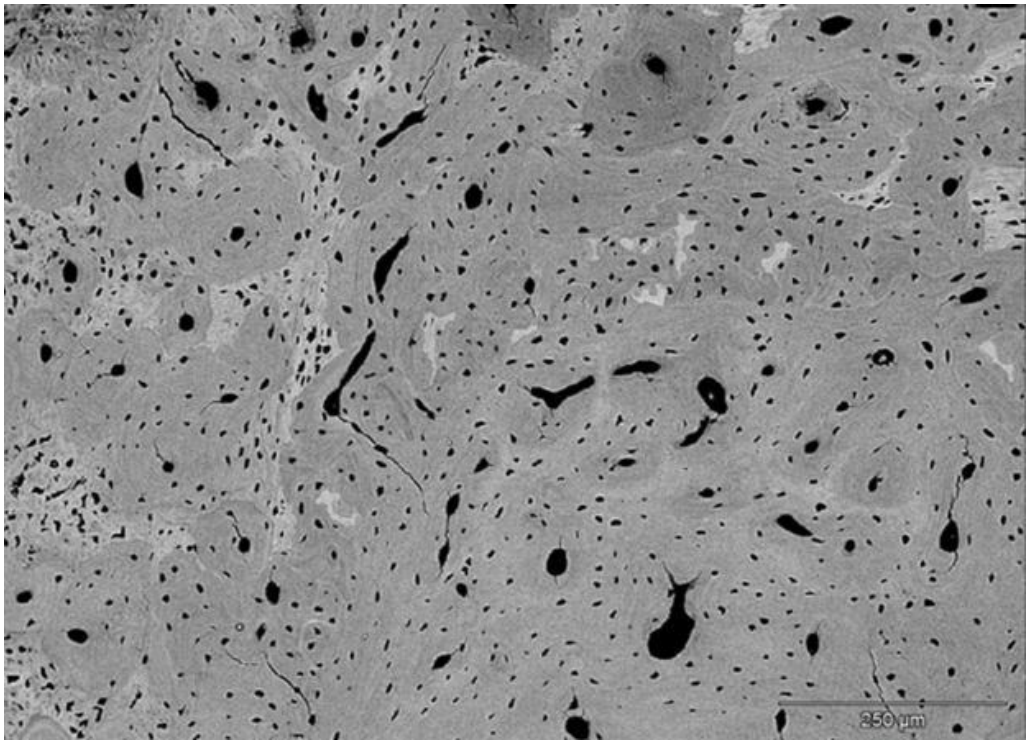

Figure 5: Cross sectional backscattered electron image of rabbit cortical bone demonstrating visible Haversian canals, osteons and lacunae.

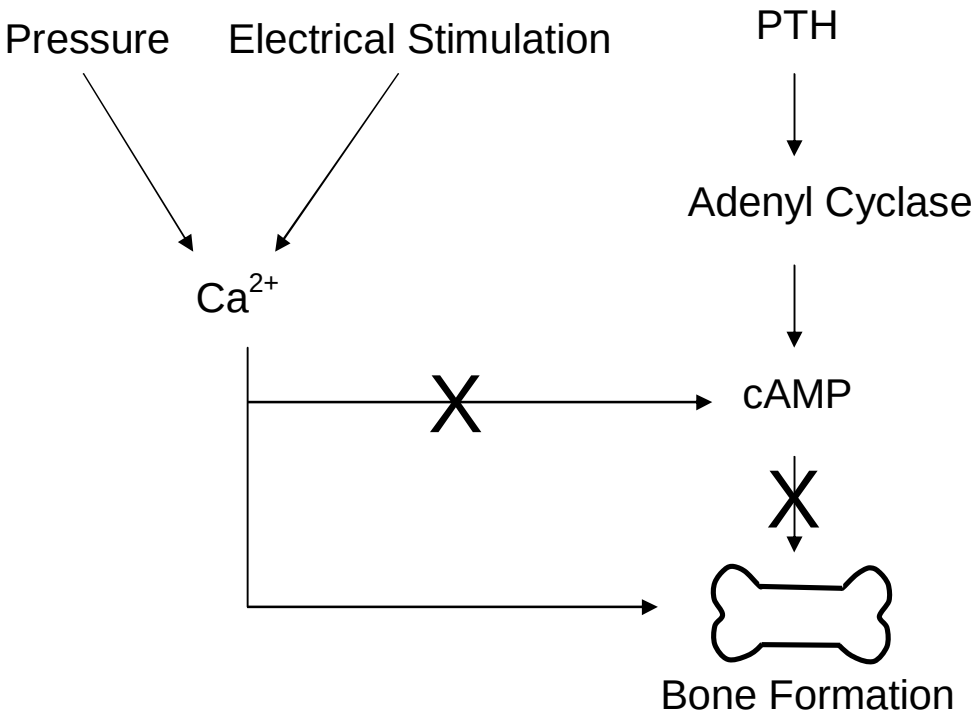

Figure 6: Schematic overview of the PTH pathway affecting bone growth. An increase in pressure or electrical stimulation leads to an increase in intracellular Ca^{2+} and bone formation. However, in situations of low pressure or no electrical stimulation exposure, PTH activates adenyl cyclase and cAMP which prevent bone formation.

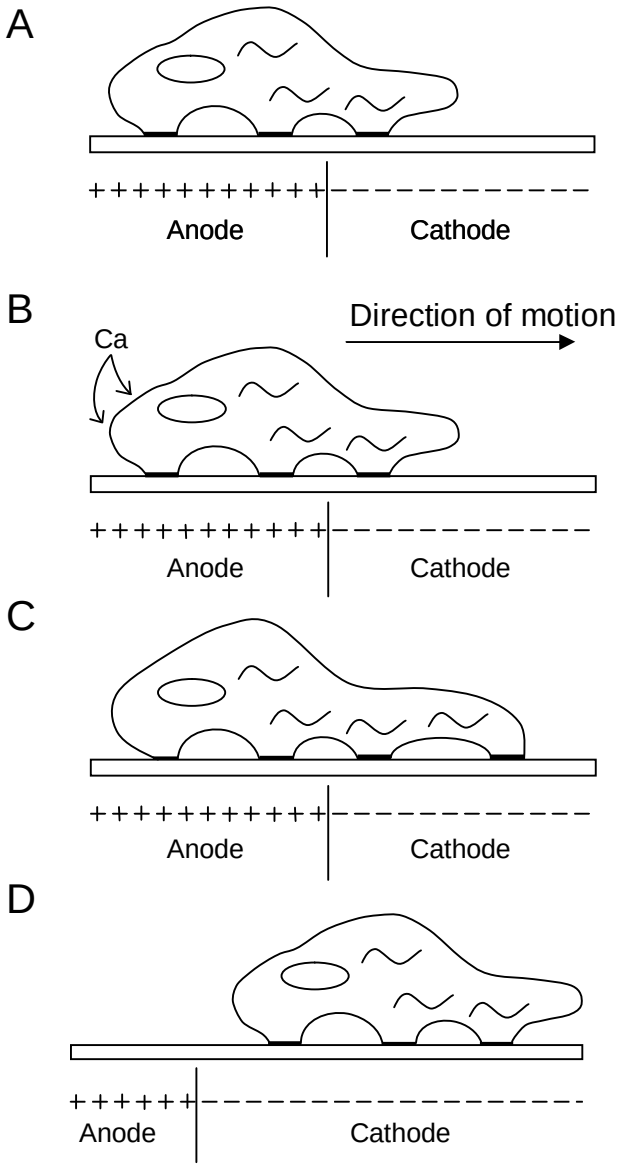

Figure 7: Osteoblasts placed in an 1-10 V/cm electric field (A) will migrate towards the cathode due to an influx of Ca^{2+} which occurs near the anode region (B). This phenomenon, termed the push-pull effect, results in attachment and release of focal adhesions (C) and galvanotaxis of osteoblasts (D).

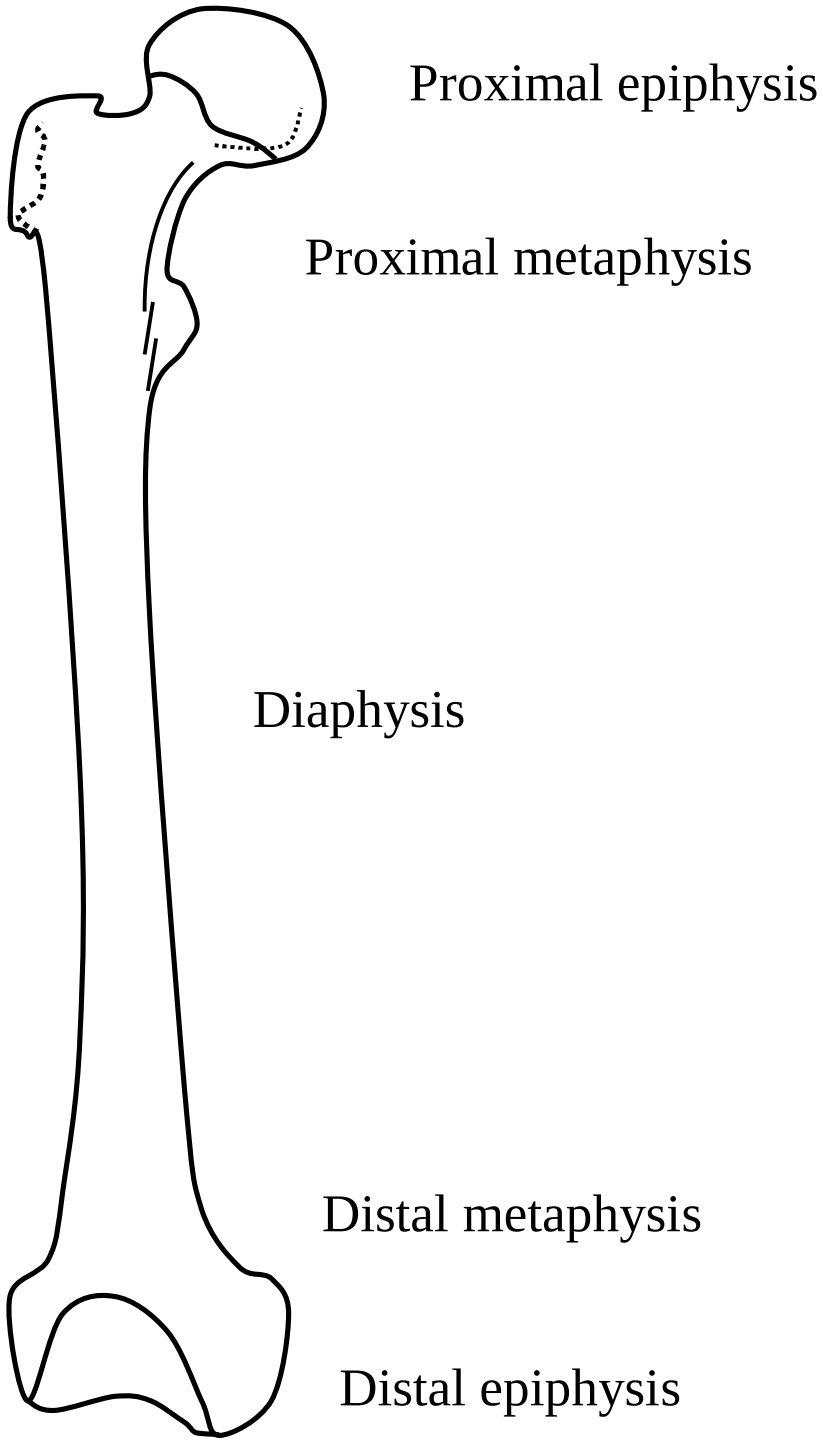

Figure 8: Representative image of human long bone subdivided into distinct regions of the diaphysis, epiphysis and metaphysis.

Table 2: Commonly used electrical treatment modalities in fracture healing applications and the advantages and disadvantages reported for each technique.

Method	Advantage	Reference	Disadvantage	Reference
Direct Current	Patient compliance	141,160	Invasive (requires surgery for electrode implantation and removal)	141, 160
	Electric field not magnetic field appears to be the dominating factor in fracture healing	72	Transcutaneous leads have infection risks and mechanical failure	147
	Clinical success rates: 63-86%	156, 169, 171,175		
Capacitive Coupling	Noninvasive	141	Requires high voltages with large limbs	177
	Clinical success rates: 70-77%	109, 176	Patient compliance	141
Inductive Coupling	Noninvasive	141	Non-weight bearing technique	134
	Clinical success rates: 64-87%	178, 179	Patient compliance	141

CHAPTER 3

DEVELOPMENT OF COMPUTATIONAL MODELING FOR PREDICTING ELECTRIC FIELD AND CURRENT DENSITIES IN THE RESIDUAL LIMB OF AMPUTEES

3.1 Introduction

To more closely approximate electric field and current density magnitudes *in vivo*, and avoid crude analytical estimations,[136] researchers have explored the use of FEA for enhancing the success of TOI.[46,75] FEA offers a plausible experimental model for better understanding the bioelectric effects in the distal residual limb for amputees seeking osseointegration technology. However, as demonstrated in Chapter 2, complications with electrical stimulation have been reported from misunderstanding the importance of electrode design and placement, as these variables have been known to directly influence current density magnitudes.[157] Previous studies using "trial and error" techniques have negatively affected patient care,[166] and therefore required a more methodical scientific approach for electrically induced osseointegration. This chapter explains how volume conductor models were developed with thresholding and FEA software programs to

better determine an electrical configuration which would ensure patient safety and theoretically induce osseointegration *in vivo*. The objectives of this study were to use the exoprosthetic portion of a TOI as a functional cathode to (1) standardize an electrode configuration for electrically induced osseointegration procedures, (2) determine the relationship between residual limb volume and electrical metrics and (3) establish electrical criteria which should lead to enhanced skeletal fixation in future *in vitro* and *in vivo* applications.

3.2 Materials and Methods

3.2.1 Patient Inclusion

Retrospective computed tomography (CT) scans were collected from 4 patients in accordance with University of Utah and Department of Veterans Affairs Institutional Review Board (IRB) and HIPAA approvals. The patient population consisted of 2 males and 2 females who were 59.0 ± 22.2 years of age at the time of radiographic review (Table 3). While in most cases high standard deviations would not be advocated because of the associated experimental variability, wide distributions in patient demographics (height: 163 ± 14.7 cm, weight: 58.1 ± 15.3 kg) were necessary in this study to determine the bioelectric effect of TOI using a broad range of residual limb volumes (Figure 9).

Transfemoral amputations in patients 1 and 2 differed significantly from that of patients 3 and 4. Patients 3 and 4 were individuals who sustained trauma-related limb loss. However, patients 1 and 2 were “artificial amputees” in the fact that software segmentation was used to simulate limb loss (Figure 9). Artificial amputees lacked a distal residual limb and muscles and tendons were not reattached using the known

myodesis and tenodesis techniques (Figure 10).[180] Instead, transfermoral limb loss was created using computer software and occurred several centimeters above the knee. The rationale for generating artificial amputees in Chapter 3 resulted in part from a limited patient population as there were only 2 individuals with lower extremity amputations and retrospective CTs at the IRB approved sites, and because a discrepancy in limb geometry and residual limb size were necessary to determine the sensitivity of FEA.

3.2.2 Using CT Scans for Amputee Reconstructions

CT files collected during the study were saved as dicom images and imported into Seg3D (version 1.11.0, Scientific Computing and Imaging Institute, Salt Lake City, UT), a volume segmentation and processing tool, used to create anatomically accurate patient specific models. The tissue boundaries of the internal organs, bone, bone marrow and adipose tissue were generated by thresholding the CT files interactively using fixed values for all of the patients' CTs (Figure 11).[46] Musculature was obtained by manually setting seed points inside the tissue and using a confidence connected filter to find all of the tissue connected to the seed points, since the complex geometry required additional image processing.[46] Because the skin was impossible to discern reliably from CT images, an estimate of the skin layer was generated by dilating the outermost visible tissue to produce a 2mm layer of homogeneous thickness (the average thickness of human skin)[23] to surround the full model. Skin was modeled with 0.26 S/m, a conductivity representative of hydrated skin, since the moisture content on the surface of the tissue would be expected to alter the electric field and the related current density magnitudes at the bone-implant construct. Segmentations were lastly manually inspected, corrected to

ensure accuracy and combined in a hierarchy into a single label map required to generate meshes for FEA (Figure 12).[46]

3.2.3 FEA

SCIRun, a problem solving environment which included modules to carry out FEA for bioelectric field problems, provided support for electrode design (version 4.0, Scientific Computing and Imaging Institute, Salt Lake City, UT). The interactive platform allowed for real-time electrode manipulation and helped to assure reproducibility in the model. A network was created and modules were organized for defining boundary conditions (Equations 1-5), tissue conductivities, mesh refinements, generating Matlab histograms and recording field data (Figure 13).

In this model, the boundary conditions were formed by the electrodes that injected electrical currents, and the homogenous Neumann boundary condition on the limb's surface, forcing the electric current to remain in the limb, as electrical conductivity of the surrounding air has been known to be zero. Since the electrodes and the implant had a much larger conductivity than the surrounding tissues, it was assumed that the osseointegrated implant (cathode) was at a constant potential; likewise, the surface electrodes (anodes) were modeled with a constant potential difference from the transcutaneous implant. Boundary conditions for the nodes in the meshes were set up to be continuous between tissue types, such that there was no discontinuity between bones and muscles (see Equation 1). The electric current was governed by Equation 2, which required that the electrical current of the bone be equal to the electrical current of the muscle and hence, electrical power could not be dissipated between tissue types.

(1) $$\varphi_{(r)}\Big|_{\partial G_{bone}} = \varphi_{(r)}\Big|_{\partial G_{muscle}}$$

(2) $$\sigma_{bone}\nabla\varphi_{(r)}\Big|_{\partial G_{bone}} \cdot \vec{n} = -\sigma_{muscle}\nabla\varphi_{(r)}\Big|_{\partial G_{muscle}} \cdot \vec{n}$$

(3) $$\sigma_{skin}\nabla\varphi_{(r)} = 0$$

(4) $$\sigma\nabla\varphi \cdot \vec{n} = 0$$

(5) φ = constant for electrodes

In order to ensure electrodes were placed at the same location on each amputee, a 10cm intermedullary device was simulated as the osseointegrated implant and set to the endosteal wall, since gaps in excess of 50 μm may lead to fibrous encapsulation without bone ingrowth.[181] External electrodes were designed with multiple configurations to assess which style produced the most homogenous electric metric distribution. Anodes consisted of a one patch electrode, two patch electrodes, one continuous band and two continuous bands (Figure 14). Electrode patches were placed as a strip covering approximately half the diameter of the residual limb and were 3 cm in thickness. Electrode bands were placed equidistant from the intramedullary implant and were 1.6 cm in thickness to replicate the size of commercially available capacitive stimulation devices.[182] Electrodes incorporated in the finite element meshing were assigned a constant potential difference from 1.0 to 2.0 volts, in ¼ volt increments, a predetermined range selected to ensure tissue integrity based on the expected tissue conductivities.

Elements in the model were treated as piecewise, homogenous, ohmic and isotropic, and were assigned conductivities using measurements reported from

physiologic tissues (Table 4). FEA was conducted using a quasi-static approach and by solving Laplace's equation for each tissue type (Equation 6).[46]

$$\nabla \cdot \sigma \nabla \varphi = 0 \quad (6)$$

3.2.3 Mesh Sensitivity Study

The models generated from retrospective CTs consisted of a hexahedral mesh with approximately 1.8 million elements, a quantity determined to be sufficient following a mesh sensitivity study for subject 1's residual limb which verified a less than 5% relative difference in voltage gradients between mesh densities (Table 5). While a 10% relative difference is usually acceptable for finite element bioelectricity problems (personal communication, Dr. Jeoren Stinstra), it was decided to maintain less than 5% in order to improve model accuracy.

3.2.4 Outcome Criteria

The overall outcome measure of "optimal potential difference" was satisfied when the current density and electric fields were at their highest attainable value within the following predetermined measures: Electric fields were restricted between 1-10 V/cm to prevent joule heating effects,[131] while current densities were limited to 1.8 mA/cm^2 to prevent localized tissue necrosis. The current density threshold was preset to 1.8 mA/cm^2 to adhere to International Electrotechnical Commissions' regulations that 2 mA/cm^2 should not be exceeded in electrical devices designed for the general population.[168] Maintaining a value below the standard of practice was also important in providing a

factor of safety since fluctuations may occur *in vivo* due to variations in ion concentrations, temperature and hydration, and variables which were not accounted for with this finite element model.

3.3 Results

Interactive placement of electrodes allowed for various computational simulations. Figure 15 illustrates one example of the differences between patients using a one band configuration. As demonstrated in the image, electric field and current density distributions varied considerably based on the occurence of the myodesis technique (artificial vs. actually amputees), residual limb geometry and the volume of the tissue types within the residual limb. Histograms generated from the FEA approximations demonstrated a wide range in skewness and kurtosis of the electric metrics despite uniform external electrode placement.

The influence of the residual limb geometry was most clearly demonstrated when comparing the four electrode types and the amputee's residual limb (Figure 16). As demonstrated in Figure 16, Patients 1 and 2 (artificial amputees), required a 100% increase in voltage in the electrical stimulation device over that of Patients 3 and 4 (trauma-induced limb loss) to satisfy the outcome criteria of an electric field between 1-10 V/cm and current density less than 1.8 mA/cm^2. Comparisons between electrode types indicated a general trend that the 2 band electrode required the lowest potential difference for the electrical system, while the 2 patch configuration required the highest potential difference (Figure 16). Because the 2 band electrode was positioned uniformly around the exterior of the residual limb and had the highest amount of conductive medium, this

electrode type also produced the most uniform electric field distributions at the simulated bone-implant interface.

3.4 Discussion

The necessity for patient-specific models using electrically induced TOI was confirmed in the study. The distribution of the electrical field at the implant-bone interface varied between subjects due to differences in anatomy and the presence of an amputation. While creating “artificial amputees” using a segmentation program was straightforward and permitted robust computations, histograms of electric field and current density magnitudes confirmed that the electrical metrics changed dramatically when compared to an amputee with trauma-related limb loss (Figures 15 and 16). The results clearly demonstrated that the 1 patch electrode generated the smallest electric field at the bone-implant interface, while the 2 band electrode configuration generated the highest field for the same applied potential. This would suggest that proper electrode placement may improve efficacy, but a 2 band configuration appears optimal as it requires the lowest voltage for the highest field strength.

Due to the limited quantity of patients in the study, statistical evaluation of patient demographics and potential differences was not feasible. However, the highest voltage gradients mapped during simulations consistently occurred in Subject 2, a patient who was in the best physical condition. The increased electrical field may have been associated with the reduction in the diameter and thickness of adipose tissue in the subject’s residual limb, since adipose tissue would raise resistivity and impede current

pathways. Minor adjustments may be necessary in the future to account for the varying anatomy of patients and spatial location of topically applied electrodes.

In order for electrically induced TOI to remain feasible, a balance must be maintained between obtaining the highest electric field (between 1-10 V/cm) while minimzing the host tissue response which may occur with metal implants. Titanium alloy was selected as the cathode in this model ($3x10^6$ S/m), since it has been regarded as one of the most biocompatible material types for total joint replacements, and has low thermal conductivity to protect tissue necrosis from heat generation.[183-185] However, if clinicians and engineers require an altered rate of electrical flow, then it would be possible to alter the material and/or the porosity, but careful attention must be paid to ensure the material does not illicit a foreign body response from electrolysis.

3.5 Conclusion

The simulations developed for electrically induced TOI may have the capabilities of expediting skeletal attachment by increasing osteoblast migration. Computation modeling has effectively shown that 1-10 V/cm electric fields may be generated using the implant as a functional cathode and topically applied anode band and patches. Using three-dimensional computer simulations may be the first step to resolving the classic problem with electrical stimulation which has been the inability to define current pathways in the human body.[99,186]

Patient-specific modeling in this study was also effective for attaining values that may be osteogenic at the implant site, but wide variations in electric field and current density distributions shown with generated histograms reaffirm the need to evaluate each

case specifically. FEA approximations from this model indicated that electrically induced TOI may be a viable option for accelerating skeletal attachment, but would require a higher sample size and larger hierarchical models for model confirmation prior to implementing this novel design principle.

Table 3: Demographical information for the patients included in the IRB approved study.

Patient	Gender	Age [yrs]	Height [cm]	Weight [kg]
1	M	60	185.4	79.9
2	F	28	157.5	50.1
3	F	80	152.4	45.5
4	M	68	160.0	56.9

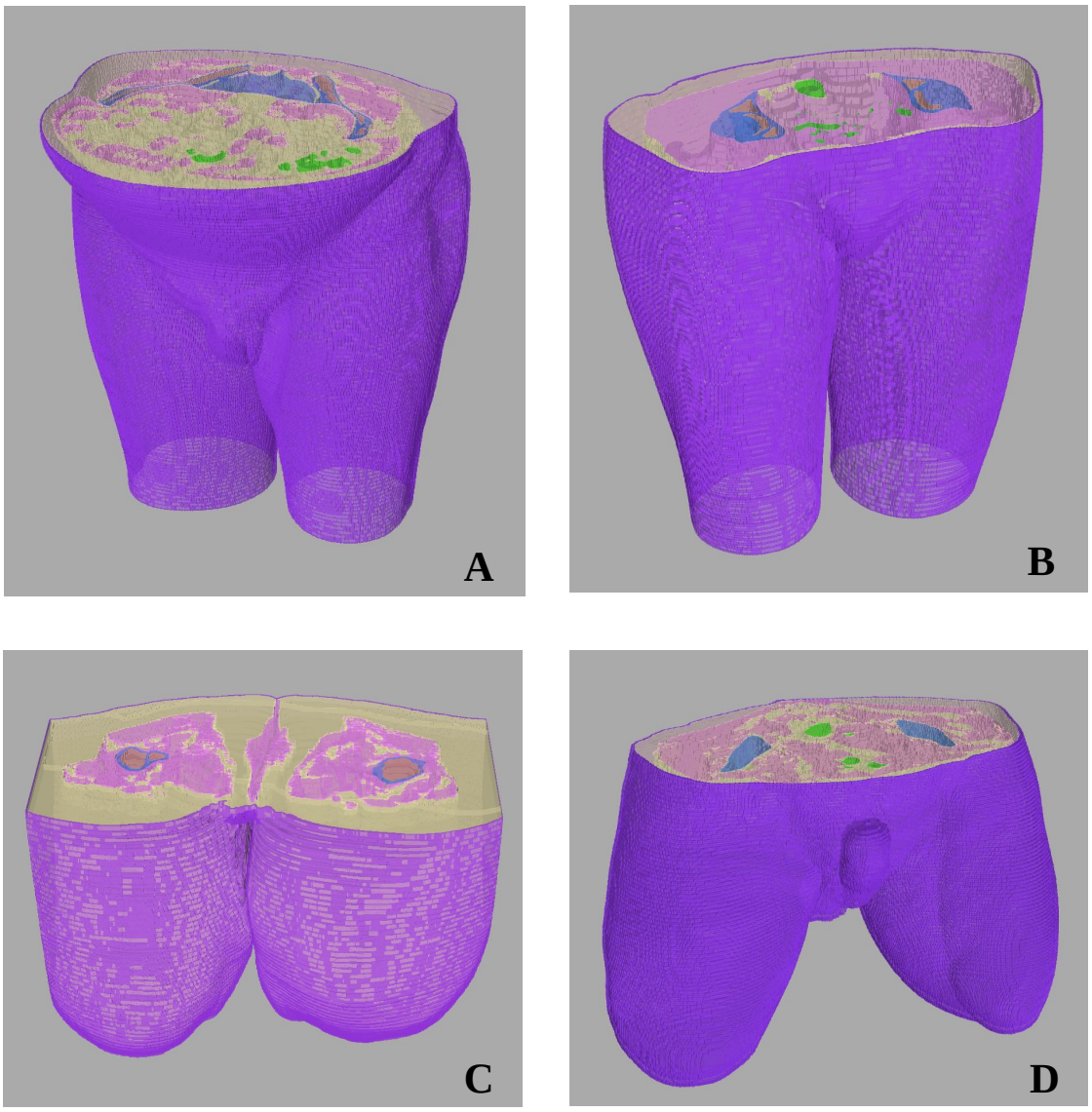

Figure 9: Reconstructions of the four amputees selected for preliminary bioelectric evaluation. Patients 1 (A) and 2 (B) were the simulated amputees without a distal residual limb while Patients 3 (C) and 4 (D) were amputees who sustained trauma-related limb loss.

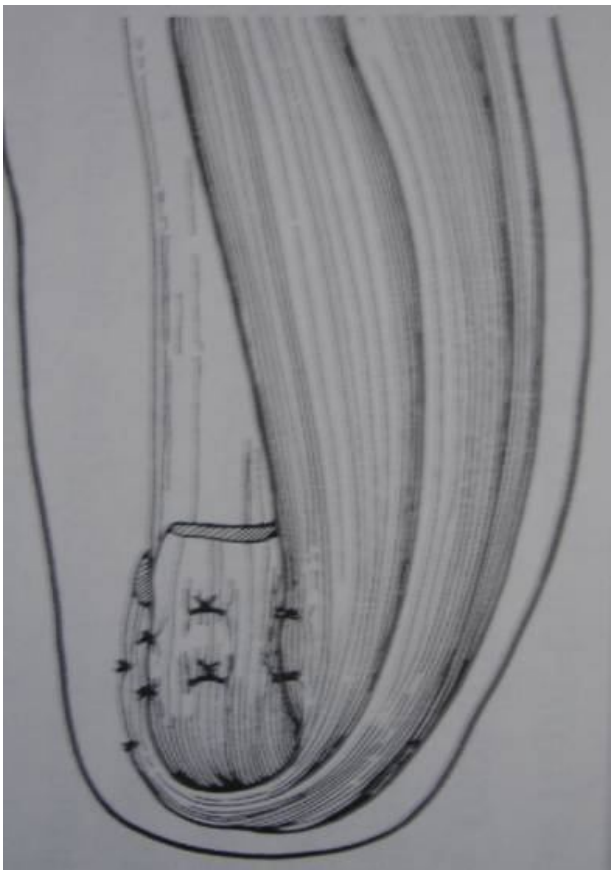

Figure 10: Representative image of the myodesis technique used for musculature reattachment during residual limb reconstruction. Because the sample population for this study used 2 simulated amputees, it is important to note that Patients 1 and 2 did not undergo this surgical procedure.

Figure 11: A sagittal cross section of an amputees' residual limb thresholded into specific tissue types. In this diagram, the bone, muscle, adipose tissue and skin are readily distinguishable, as well as a small quantity of abnormal bone growth, termed heterotopic ossification (HO) distally.

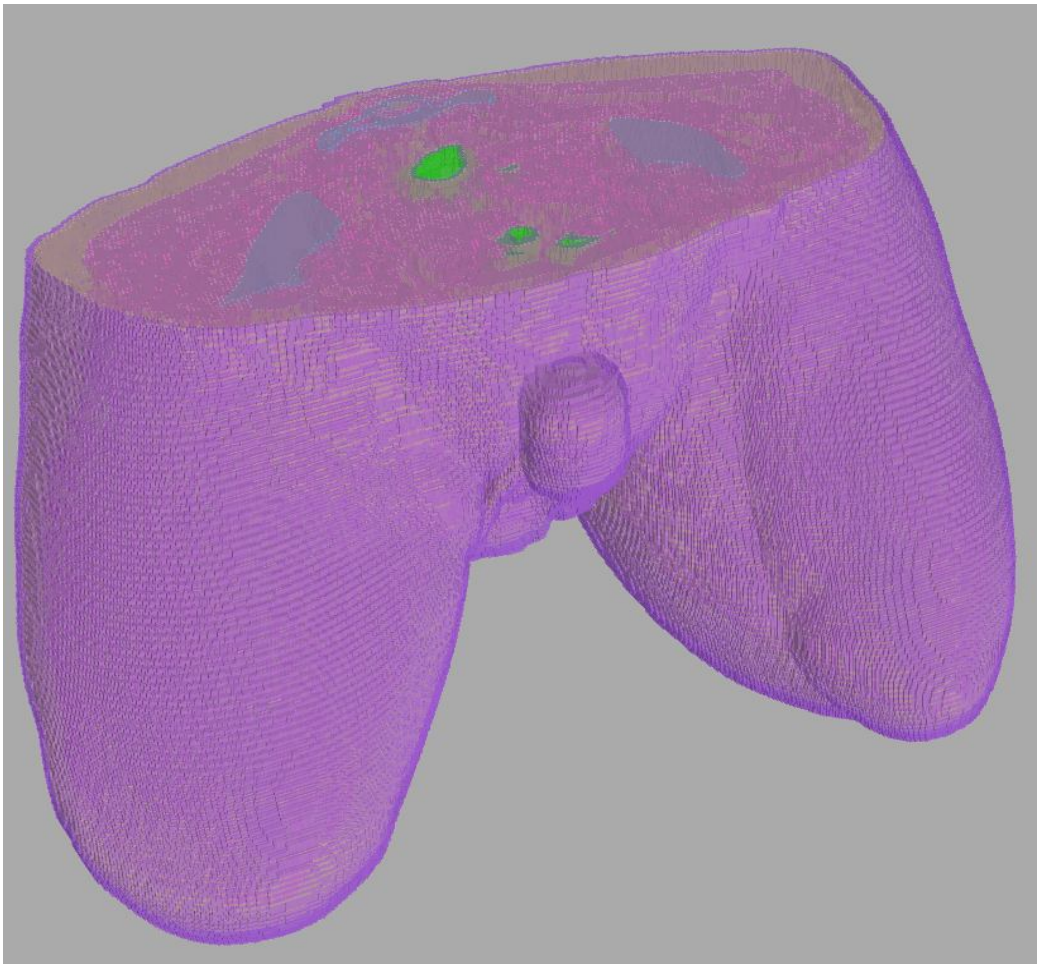

Figure 12: A unilateral hierarchical model was assembled as a representative image consisting of skin (purple), adipose tissue (yellow), musculature (pink), bone (blue), bone marrow (orange) and internal organs (green). Each tissue type was assigned a specific conductivity using the SCIRun software package.

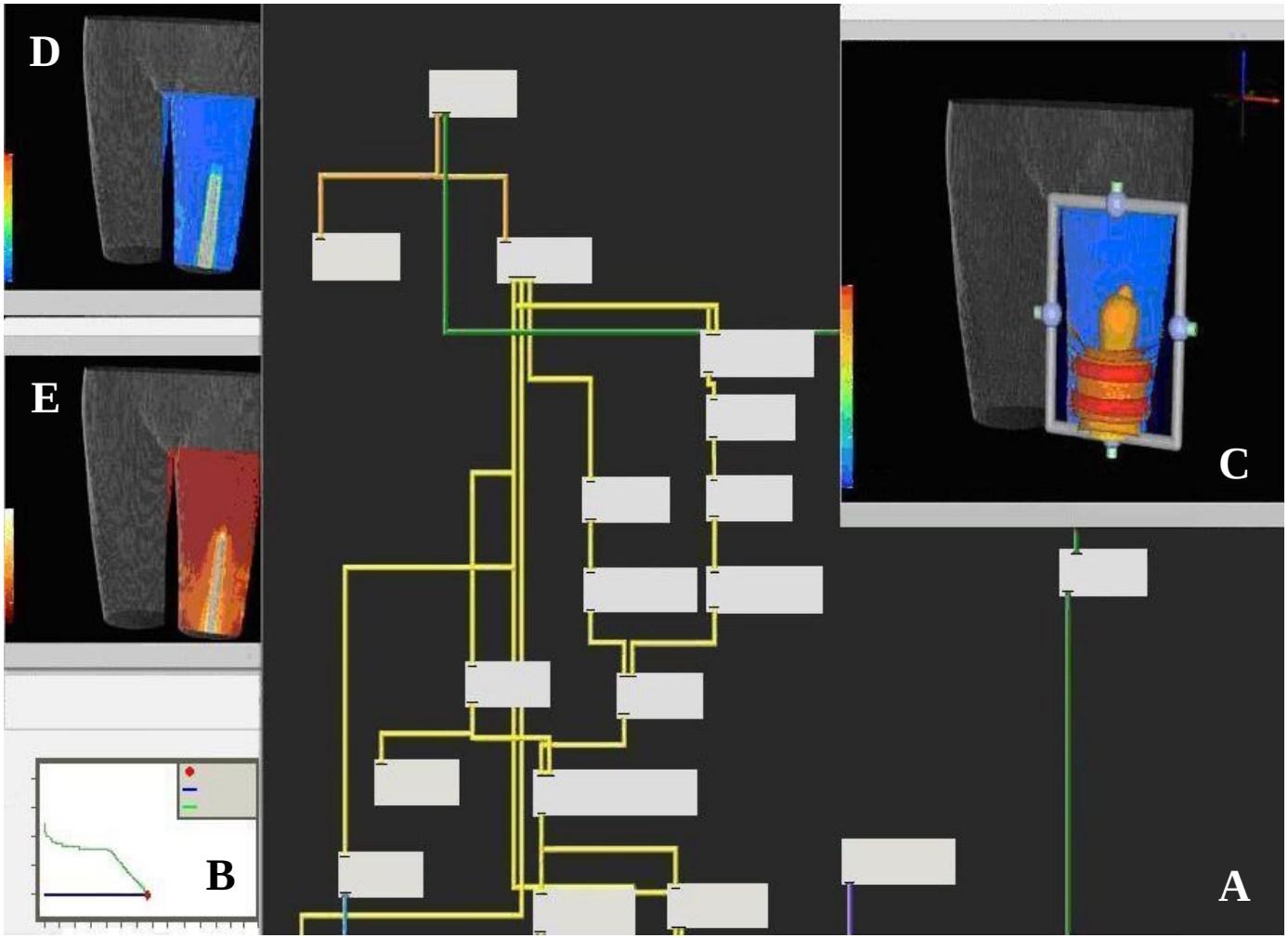

Figure 13: Representative image of a partial network used for inserting model boundary conditions (A), performing iterative solving (B), design electrodes (C) and calculating the electric field (D) and current density (E) at the bone-implant interface.

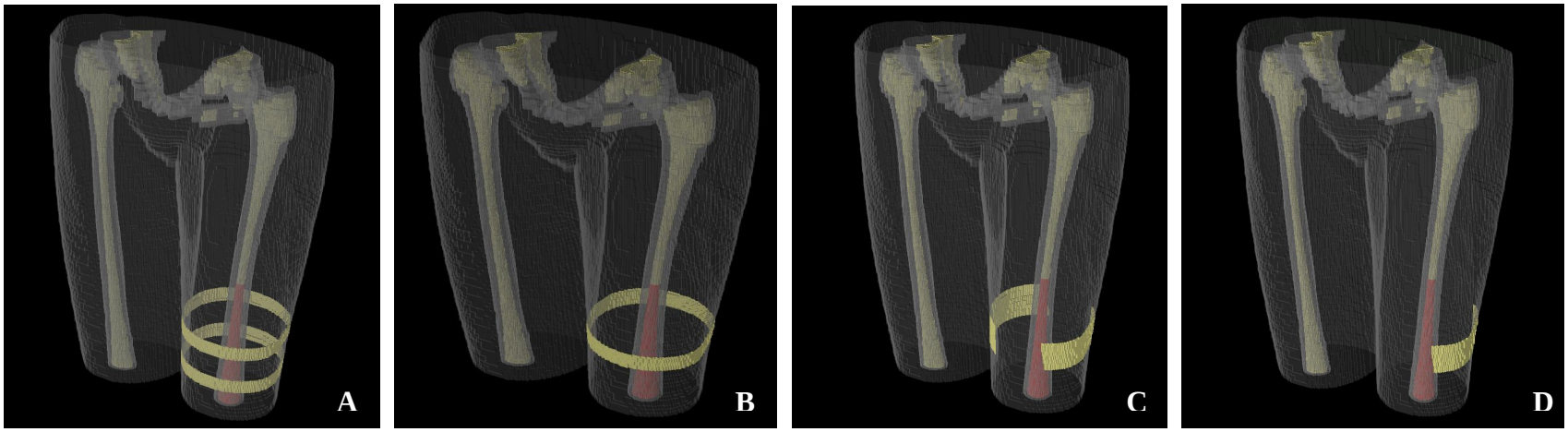

Figure 14: Schematic overview of the four electrode designs developed for investigating the utility of electrically induced osseointegration. The potential anode configurations consisted of two bands (A), 1 band (B), two patches (C), and 1 patch (D).

Table 4: Conductivities assigned to the segmented tissues used for FEA in SCIRun.

Tissue Type	Conductivities [S/m]
Organ	0.22
Skin	0.26
Adipose	0.09
Muscle	0.25
Cortical Bone	0.02
Bone Marrow	0.07

Table 5: Sensitivity study used to determine the appropriate mesh density prior to conducting FEA.

Mesh	Elements	Nodes	Relative Difference
100 100 050	149089	161131	0.0995
125 125 075	350180	371472	0.0802
150 150 100	673032	706082	0.0545
175 175 125	1146778	1194044	0.0527
200 200 150	1796690	1860772	0.0439
250 250 200	3745038	3850202	0.0364
275 275 225	5097243	5226587	0.0301
300 300 250	6742588	6898729	0.0000

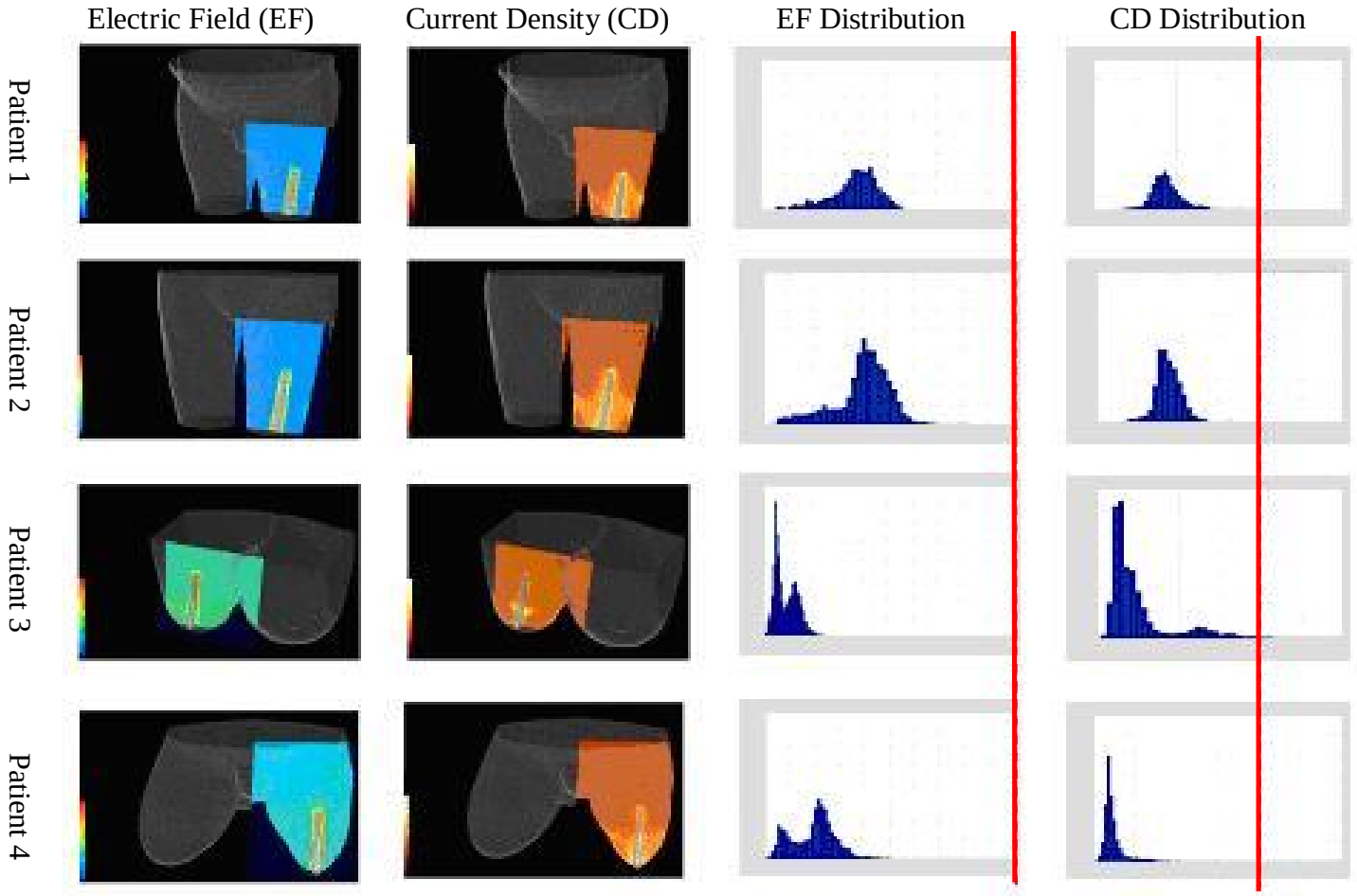

Figure 15: This figure demonstrates one example of the FEA performed in the study. The color map reflects the strength of the electric field in the lower part of the limb. The corresponding histograms (right) represent the electric field and current density strengths of the 6,000 elements surrounding the implant site and the homogeneity of the field. Note that histograms demonstrated a broad variation among patients despite using the same 1 band electrode configuration.

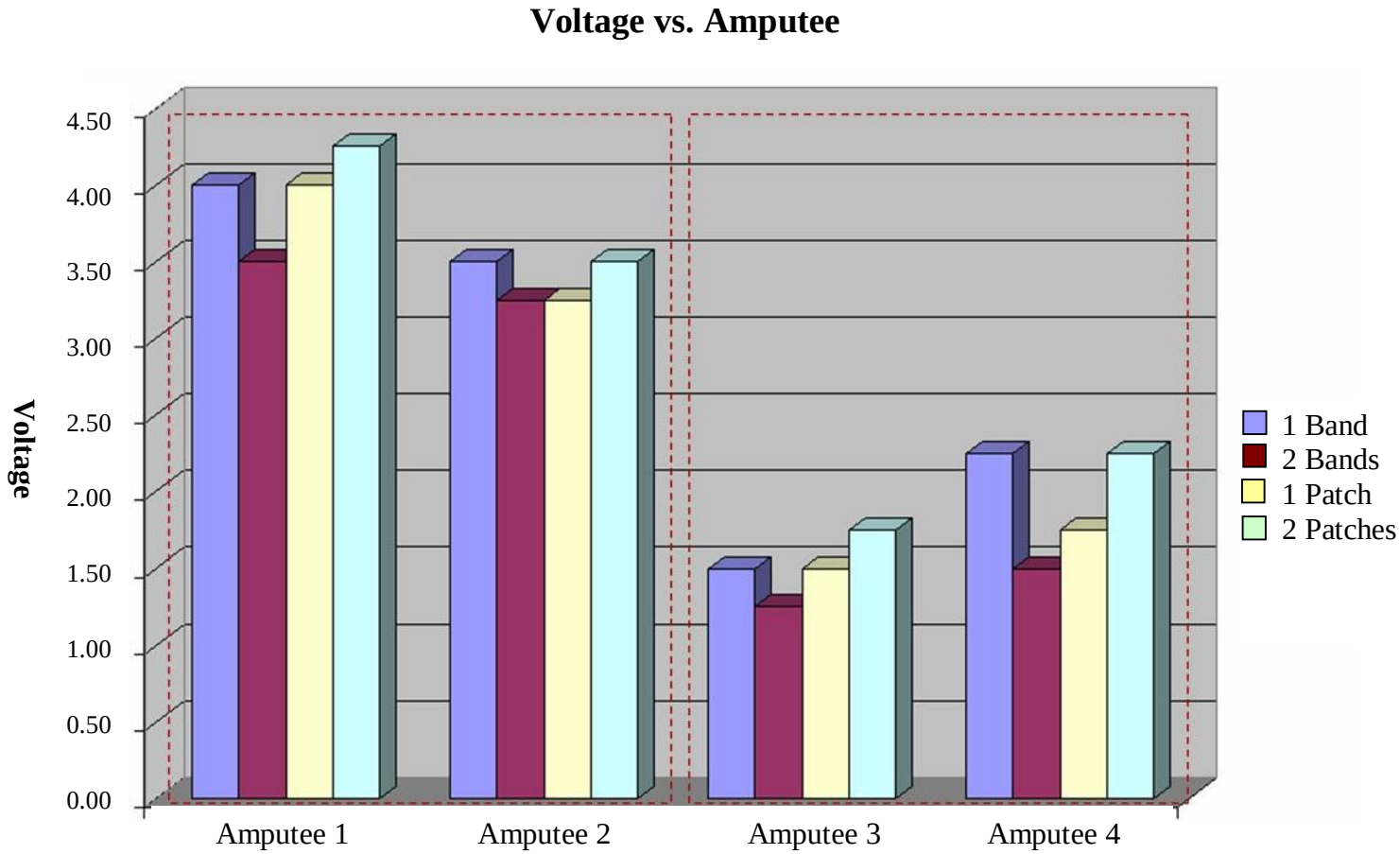

Figure 16: Comparison between the 4 included patients and electrode configurations. These results confirm the requirement for individual patient modeling as the potential difference depends on the ptand electrical setup. Distributions of electric fields were not homogenous in each case and may require manipulation of the applied voltage to attain theoretical uniform bone ingrowth in the future.

CHAPTER 4

VOLUME CONDUCTOR MODELS WITH HETEROTOPIC OSSIFICATION FOR ASSESSING THE INFLUENCE OF ECTOPIC BONE GROWTH ON BIOELECTRICITY

4.1 Introduction

Improving skeletal fixation of osseointegrated implants with controlled electrical stimulation may accelerate rehabilitation protocols for individuals with limb deficiencies. However, before employing this technique in human subjects, extensive scientific experimentation must be conducted to better understand the bioelectric properties and pathways through human residual limbs. Results from Chapter 3 demonstrated the potential of computer simulations for predicting electric fields and current density magnitudes in the distal residual limb of amputees. However, prior to implementing electrical stimulation as a rehabilitation tool for service members with limb loss and a TOI, safety and efficacy must be evaluated with a larger patient population, especially given the variations that exist in residual limb volume, geometry and factors such as heterotopic ossification (HO).

HO has been reported as "bizarre overgrowth" of mature bone in the neighboring soft tissue[187] and was evident in the first patient series investigated in Chapter 3 (Figure 11). This lamellar bone formation[152] has been reported as metabolically active,[188] variable in nature[188] and "serpentine-like" (connecting to the periosteum).[189] Reports of HO have been replete in the orthopedic literature and known to occur predominately in periarticular regions following total hip arthoplasty,[188,190] head injury,[191] spinal cord injury,[192,193] rotator cuff surgery[194] and burns.[195] While the etiology of HO has not been fully understood,[190] there has been a general agreement in the literature that HO is associated with damage to soft tissue and inflammation,[190,196] and is most pronounced in combat-related trauma to service members following blast injuries.[2]

The frequency of HO from improvised explosive devices (IED) and rocket propelled grenades (RPG) in OIF and OEF have been reported as high as 63% in the wounded service members.[187] Because HO may manifest months after a blast injury and has a maturation rate upwards of 18 months,[191,197] problems may arise with poor prosthetic fit for those requiring assistive ambulatory devices.[198] An improper interface between the residual limb and prosthetic socket may also lead to skin breakdown[26] and significantly limit the mobility of individuals with limb loss,[2,199] particularly injured servicemen and women who wish to return to active duty or an energetic lifestyle.[2,27]

The variability of HO formations in subjects with combat-related limb loss may alter the electric field and current density distributions at the bone-implant construct for those with electrically induced TOI. As noted previously, the anatomy and geometry of residual limbs has been known to affect the potential difference during FEA and HO inclusion and may provide future insight into the need for patient-specific modeling in a

representative patient population prior to clinical implementation of these design principles. Therefore, the goals of Chapter 4 were (1) to demonstrate that safe and effective electric stimulation of osseointegrated implants was possible even in patients with significant HO, (2) to show that patient-specific modeling and simulation was necessary to determine the relevant metrics for such stimulation, (3) to develop a quantitative method for determining the volume of HO and (4) to characterize the prevalence, the extent and the structure of HO in returning service members.

4.2 Materials and Methods

4.2.1 Study Population

In order to account for variations in patient anatomy and HO in service member's residual limbs, CT scans were obtained retrospectively from Walter Reed Army Medical Center in accordance with IRB approval. CT scans were selected as the preferred imaging modality and femoral slice thicknesses ranged from 1.0 to 2.5 mm for all subjects included in the study. Inclusion criteria required the absence of metallic implants or high aggregations of shrapnel in the residual limb to prevent image artifacts during three-dimensional reconstructions.

Eleven male service members satisfied the above criteria and were included in the study. Subjects were on average 28.3 ± 5.0 years at the time of injury, and 84.5 ± 11.3 kg and 181.2 ± 4.4 cm prior to injury. While age was routinely recorded for each subject, weight and height were reported in only 10/11 and 6/11 of the patient's medical records, respectively. The study population consisted of transfemoral amputations with an average limb length of 26.7 ± 6.1 cm, as measured from the apex of the greater trochantor to the

most distal bone in the residual limb using CT scans and computer software (OsiriX 3D, version 3.1). Ten (91%) subjects included in this study sustained a limb amputation as a result of a combat-related injury (9/11 OIF, 1/11 OEF), while one subject sustained a limb loss from a nonmilitary incident. The injury mechanism most frequently reported was IEDs, which resulted in 82% of traumatic amputations (9/11), while 9% were the direct result of an RPG (1/11), and a motor vehicle accident (1/11) (Table 6).

4.2.2 Image Reconstructions

Anatomically accurate reconstructions were created using the protocol developed by Isaacson et al.[46] and described previously in Chapter 3. In short, retrospective CT scans were imported into Seg3D as dicom images and thresholded into the specific tissue types (Figure 17). Six-layer hierarchical models were developed and consisted of internal organs, adipose tissue, bone, bone marrow, musculature and skin. However, for patients who experienced ectopic bone growth, additional inspection and manual thresholding were necessary to ensure that all HO sections were included in the data set. As mentioned previously, HO has been known to manifest itself as bony islands or connected in a serpentine-like structure to the periosteum,[189] and therefore, each axial cross section was carefully inspected to ensure all HO was included in the datasets.

4.2.2.1 Determining the Volume of HO Within the Residual Limb

The bioelectric effect of HO was evaluated by computing the volume of ectopic osseous overgrowth throughout the residual limb. Axial cross sections of CT scans were

manually inspected and all "small islands"[188] and "serpentine"[189] HO formations were included (Figure 18). The entire volumetric data was collected using customized software that multiplied voxel height and width by the slice thickness to determine the volume of HO (Analyze 9.0, Mayo Clinic, OH). Three-dimensional reconstructions were created in OsiriX 3D to visualize the HO and were necessary to fully understand the intricate morphology of heterotopic bone[189] (Figures 19-22).

4.2.3 Finite Element Analysis

FEA was performed using the protocol developed by Isaacson et al.[46] and described previously in Chapter 3. In short, 6-layer hierarchical models of amputee residual limbs were used to generate the meshes for FEA. The TOI was positioned against the endosteal wall of the reconstructed residual limb and two electrical bands were positioned 2 cm from the most distal and proximal aspects of the implant (Figure 23). The 2 band electrical configuration was selected since it had previously demonstrated that it could produce the most uniform electrical metric distribution it and also required the lowest voltage input for safe and effective electrically induced TOI (Chapter 3).

4.2.4 Statistical Evaluation

The volume of HO in each service members' residual limb was compared to the optimal potential difference to determine if ectopic bone growth correlated with the electric field and current density at the bone-implant interface. HO formation was also

independently assessed to determine if demographical information (age, height, weight, residual limb length) correlated with the volume of HO since inconsistencies have been presented in the orthopedic literature.[193,196] All statistical evaluations were performed by computing Spearman's rho correlation coefficients and nonparametric statistical evaluations given the limited sample size. In addition, to accurately associate the predictor and outcome measures, without introducing overfitting or having confounding variables, each factor was correlated independently. All statistical comparisons were conducted with commercially available software and $\alpha = 0.05$ (SPSS, Inc., Chicago, IL, USA).

4.3 Results

For all of the reported cases, voltage gradients at the bone-implant interface were within the required range and therefore, the limiting factor for selecting the optimal potential difference was based on current density magnitudes (Figure 24). Electric fields fluctuated from 1.30-3.10 V/cm for all patients, a value which should theoretically induce osteoblast migration *in vivo*[84] (Table 7). However, current densities ranged from 0.66-2.63 mA/cm^2 for the potential differences selected, and confirmed that individual adjustments would be necessary if this technology were to be implemented clinically, as some current densities exceeded the recommended threshold (Figure 25, Table 8).

Investigation of the current densities at the periprosthetic interface demonstrated lower magnitudes occurred when the volume of HO increased (Figure 25). For the potential differences selected in Subjects 2, 3 and 11, current densities remained below the 1.8 mA/cm^2 threshold. In each of these cases, a dense aggregation of HO was located

at the anode site and resulted in more resistive medium at the point of current injection. This trend was consistent throughout the study and results of a Spearman's rho correlation coefficient, assessing the relationship between the volume of HO and the optimal potential difference, were statistically significant ($p=0.024$, $r=0.670$).

The volume of HO was also compared to demographic information provided in the subjects' medical records to determine if correlations existed between patient history and HO. While the orthopaedic literature has speculated that the frequency of HO may be dependent on genetic predispositions[196] and body type, there has been little evidence to directly support these claims. The results from this study have indicated that only age was statistically significant ($p=0.041$, $r=-0.622$) and that the volume of HO decreased with increasing age.

4.4 Discussion

Ectopic bone formation presents a difficult challenge for rehabilitation and post-amputation quality of life. While HO can be detected early as indicated by redness, swelling in the periarticular regions and increased alkaline phosphotase levels,[200] few treatments are available to quell the metabolically active osseous growth.[196] Non-steroidal anti-inflammatory drugs and irradiation treatments have been available,[194] but present additional health risks to the patient. Compounding this problem has been that the presence of significant HO within a residual limb may prohibit the use of a prosthesis. Therefore, electrically induced osseointegration offers a potential alternative to traditional prosthetic socket fitting, may promote bone remodeling and avoid frequent complications with HO. It should be noted that it would be highly unlikely that electrically induced

osseointegration would increase HO formation in the residual limb, since HO develops from inflammation and trauma,[190,196] and is not solely dependent on electrical signals. While electrical stimulation has demonstrated success in healing nonunions,[160] there has been no mention in the peer-reviewed literature of generating HO from electrically induced fracture healing applications with direct current, inductive coupling or capacitive coupled devices.

In this experiment, FEA demonstrated that HO will significantly affect the bioelectricity in the residual limb, since larger volumes of HO required a higher potential difference to satisfy the electric field and current density criterion needed to theoretically accelerate bone healing using simulations. Therefore, effective use of electrical stimulation in this patient population would require altering the voltage in the system or modifying the band placements slightly to avoid resistive HO medium on a personal basis. The only exception noted in this trend was with service member 9 who had a smaller residual limb size, and a reduction in soft tissue may have offset the resistive effect of HO. While the admission height for this patient was not available for retrospective review, service member 9 was 11.5 kg below the average weight of the other subjects in the study and may have also had associated decreased muscle mass or adipose tissue.

When assessing the correlation between age and HO frequency, our results indicated that higher volumes of HO were most prevalent in younger subjects. The inconsistent reporting of age-related ectopic bone formation has been subject to debate in the orthopedic literature[193,201] and a discrepancy still exists since HO studies are often small, unrandomized and lack control groups.[202] A contributing factor in age-related HO may be the result of the decreasing proliferation of stem cells and progenitor cells which

occurs naturally with age[203] since "skeletal tissue is a complex, multicellular, multifunctional system mutually interactive with and dependent on all other organ systems."[204] Evidence of the decline in stem cell regeneration has been a well known phenomenon in older individuals in which the cavities of long bones become vacant and bone marrow resides only in the pelvis, sternum and vertebrae.[133] The decreased bone forming capacity of aged osteoblasts and reduced cell population with age[204] may limit the likelihood of developing HO, but was not likely the case in our study. Because the patient population in this study consisted of a small sample of relatively young service members (28 ± 5.0 years), age was not likely to be a causative factor for HO formation. The statistical trend reported in the study was most likely the result of comorbidities, which have been highly prevalent with blast injuries[5] and may have contributed to the HO formation. In fact, previous peer reviewed publications have demonstrated that the likelihood of developing HO significantly increased with head and spinal cord injuries, variables which were not assessed in the study. To confirm the hypothesis of age-related HO, a study must be organized with a more uniform patient population and a wider age range distribution to prevent confounding variables.

4.4.1 Innovation

In this sample population of injured service members, the frequency of HO occurred in 73% of the cases (8/11) and was variable in severity and location. The formation of HO resulted in "serpentine"[189] structures which connected to the skeleton and "small islands"[188] in the neighboring soft tissue. To help categorize the HO in a non-subjective manner, thresholding software provided volumetric measurements which

assisted in determining the extent of HO in each person's residual limb. To the authors' knowledge, this was the first grading criteria to directly quantify the volume of HO in patient extremities. Traditional methods for determining the magnitude of HO have included measuring the length of HO on anteroposterior radiographs,[205] developing grading scales to group HO severity based on a percentage of occupied space around the affected area[190] or designing studies which subjectively include patients only displaying signs of decreased motion or pain.[206] These techniques have been very limited because only three-dimensional reconstructions or direct volume measurements have the ability to completely demonstrate the intricate morphology of HO.[189] Additionally, grading criteria's which group HO by percentages and classifications of mild, moderate and severe[207] tend to mislead the scientific community since readers may assume that a higher value of HO (severe vs. mild) may result in more pain or impaired movement for a patient, but this may not necessarily be the case. Reduced patient activity levels have often been the result of the location of HO in relation to the periarticular region, neurovascular damage and individual patient pain tolerances.

4.4.2 Computational Modeling Limitations

Because our model used a quasi-static approach, the current density and electric fields in this experiment scaled linearly. Therefore, the direct relationship depicted in Figure 26 demonstrated that the optimal potential difference may be determined for each patient by evaluating individual trend lines derived from the FEA. The ability to use a simple algorithm may be an important tool for improving periprosthetic attachment; however, fluctuations in temperature, hydration and ion concentration will undoubtedly

affect recordings *in vivo*. While computational modeling has a broad utility, FEA in this study only served to provide initial proof of concept for future electrically induced osseointegration studies.

4.4.3 Study Limitations

While osseointegration is currently being practiced in Europe and Australia (Chapter 1), this technology has yet to be expanded in the United States and will not be available until Food and Drug Administration approval is obtained. Therefore, since our model can not be validated until osseointegration technology is accepted as a standard of practice, further investigation will require a larger sample population to better understand the effect of HO in residual limbs using these extrapolations.

Prior to use clinically, electrically induced osseointegration will also require further FEA refinements. For example, the tissue conductivities used in this experiment were fixed and treated as homogenous, ohmic and isotropic and did not vary based on anatomical location, temperature or hydration. While these basic model simplifications were effective for the testing of the proposed study aims and served as initial proof of concept for further investigations, it seems reasonable from a model perspective that interpersonal differences may have significantly affected the electric metrics at the bone-implant construct. Individual variances in tissues may arise particularly in returning service members because IED injuries generate a high quantity of scar tissue formation, and the peer-reviewed literature has indicated that the hydration of scar tissue varies from that of normal physiologic tissue, and would therefore have a different localized conductivity.[208]

Direct comparisons which have resulted from this investigation may have also been influenced by slight variations in patient anatomy. Because the service members used in this study varied in residual limb size, the percutaneous osseointegrated implant was set to the endosteal wall to ensure uniform skeletal attachment prior to FEA. While this simplification ensured model reproducibility for host bone-implant contact, it did create another variable in itself, given the fluctuations in medullary canal diameters. Because the service members used in this patient population varied in height and weight, there is reason to believe that custom-fitting the prosthetic device to the residual limb may have slightly altered the diameter of the metal cathode. While its doubtful that this decision would have introduced large variations in the data, given the much greater conductivity of the cathode than that of human tissue, a study by Mahaisavariya et al. did show that medullary canal diameters ranged from 10.3 mm at the greater trochantor to 11.8 mm in the metaphysis of 98 human cadaveric femurs (ranging from 22-83 years).[209]

One limitation of the FEA research conducted in this study was the assumption that tissue was homogenous, ohmic and isotropic. While it has been well known that bone is a highly organized anisotropic composite structure,[87] this tissue type, like the other five reconstructed in this experiment (bone marrow, adipose tissue, musculature, internal organs and skin), were modeled with constant tissue properties to reduce experimental variations. Future model validations will be useful for determining the influence of assuming tissue fiber directions, since tissue conductivity has been known to fluctuate in the same tissue or organ due to changes in orientation.[174] Bone, for example, has been reported as 100% more resistive in the circumferential direction compared to longitudinal direction[98] and may impact model accuracy.

A final limitation of our study design resulted from using a sample population that consisted of only servicemen. Because female subjects who had retrospective lower extremity CTs did not satisfied the preexisting criterion (the absence of metallic implants or high aggregations of shrapnel in the residual limb to prevent image artifacts during three-dimensional reconstructions), this investigation was unable to evaluate the effect of gender as a causation for HO development; which has been an area of frequent debate in the orthopaedic literature.[188,193,201] While it is not possible to comment on current data at this moment, it is very unlikely that HO formation is gender-specific and would more likely attributed to the size of the residual limbs. In general, males tend to have an increased volume of muscle and since osteoblast progenitor cells reside in the neighboring soft tissue,[196,210] a greater volume of muscle mass may increase the likelihood of HO formation. Previous studies have indicated that HO formation generally occur in tissues with high aggregations of fibroblasts[188] and between 3 weeks to 6 months after injury.[200,211] This commonality may be the result of over-expression of bone morphogenetic proteins,[210] which may directly increase alkaline phosphotase levels[212] and contribute to HO development.

4.5 Conclusion

Osseointegration may offer significant improvements in prosthetic management of individuals with limb loss, especially those with complex residual limbs with HO and subsequent difficulty with socket fit and comfort. Controlled electrical stimulation may accelerate rehabilitation programs for osseointegrated implants once safety and efficacy has been verified clinically, but research has presently shown that current density must be

controlled in the distal residual limb on a patient-specific basis using FEA. Statistical evaluations in this model demonstrated that the volume of HO compared to age and volume of HO compared to the optimal potential difference were significant. Therefore, if electrical stimulation were to be used in the future for individuals with transcutaneous osseointegrated implants, electrode placement must be carefully based on the volume of HO, age of the patient population and comorbidities from blast injuries.

Table 6: Demographical information of the service members included in this sample population.

Patient	Age [yrs]	Injury Mechanism	Event	Admission Height [cm]	Admission Weight [kg]	Length of Available Bone [cm]	Volume of HO [cm^3]
1	27	IED	OIF	175.26	90.56	28.40	47.88
2	24	IED	OIF	177.80	90.72	30.00	74.25
3	22	IED	OIF	187.96	80.00	35.10	115.96
4	32	IED	OIF	-	90.00	25.90	0.00
5	30	IED	OIF	-	-	23.30	26.53
6	39	RPG	OEF	180.34	67.92	13.00	0.00
7	24	IED	OIF	-	106.50	31.50	12.75
8	28	IED	OEF	182.88	90.00	24.40	47.78
9	23	IED	OIF	-	74.00	21.20	77.43
10	31	IED	OIF	-	73.30	29.60	0.00
11	31	MVA	NBI	182.88	81.80	30.70	261.89

* IED = improvised explosive device
* RPG = rocket propelled grenade
* NBI = nonbattle injury
* MVA = motor vehicle accident

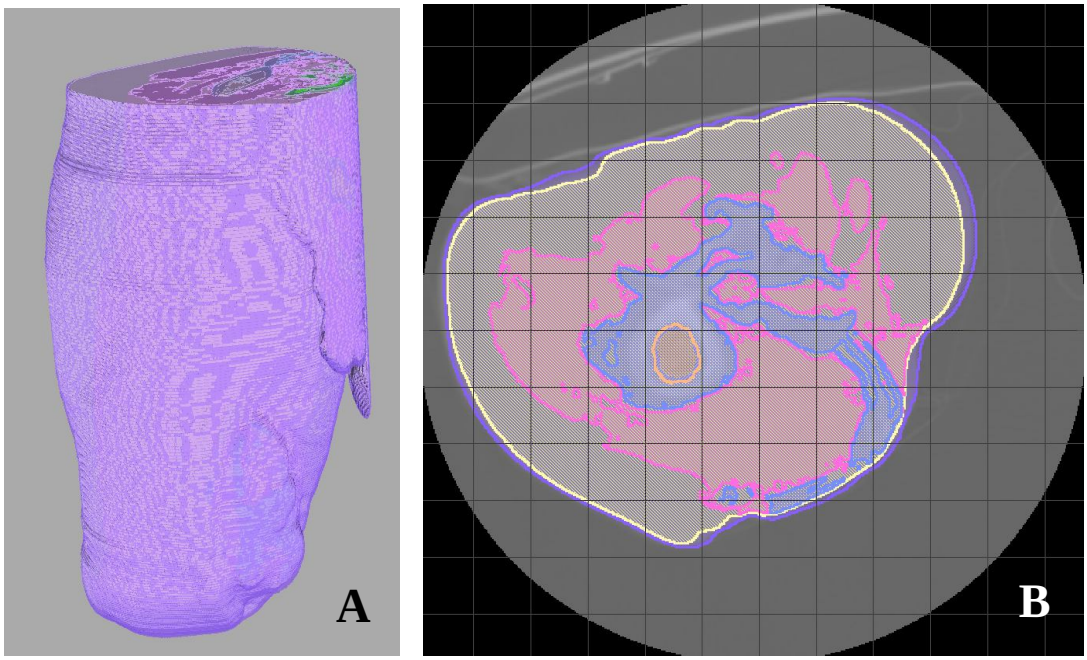

Figure 17: A unilateral hierarchical model was assembled as a representative image consisting of skin (purple), adipose tissue (yellow), musculature (pink), bone (blue), bone marrow (orange) and internal organs (green) (A). Each tissue type was assigned a specific conductivity using SCIRun. Addtionally, a large serpentine-like mass of HO was identified in the distal anterior aspect of the residual limb and was demonstrated in more detail in an axial cross section of the affected limb (B).

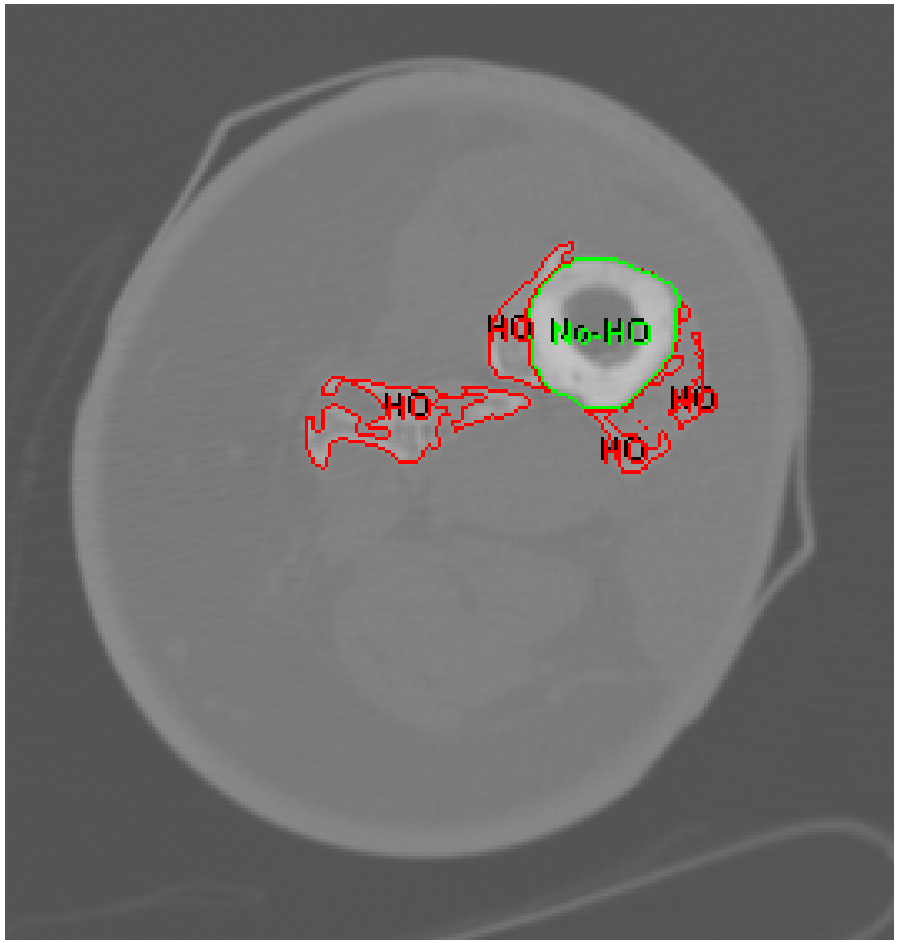

Figure 18: Representative image of the axial CT slice from an amputee's residual limb being used for volumetric assessment. In this cross section, there is clear distinction between ectopic bone growth and femur in the injured service member.

Figure 19: Representative image of a service member with no HO.

Figure 20: Representative image of a service member with 26.53 cm^3 of HO.

Figure 21: Representative image of a service member with 74.25 cm^3 of HO.

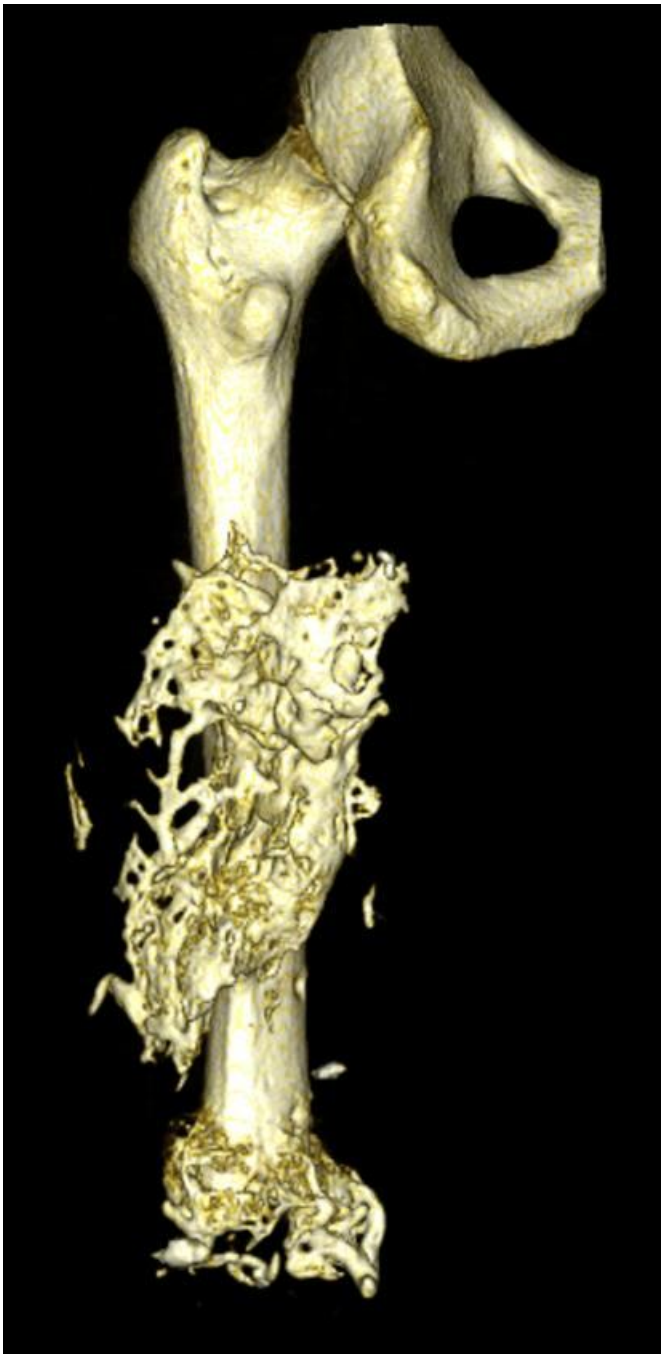

Figure 22: Representative image of a service member with 115.96 cm^3 of HO.

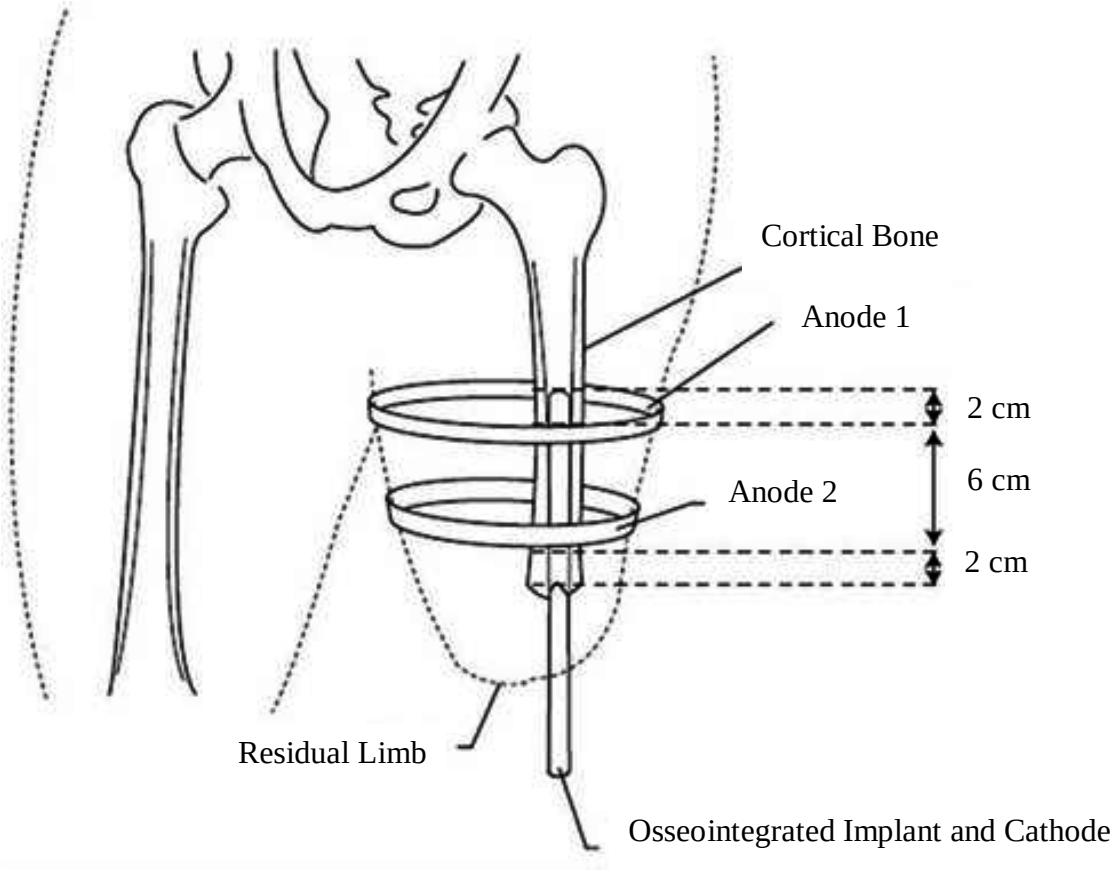

Figure 23: External electrode placement was standardized by placing 2 electrode bands 2 cm from the most distal and proximal ends of the osseointegrated implant to create a homogenous electric field at the bone-implant construct.

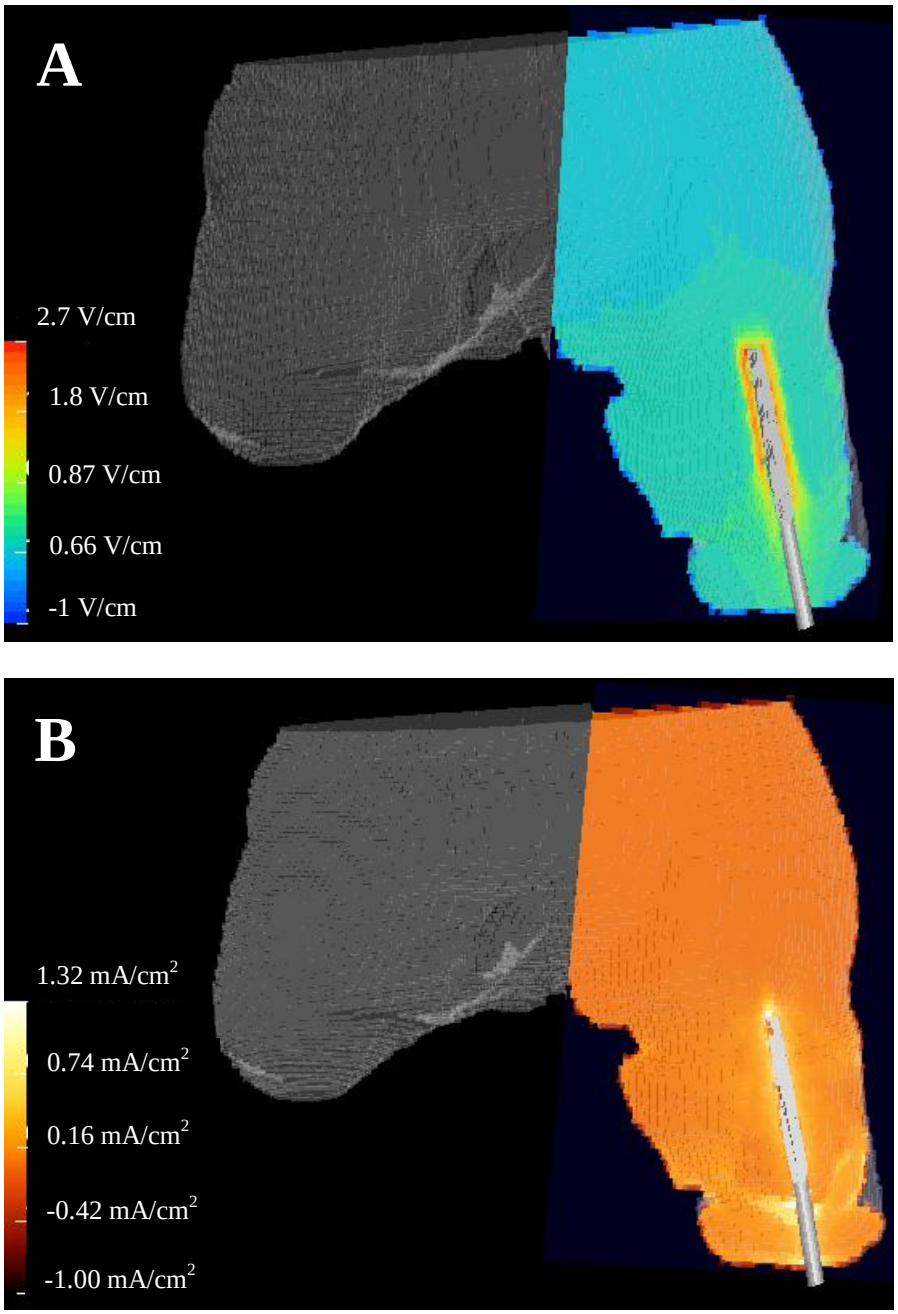

Figure 24: Electric field (A) and current density (B) distributions for service member 2 using an initial input potential of 2 volts.

Table 7: Voltage gradients at the bone implant-interface given in units of V/cm.

Patient	**Potential Difference**				
	1.00 V	**1.25 V**	**1.50 V**	**1.75 V**	**2.00 V**
1	1.3	1.6	2.0	2.3	2.6
2	1.4	1.7	2.1	2.4	2.7
3	1.4	1.7	2.1	2.4	2.8
4	1.5	1.9	2.3	2.6	3.0
5	1.5	1.9	2.3	2.7	3.1
6	1.3	1.6	1.9	2.2	2.5
7	1.4	1.7	2.1	2.4	2.8
8	1.4	1.8	2.1	2.5	2.8
9	1.4	1.7	2.1	2.4	2.8
10	1.5	1.9	2.3	2.7	3.1
11	1.4	1.7	2.1	2.4	2.7

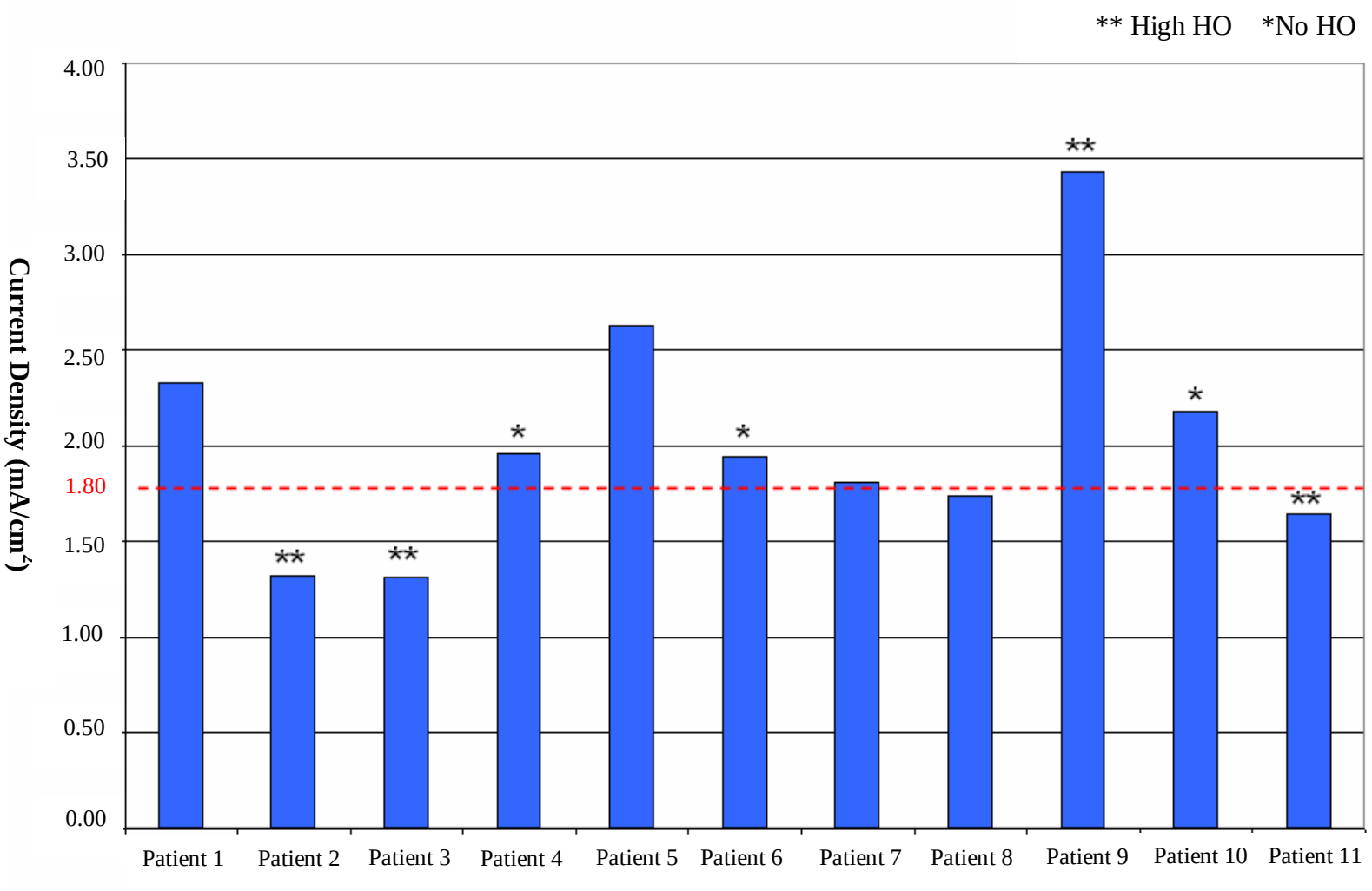

Figure 25: Current densities in the distal residual limb computed using FEA. The critical current density threshold (1.8 mA/cm^2) was selected because it was less than the required 2.0 mA/cm^2 to allow for a factor of safety (indicated by the horizontal dashed line).

Table 8: Current densities at the bone implant-interface given in units of mA/cm^2.

Patient	Potential Difference				
	1.00 V	**1.25 V**	**1.50 V**	**1.75 V**	**2.00 V**
1	1.170	1.460	1.750 *	2.040	2.330
2	0.658	0.822	0.986	1.150	1.320*
3	0.656	0.820	0.984	1.150	1.310*
4	0.980	1.220	1.470	1.710*	1.960
5	1.320	1.640*	1.970	2.300	2.630
6	0.970	1.210	1.450	1.700*	1.940
7	0.907	1.130	1.360	1.590*	1.810
8	1.010	1.260	1.520	1.770*	2.020
9	0.872	1.090	1.310	1.530	1.740*
10	1.090	1.360	1.630*	1.910	2.180
11	0.784	0.980	1.180	1.440	1.640*
* signifies the recommended threshold for current density					

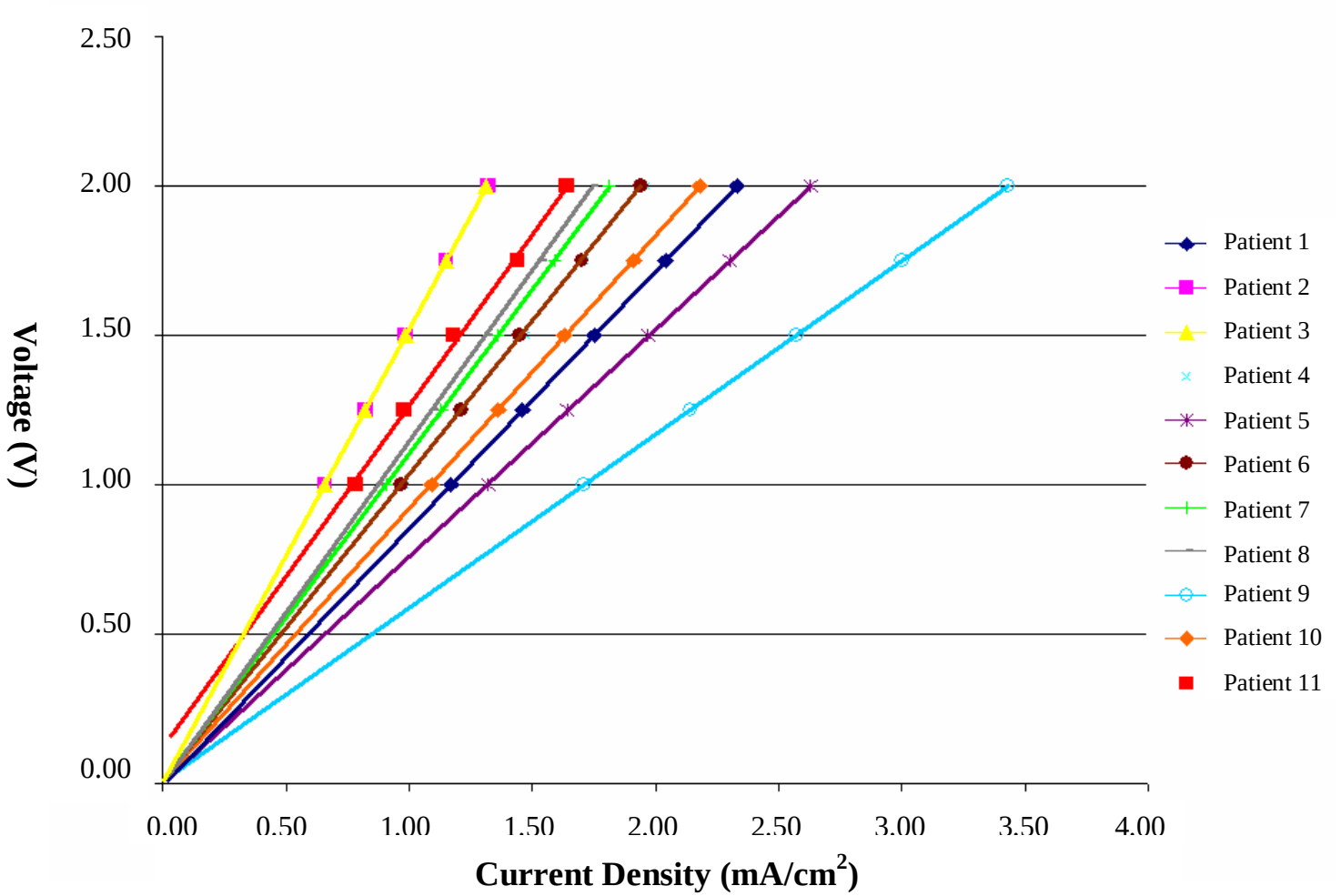

Figure 26: General trend lines for each service member selected in the study demonstrate that the optimal potential may in future be selected using an algorithm on a patient specific basis.

CHAPTER 5

IN VITRO CELL CULTURING ASSESSING THE EFFECT OF DIRECT CURRENT ON OSTEOBLASTS

5.1 Introduction

Researchers in the fields of bioelectricity and orthopaedics have generally agreed that the cell membrane is the site of prime electromagnetic field interactions,[122] but the mechanism for enhanced bone growth at the cellular level has remained largely unknown.[125] Brighton and his colleagues have provided some insight, noting that the initial event with capacitive coupling apparatuses has been Ca^{2+} ion translocation through cell-membrane voltage-gated calcium channels, whereas inductive coupling and combined electromagnetic fields have initiated with the release of Ca^{2+} from intracellular stores.[130] Regardless of the electrical stimulation modality used, fluctuations in membrane potentials have correlated with osteoblast proliferation, orientation and cellular activity.[213]

As noted in Chapter 2, the skepticism has existed with electrical stimulation largely in part from the misinterpretation of current vs. current density in the peer reviewed literature.[75] When implemented properly, electrical stimulation has the ability to

significantly improve clinical outcomes and has demonstrated success in cases where bony nonunions would not heal even with using autograph bone transfer to the defect site.[176] Therefore, to demonstrate the effectiveness of electrical simulation, and provide additional insight to the cellular response to electrical stimulation, Chapter 5 details how *in vitro* testing was necessary as a first measure to confirm safety and efficacy of using an exoprosthetic as a functional cathode prior to *in vivo* use.

The distinct advantage of culture dishes and flasks as a preliminary step for assessing electrical stimulation is that these setups can be regulated for temperature, oxygen concentration, medium concentration and provide insight for cellular adaptation in a very controlled environment.[213] However, while *in vitro* tests may be useful for determining which electric metrics may negatively impact cellular integrity, *in vitro* tests alone cannot simulate the three-dimensional bone tissues which occur *in vivo* and results from Chapter 5 should be carefully interpreted.

Successful implementation of electrically induced osseointegration required additional *ex vivo* confirmation to ensure tissue integrity prior to animal models and clinical trials in our wounded service members. The voltage selected for this experiment was based on the data collected in Chapters 3 and 4, which indicated that a 1.2 V/cm electrical field would be attainable at the periprosthetic interface. However, if a decrease in cell proliferation occurred or if cellular integrity was negatively impacted using this design principle, then further alteration to the electrical setup would be necessary prior to *in vivo* usage. The aims of Chapter 5 were to (1) examine the effect of controlled electrical stimulation on osteoblasts *in vitro,* and (2) compare the viability in unstimulated and electrically stimulated cell populations.

5.2 Materials and Methods

Determining osteoblast viability and proliferation with DC electrical stimulation was conducted using a modified cell culturing chamber adapted from *Soong et al.*[131] Plexiglas cell chambers (22.0 cm x 11.5 cm x 11.5 cm) were designed to house two 100 mL beakers with NaCl electrolytic solutions, two agar salt brides and a 100 mm Petri dish for cell growth (Figure 27). To ensure reproducibility, 5 mm holes were drilled on the top of the chamber for uniform placement of electrodes and agar bridges (Figure 28). A transfected osteoblast cell lineage (ATCC, CRL-11372, Manassas, VA, USA) was selected to reduce experimental variation since it has been well regarded that over-sub culturing may alter a cells' phenotype over time[214] and lead to false positives during data anaylsis.

Approximately 6.9 x 10^5 osteoblasts cells were placed in a 100 mm Petri dish (Greiner Bio-One, Monroe, NC, USA) and incubated for 24 hours at 37ºC and 5% CO_2 (Thermo Forma Inc., Series II Water Jacketed CO_2, Marietta, OH, USA) prior to experimentation (Figure 29). Cells were grown in a culture medium consisting of Dulbecco's Modified Eagles Medium (DMEM) (ATCC, Cat No. 30-2002, Manassas, VA, USA), 10% fetal calf serum, 5 μg/ml amphotercin B (to prevent mold/fungal contamination) and 50 mg/ml penicillin/streptomycin (to prevent bacterial colonization). Osteoblasts were portioned into 2 separate Petri dishes and used as comparisons between an unstimulated control group (Group 1), and an electrical stimulation group (Group 2).

Platinum wires were placed in the 0.9% NaCl solutions to isolate the cells from electrolysis generated during electrical stimulation. Electrical current in Group 2 cells was transmitted from the platinum electrodes through the 3% agar salt bridge created

from borosilicate glass (Pyrex, Lowell, MA, USA) with an inner diameter of 5mm. Borosilicate glass was selected in the experiment for agar bridge construction because the material is highly ductile when heated and allowed for reproducible fabrication (5.5 cm width x 10.5 cm in length for an approximate agar bridge volume of 5.2 cm^3). The glassware and salt bridges used in the experiment were sterilized by autoclaving for one hour prior to use in the incubator. However, the custom fabricated cell chambers and Petri dishes were wrapped in sterile surgical drapes and sterilized with ethylene oxide (ETO) since autoclaving would have caused shape distortion of the plastics due to the higher temperatures (autoclaving: 250ºF, ETO: 150ºF).

Electrical current was applied to Group 2 osteoblasts using a DC voltage supply (BK Precision, Model 1665, Yorba Linda, CA, USA) and 20 gauge Teflon coated wire (NTE Electronics, Inc., Bloomfield, NJ, USA) connected to the platinum electrode. Electrical current was recorded using a digital multimeter (accuracy ± 0.05%) (Fluke Corporation, Model 87V True RMS Multimeter, Everett, WA, USA) and all wires were soldered to prevent accidental dislodging during experimentation. A 6.35 volt potential difference was selected for the Group 2 cells, since the salt bridge poles were 5.5 cm apart and would result in an approximate electric field of 1.2 V/cm. This was a value demonstrated to be attainable with FEA and would theoretically result in galvanotaxis and galvanotropism *in vivo*.[80,84] The DC power supply was set to constant current mode and the electric metrics were monitored throughout the experiment.

5.2.1 Cell Collection and Analysis

At the final time period of 72 hours, Petri dishes from Group 1 and Group 2 osteoblasts were removed from the incubator and imaged to determine cellular morphology (Olympus, Model DP11, Center Valley, PA, USA). After visual inspection and image capturing, the Petri dishes with the attached cells were placed in a laminar flow biosafety cabinet to prevent contamination during cell and media collection (NuAire, Inc., Plymouth, MN, USA). Medium from each group was carefully poured into a 50 mL polypropylene test tube (Greiner Bio-One, Monroe, NC, USA) and examined for differences in pH and medium conductivity (Denver Instruments, UB-10 pH/mV meter, Bohemia, NY, USA). The UB-10 pH/mV meter had an accuracy of ± 0.005 pH and ± 0.2mV and was used to determine the effect of the electrical chemical reaction that may have occurred during electrical stimulation usage in Group 2 cells.

Osteoblasts attached to the Petri dishes were removed using an ATCC protocol in which 10 mL of phosphate buffered saline (PBS) was added to the Petri dish and removed by vacuuming. One and a half mL of 0.25% trypsin (ATCC, Trypsin, Cat No. 30-2101, Manassas, VA, USA) was added to the Petri dish and cells detatched slowly between 1 to 2 minutes. The liquid/cellular mixture was removed from the Petri dish and placed in a 50 mL polypropylene test tube with 5 mL of media and fetal calf serum to quench the trypsin. To ensure all cells were removed from the polystyrene surface, 5 mL of media and fetal calf serum were once added to each Petri dish and the polystyrene surface was gently squeegeed with a cell scrapper (Corning Inc., Corning, NY, USA) to mechanically displace any residual cells. The second batch of media/cells was added to the 50 mL polypropylene test tube with the previously harvested osteoblast cells.

To collect the cells in the suspension (DMEM, FCS, trypsin), the 50 mL polypropylene test tube was centrifuged at 125x gravity for 10 minutes to obtain a cell pellet (Beckman Coulter, Inc., Model TJ-6, Brea, CA, USA). The supernatant liquid was carefully removed after centrifugation with vacuuming and 1 mL of DMEM and FCS was added to the cells. The cell pellet was gently pipetted up and down to break up the aggregation and 50 μL was collected from the polypropylene tube and combined with 50 μL of 0.4% weight/volume trypan blue in a 0.65 mL microtube (Genemate, Kaysville, UT, USA) to determine cellular viability. The 100 μL of cells and trypan blue were pipetted vigorously to ensure thorough mixing, and 10 μL was removed for hemacytometry analysis (Olympus, Model CX31, Center Valley, PA, USA). Cell count and viability was conducted at 100x magnification according to standard laboratory procedures (Figure 30).[215]

5.2.1 Statistics

The percent viability between unstimulated osteoblasts (Group 1) and osteoblasts exposed to continuous DC electrical stimulation (Group 2) was performed using an independent samples t test after verifying homogeneity of variance using Levene's test. All statistical comparisons were conducted with commercially available software and $\alpha = 0.05$ (SPSS, Inc., Chicago, IL, USA).

5.3. Results

Osteoblast groups demonstrated similar cellular morphology and viability for the 10 quadrants examined using hemacytometery (Figure 31). Group 1 osteoblasts had a 97.4 ± 2.0% viability compared to 95.8 ± 2.2% in Group 2 (Table 9). Statistical comparison between percentage viability for the 10 trials for Groups 1 and 2 were not statistically significant (p=0.102). Media collected during the 36 hour experimental period revealed a slightly alkaline pH in Group 2 Petri dishes (Group 1: pH = 7.33 and Group 2: pH = 7.46) and higher media conductivity (Group 1 = 19.8 mV and Group 2 = 27.5 mV) than that of the unstimulated control osteoblast cells.

5.4 Discussion

Hemacytometry analysis indicated that the addition of DC did not affect osteoblast viability or cell morphology. While no statistical differences occurred between treatment groups, it should be noted that consistently higher cell counts were observed in Group 1 osteoblasts. However, it has been difficult to draw conclusions based on cell proliferation since Petri dishes were seeded with approximately 6.9×10^5 osteoblasts, and may not have been exact in both cases. While hemacytometry has remained the gold standard technique for cell counting in the literature,[216] others have cautioned that there has been high variability using this measure.[217] Fedoroff and Richardson noted that "the average error in counting cells, using the hemacytometer, approaches 15-20%, but may be kept as low as 5-8%. Errors inherent in cell enumeration using this method have been caused by inadequate suspension of cells, inaccurate dilution, overfilling the

hemacytometer chambers, too few or too many cells in the sample to be counted, and inaccurate counting."[218]

Cell culturing media indicated that the osteoblasts exposed to electrical current had a more alkaline pH and higher media conductivity than that of Group 1 cells. As stated in Chapter 2, gradients have been known to exist at the epiphyseal plate during growth with the lowest oxygen tension occurring at the cartilaginous junction[145] having a localized alkaline pH of 7.70.[146] The 0.13 increase in medium pH for the electrically stimulated cells compared to the untreated control cells (Group 1: pH = 7.33, Group 2: pH = 7.46), may function as important mesenchymal stem cell initiators *in vivo* and enhance skeletal attachment of a TOI.

While cell viability and proliferation appeared not to be influenced by DC, a 39% difference in media conductivity was evident between cell groups. However, determining a relationship between medium conductivity and DC may be difficult to assess given that the osteoblastic cell count in each Petri dish was approximately, but not exactly, 6.9×10^5 cells. Brighton et al. noted that with inductive coupling and combined electromagnetic fields, the interaction between electrical current and the cellular membrane initiated with the release of Ca^{2+} from intracellular stores.[130] Therefore, the discrepancy in medium conductivity between groups (Group 1 = 19.8 mV and Group 2 = 27.5 mV) may have resulted from DC and would confirm previous published observations. However, it may be possible that the cells in the untreated Petri dishes had a higher cell count initially and the decreased medium conductivity of Group 1 osteoblasts may have been signs of a depleted cell culturing medium.

5.5 Conclusion

Controlled electrical stimulation demonstrated that DC did not impact osteoblast viability or morphology in custom designed cell chambers. Media collected after a 72-hour incubation period indicated that electrically treated cells had a more alkaline pH and higher medium conductivity. These observations remain optimistic, as an alkaline environment has been known to occur at the growth plate and functions as an important element in bone growth and maintenance. Higher medium conductivity for the osteoblasts exposed to DC may confirm Brighton et al. who noted that the interaction between electrical current and the cellular membrane initiated with the release of Ca^{2+} from intracellular stores. However, analyses conducted with hemacytometry have associated cell count errors and a higher aggregation of cells in the untreated group may have influenced nutrient consumption, a factor which cannot be negated. DC appears to hold promise for altering localized pH and in future may improve skeletal fixation of a TOI, but additional *in vitro* studies would be required using more sensitive cell counting techniques.

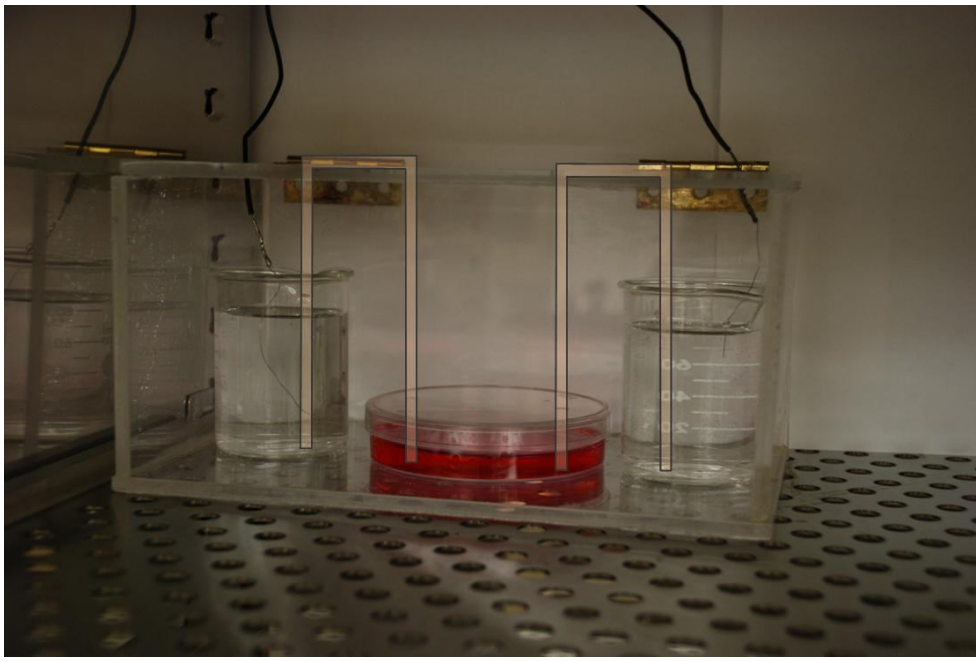

Figure 27: Photograph of the custom cell chamber created for *in vitro* evaluation of DC electrical stimulation. Cells were incubated in the 100 mm Petri dish and agar bridges connected the cell population to the electrolytic solution containing the electrodes. The cells were not placed in direct contact with the electrodes to prevent contamination.

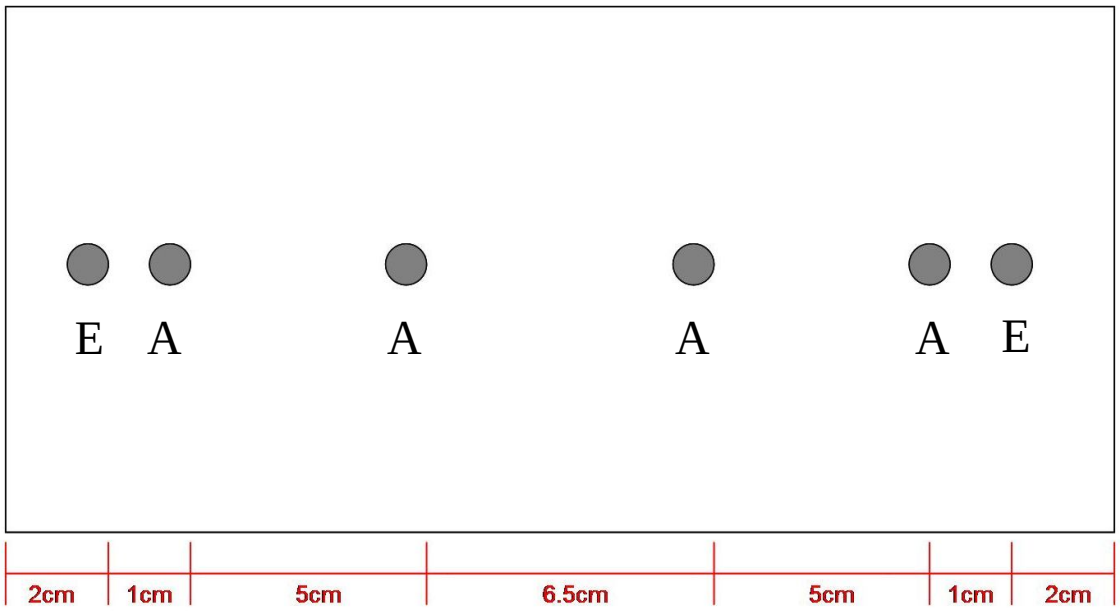

Figure 28: Pictorial representation of the top view of the cell chamber with holes drilled in specific locations to ensure uniform data collection. Electrodes (E) were placed furthest from the center of the chamber and an electrical current was passed via agar salt bridges (A).

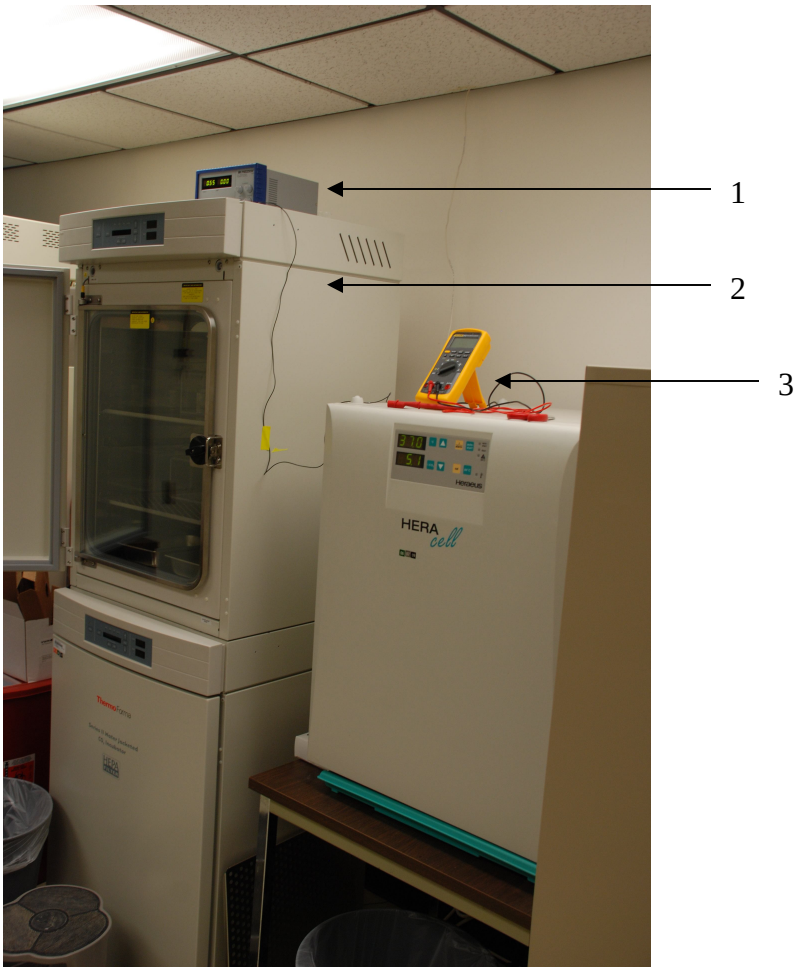

Figure 29: Gross photography of the circuitry used for cell culturing. The set up included (1) a power source, (2) incubator and (3) digital multimeter.

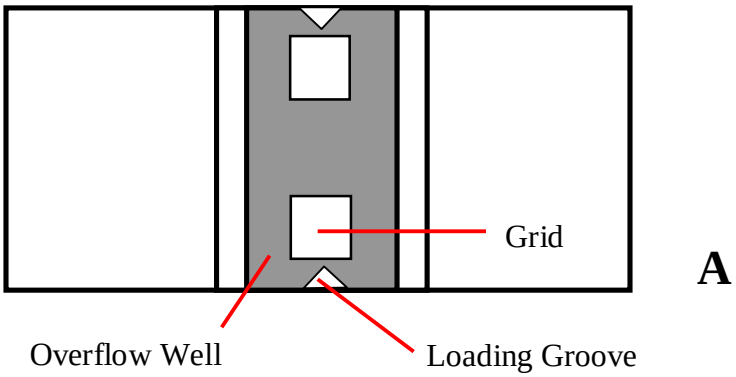

A

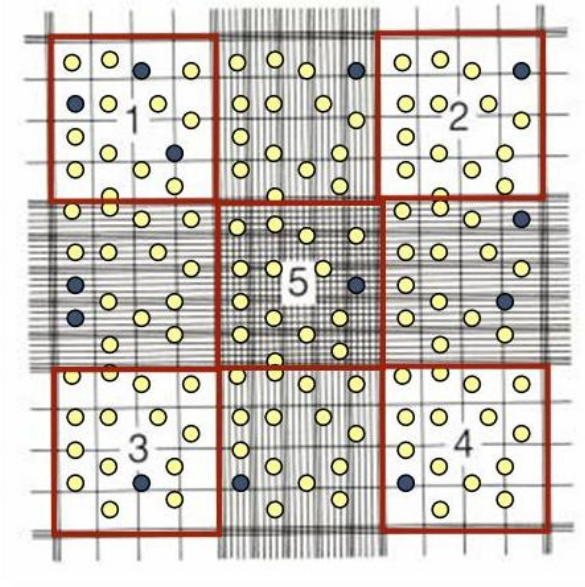

B

Figure 30: Illustration of a hemacytometer and the grid used for determining cell viability (A). A magnified view of the grid has been depicted below (B) and shows the five quadrants used in this experiment for determining cellular viability (outlined in red boxes); osteoblasts which are no longer viable stain blue due to the penetration of the trypan blue dye.

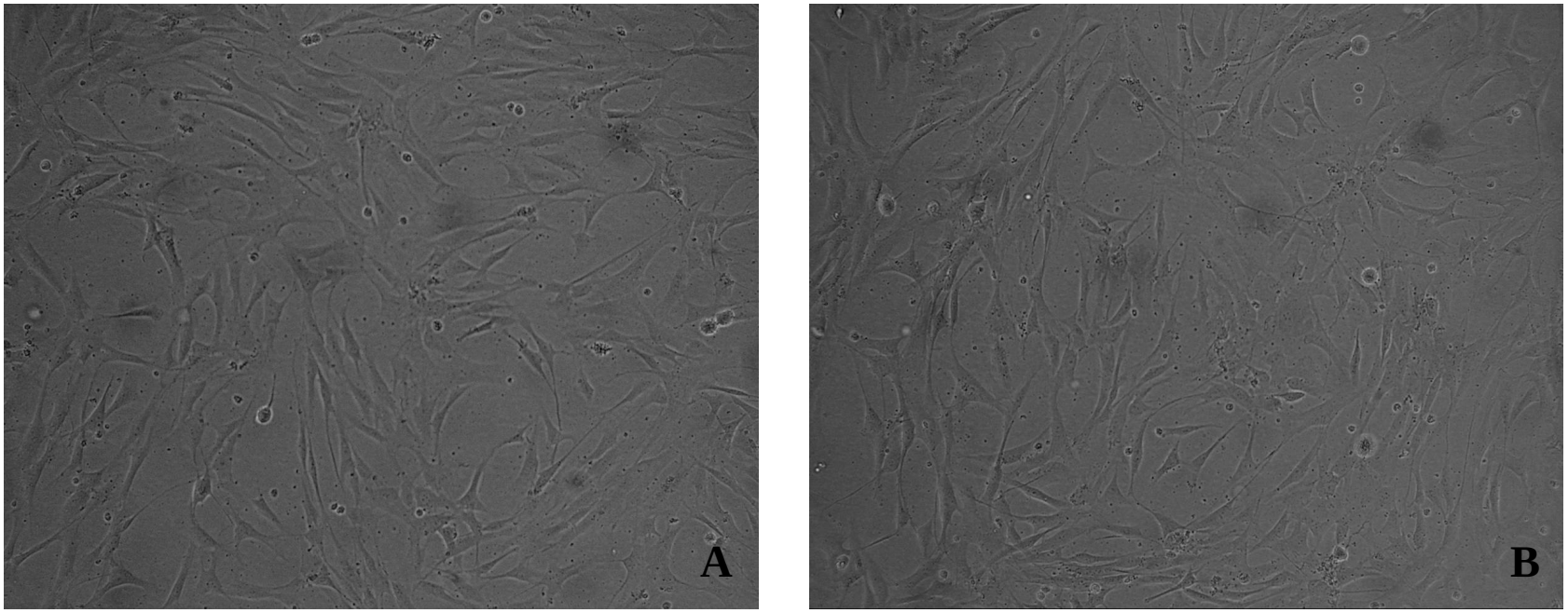

Figure 31: Representative image of cell morphology prior to the trypsinization process for both the untreated (A) and electrically simulated (B) osteoblasts. Note: There appears to be no differences in cellular morphology as both cell groups have spindle shapes with extended processes.

Table 9: Cell count and viability comparison between the osteoblast groups. Group 1 osteoblasts were unstimulated controls while Group 2 were cells exposed to DC.

Quadrant	**Group 1**		**Group 2**	
	V	NV	V	NV
1	179	4	113	4
2	176	9	103	3
3	126	3	105	6
4	107	2	146	4
5	101	7	117	2
6	142	0	81	3
7	106	1	91	8
8	122	3	97	2
9	132	3	88	4
10	124	2	68	4

* V = viable, NV = nonviable

CHAPTER 6

ELECTRICALLY INDUCED OSSEOINTEGRATION *IN VIVO*

6.1 Introduction

The peer-reviewed literature has indicated that direct current appears to be the most useful electrical stimulation modality for increasing bone growth,[219] but to date, there have been no human or animal studies that have evaluated the effect of skeletal fixation of intramedullary implants using this modality. Previous animal models have only demonstrated the effectiveness of electrical stimulation in fracture healing applications by measuring the percentage of new bone growth in the medullary canal around a cathode site with a small diameter stainless steel wire. However, these experiments have not used an appropriately sized implant placed in apposition to the endosteal wall and have lacked time zero data for baseline comparisons.[219] While animal models used by Brighton and Friedenberg have demonstrated the ability of electrical stimulation to generate new bone formation,[158,219] other animal studies have shown noticeable bone retardation from improperly controlled electric metrics.[167] The inconsistencies in bone growth have been attributed to varying electrical system design, electrode proximity and lack of finite element analysis.[75]

To demonstrate the ability of electrical stimulation to increase bone growth around a TOI, and avoid complications with excessively high current densities reported clinically,[166] FEA was used in this study to determine the appropriate potential difference conducive for bone growth and was validated with *in vivo* experimentation. The ability to predict electric fields and current densities in the limb prior to using electrically induced osseointegration *in vivo* was a unique idea that has not been conducted previously. The same design principles developed in Chapters 3-5 were employed in Chapter 6 with expectation that these previously established methods would result in successful histological and biomechanical data in this application. The hypotheses of Chapter 6 were that (1) DC would expedite periprosthetic bone mineral apposition rates, and (2) increase skeletal attachment strength at the bone-implant interface.

6.2 Materials and Methods

6.2.1 Experimental Model

Twenty-five adult female New Zealand white rabbits (4.7 ± 0.2 kg) were used in a Department of Veterans Affairs and University of Utah IACUC-approved research protocol. Animals were sacrificed at zero, 3 and 6 weeks to evaluate the rate and magnitude of electrically induced osseointegration over time, and assigned to histological (Group I) and biomechanical (Group II) test groups after necropsy. In order to limit bias, the animals were grouped based on their surgical order: even number rabbits were assigned to Group I and odd numbered rabbits were assigned to Group II. Time zero rabbits were used for both Group I (left hind limb) and Group II (right hind limb) animals. Although no bone remodeling would be expected to occur at time zero, these animals

were needed for baseline comparisons and to maintain *a priori* power calculations. All analyses were conducted postmortem and the final time point of 6 weeks was selected because it has been reported as the time required for rabbit cortical bone remodeling.[61,220] Five and 16 days prior to euthanasia, 40 mg/kg intramuscular (IM) Tetracycline injections (Vedco Inc., Saint Joseph, MO, USA) were administered twice daily in the right thigh of the Group I rabbits. Tetraycline was used to determine the mineral apposition rate (MAR).[221] Animals were euthanized with 1 ml of Beuthanasia intravenously (Merck & Co. Inc., Whitehouse Station, NJ, USA).

6.2.2 Surgical Preparation

Fentanyl patches, 25 mcg/hr (Watson Lab, Corona, CA, USA) were applied to the skin 1 day prior to surgery to minimize postsurgical pain. Animals were sedated using Ketamine, 40 mg/kg, IM (Vedco Inc., Saint Joseph, MO, USA), Xylazine, 5 mg/kg, IM (Vedco Inc., Saint Joseph, MO, USA) and Buprenex, 0.01 mg/kg, IM (Bedford Laboratories, Bedford, OH, USA) in order to clip the hind limbs and sacral region prior to surgery. General anesthesia was maintained with isoflurane by inhalation (Vet One, Meridian, ID, USA). Surgical sites were prepared using Betadyne scrub followed by alternating application of 70% isopropyl alcohol (Humco Holding Group, Inc., Texarkana, TX, USA) and Betadyne solution (Cardinal Health, Dublin, OH, USA). Cefazolin, 10 mg/kg (West-Ward Pharmaceutical Corporation, Eatontown, NJ, USA) was given immediately prior to surgery to reduce infection risks. Rabbits were housed in individual cages for 1 week following surgery and then relocated to a group housing pen to allow for more dynamic bone loading.

6.2.3 Surgical Procedure

With the animal in a lateral decubitus position, an incision was made over the abductors of the hip and dissection carried to the region of the greater trochanter. The proximal femoral canal was hand reamed on the medial side of the greater trochanter and the proximal shaft drilled (Stryker, Kalamazoo, MI, USA) to accommodate the intramedullary implant. This implant served as the cathode for electrical stimulation. Careful attention was made to protect bone viability by minimizing drilling time and using saline irrigation.[222,223] Implants were placed in the metaphyseal and proximal diaphyseal regions of the femur and resided in apposition to the host bone (Figure 32).

After placement of the intramedullary implants, electrical leads were connected to a custom fabricated battery pack which was implanted subcutaneously in the sacral region of the rabbit. Redundant skin, at this anatomical site, readily accommodated a small battery box (65 mm x 20 mm) constructed from polyvinylchloride (Figures 33 and 34). The battery box contained a lithium 1.8 volt battery (Energizer Holdings, Inc., St. Louis, MO, USA) and a 1.8 kΩ carbon resistor, which were used to regulate the potential difference between the intramedullary implant (cathode) and intramuscular electrode (anode). The battery box was also designed with a smooth cylindrical shape to prevent skin erosion and limit interference with rabbit movement. All leads were sealed to prevent fluid penetration with instant KRAZY GLUE® (Elmer's Products, Inc., Columbus, OH, USA). To reduce the risk of infection[224] and prevent mechanical breakage,[147] all electrical wiring was connected through a subcutaneous tunnel from the hip region to the back of the animal so that none of the components were exposed to the exterior environment (Figure 35). To ensure sterility, all implants were passivated with

35% nitric acid and autoclaved prior to surgery. The battery packs and wires were cleaned with Hibiclens (Chlorhexidine Gluconante solution 4.0% weight/volume, Molnlycke Health Care US, LLC, Norcross, GA, USA) and rinsed with 70% ethanol prior to implantation.

Electrical leads to the anode and cathode were attached and conductivity maintained using silver epoxy adhesive (Ellsworth Adhesives, SEC1233, Germantown, WI, USA). A 20 gauge Teflon coated wire (NTE Electronics, Inc., Bloomfield, NJ, USA) slid securely into the center of the cathode, so that no biological fluids contacted the silver epoxy on this electrode. The anode, placed in the musculature, was fabricated with a slotted groove to attach the wire and a medical grade silicone elastomer was used to prevent contact between the silver epoxy and host tissue (NuSil Silicone Technology LLC, MED-4210, Carpinteria, Ca, USA). To prevent detachment, the elastomer selected had a tensile strength greater than 7,100 kilopascals and tear strength of 15.7 kilonewtons per meter (MSDS information provided by NuSil Silicone Technology LLC). The layer of silicone elastomer was added to the anodes (control and electrical implants) to avoid any negative impact of the silver to the surrounding tissues.

Each rabbit used in this study had an intramedullary implant (cathode) placed in the metaphyseal to the diaphyseal region of the femur and a rectangular electrode (anode) sutured in place in the adjacent musculature, approximately 1.5 cm away from the periosteum of the bone. In this experiment, only the left hind limb served as a continuously electrically stimulated implant (ESI) with a potential difference of 0.55 volts. The voltage was based on finite element analysis (FEA) predictions.[46] The contralateral limb served as the unstimulated control implant (UCI). A bilateral animal

model was selected because it limited the number of specimens required to test the experimental hypotheses and allowed each animal to serve as its own control for comparison of electrical stimulation. Electrical devices were checked after fabrication, prior to surgery and at necropsy to ensure battery packs were operating properly throughout the experiment (Fluke Corporation, Fluke 87 V True RMS Multimeter, Everett, WA, USA).

6.2.4 FEA Predictions for Establishing Potential Differences

Determining an appropriate potential difference, conducive for bone growth and osseointegration, was done using a protocol developed by Isaacson et al.[46] Computed tomography scans were obtained of a disarticulated rabbit hind limb to determine the geometry and positioning of tissues for three-dimensional reconstructions. The entire rabbit limb was carefully segmented using thresholding software and compiled into a hierarchical volume conductor model which served as the mesh for FEA (Seg3D version 1.11.0, Scientific Computing and Imaging Institute, Salt Lake City, UT) (Figure 36). Each tissue type was assigned a specific conductivity in the FEA program based on peer-reviewed reported values,[46] and electrodes were placed at the same anatomical site as in the surgical procedure described previously (SCIRun version 4.0, Scientific Computing and Imaging Institute, Salt Lake City, UT) (Figure 37). Simulations were generated after conducting FEA mesh refinements to ensure that the numerical approximations would be as accurate as possible. The electric field and current density were predicted between the intramedullary implant (cathode) and rectangular anode located in the musculature (Figure 37). Based on FEA predictions and the electric metric restriction criteria

established previously by Isaacson et al.,[40] a 0.55 volt potential difference would have theoretically produced a 1.2 V/cm electric field and a 1.82 mA/cm^2 current density at the periprosthetic interface *in vivo* and would accelerate osseointegration.

6.2.5 Implant Size and Characterization

Placement and sizing of implants were based on preoperative morphological measurements from rabbit cadavers and a previously established model assessing implant attachment in the femoral diaphysis of rabbits.[225] All cathodes were grit-blasted to replicate the exterior of the Zweymuller hip implant, which required no stem revisions in follow up periods averaging 11 years, thus demonstrating the potential of this surface structure to attain firm skeletal attachment.[226] The sterile cylindrical intramedullary implants (cathodes) used in the rabbit model were 4 mm in diameter x 25 mm in length (Figure 38). Electric fields were generated between the cathode at the bone-implant interface to a 1 mm x 4 mm x 20 mm rectangular electrode (anode) placed in the musculature of the rabbit (Figure 39). Electrical components were fabricated from titanium alloy (Ti-6Al-4V), coated with a 1200 angstrom layer of gold to increase conductivity (Spire Corporation, Bedford, MA, USA) and anodes were sutured in place to prevent migration. A uniform gold coating with 99.999% purity was used on the electrode surface to prevent polarization and minimize resistance.[79,103] A gold-titanium alloy surface would not be expected to generate galvanic current between the materials, and gold has been used effectively for osseointegration in both cortical and cancellous bone in dental applications.[227] Electrode coatings were characterized prior to implantation

and determined to be homogenous using prolifometry, scanning electron microscopy (SEM) and x-ray photoelectron spectroscopy (XPS) surface analysis techniques.

6.2.5.1 Profilometry

Following implant fabrication and prior to insertion in the rabbit, an optical profilometer (Zygo New View 5032, Zygo Corporation, Middlefield, CT, USA) was used to ensure that the grit-blasted cathodes had a similar average surface roughness (Ra) as a clinically successful Zweymuller hip implant. Three gold-coated cathodes were passivated in 35% nitric acid and autoclaved prior to analysis. Ten points were randomly selected on the cathode surface and the implant was fixed under the microscope objective lens using molding clay to prevent image artifacts. Surface profiles and Ra were collected for each implant type.

6.2.5.2 Scanning Electron Microscopy (SEM)

A scanning electron microscope (JSM-6100, JEOL USA, Inc., Peabody, MA, USA) was used to ensure the integrity of the implant coating prior to impaction in the medullary canal and also to determine the surface composition for the gold-titanium alloy electrodes. To make certain the conductive coatings would not shear from the implant surface during impaction, a carcass rabbit limb was obtained and prepared in accordance to the IACUC approved protocol described above. After implant insertion, the host bone was carefully bivalved, coated with carbon to enhance visualization in the SEM and analyzed using spectral analysis to determine element type along the endosteal wall. High

quantities of gold particulate on the bone surface would increase the likelihood of a foreign body response in the body, decrease the conductivity of the electrode and would have required changes in implant manufacturing prior to *in vivo* assessment.

Spectral analysis was also performed to determine element types on the surface of the electrodes and ensure that there was a uniform gold coating. It has been well known that gold is a faradic electrode and allows free exchange of electrons in an electrolytic medium, while titanium and its alloys are capacitive electrodes and store electrical charge.[228] Therefore, having an electrode with high quantities of titanium, vanadium or aluminum would decrease the electrical conductivity of the system and have the potential to lessen osseointegration as well. As noted above, electrodes were prepared for analysis using a combination of passivation and autoclaving processes.

6.2.5.3 X-ray Photoelectron Spectroscopy (XPS)

An XPS (Kratos Analytical Ltd, Ultra DLD Imaging XPS, Manchester, UK) was used in addition to SEM because of the increased surface sensitivity of this technique. XPS has been known to provide accurate profiles of surface elements at depths between 0.005 to 0.01 μm and would either confirm or reject spectral analysis conducted with SEM. As with spectral analysis, XPS provided a quantitative measure of element type along with surface energy bonding to determine the attachment strength of the gold layer. As noted above, electrodes were prepared for analysis using a combination of passivation and autoclaving.

6.2.6 Rabbit Specimen Processing

At the time of euthanasia, the soft tissue and skin were resected around the implant sites and were carefully excised *en bloc*, photographed, radiographed, fixed in formalin, dehydrated in ascending grades of ethanol and embedded in polymethylacrylate (PMMA) according to standard laboratory procedures.[229,230] Following PMMA embedment, 2 mm slices were sectioned using a high-speed, slow-feed cut-off saw with a diamond-impregnated rotary blade (Lapidary Slab Saw, Model LS10, Lortone, Inc, Mukilteo, WA, USA).[231] The amount of bone ongrowth, known as the appositional bone index (ABI), was measured at the cathode for cortical bone-implant attachment with high resolution contact microradiographs (Faxitron X-ray Corporation LLC, Lincolnshire, IL, USA).[230] ABI was computed by measuring the bone in direct contact with the implant ($\Sigma L1$) compared to the total length of bone-implant contact available ($\Sigma L2$) as: $((\Sigma L1/\Sigma L2) \times 100)$.[229]

To analyze the host and periprosthetic bone in the vicinity of the grit-blasted intramedullary implants, backscattered electron imagining (BSE) was performed on an average of 6 regions. Specimens were ground, polished and sputter-coated with gold to increase conductivity in the SEM (Anatech LTD, Hummer 6.2 sputtering systems, Battle Creek, MI, USA) (Figure 40). Porosity analysis was conducted by subdividing the cortical bone-implant areas into 8 equal regions to determine if a regional angiogenic effect existed with electrical stimulation and whether porosity was spatially dependent on electrode proximity (Figure 41). The midcortex was selected for porosity analysis to reduce confounding variables, as the endosteal region was disturbed during initial implant placement. Specimens were examined between 10-2000x magnifications, at a working

distance of 15 mm using 20 kV accelerated voltage and a 70 μm aperture setting. Images were captured and thresholded using customized SEM software (NSS, version 2.2).

Two millimeter cathode sections were ground to approximately 50 μm and polished to determine MAR using a mercury illuminating source microscope (Nikon Hg-100, Nikon Inc., Melville, NY, USA) equipped with image capturing software (Magnafire SP, Optronics, Goleta, CA, USA and Image-Pro Plus, Media Cybernetics, Inc., Bethesda, MD, USA). Three osteons were imaged for each bone cross section. Ten perpendicular measurements were traced between bone labels and the average length was used to determine growth rates according to Willie et al.[221] Following MAR assessment, bone cross sections were stained with Sanderson's bone stain (Dorn & Hart Microedge, Inc., Villa Park, IL, USA) around the cathode and hematoxylin and eosin (H&E) (Richard-Allan Scientific, Kalamazoo, MI, USA) around the anode to provide qualitative results of tissue and cellular integrity. Histological sections were examined by a pathologist blinded to the specimen source to ensure unbiased data collection.

The degree of skeletal attachment at the bone-implant interface for Group II animals was determined using a uniaxial push-out test. Radiographs taken prior to implant testing were used to compare the percentage of the implant in apposition with cortical and cancellous bone, since it has been known that skeletal fixation is greater in cortical bone[232] and may influence the maximum force required to displace the intramedullary implant. The disarticulated rabbit femurs were carefully sectioned (Craftsman 10" Direct Drive Band Saw, Sears Holding Corporation, Hoffman Estates, IL), ground and polished to the implant surface and then fully submerged in 0.2 molar sodium cacodylate buffer solution (SCBS) prior to testing (Electron Microscopy Sciences,

Hatfield, PA, USA). SCBS was used to prevent bacterial attachment and bone degradation prior to testing and was necessary for maintaining the host bone bed until each bone was properly analyzed. To ensure uniformity, all test samples were temporarily stored in the medium for 1 week. Implant push-out tests were conducted with a servo-hydraulic testing machine (Model 8800, Instron Corp., Norwood, MA), and all bone specimens were rinsed in deionized water to remove SCBS residue and immersed in 0.9% NaCl prior to testing to prevent dehydration.[117] A uniaxial force was applied at a constant rate of 0.1 mm per second for 4 mm of displacement. A force versus displacement curve was generated to determine the maximum push-out force of the osseointegrated implant.

6.2.7 Statistical Evaluation

The animals in Groups I and II were subdivided equally and assessed with biomechanical testing and histological analyses. Osseointegration was evaluated using a one-way analysis of variance (ANOVA) parametric statistical test to determine the correlation between predictor variables (UCI, ESI) and the predetermined outcome measures (ABI, MAR, porosity and mechanical push-out forces). Post-hoc analyses were performed with a Tukey test when statistical significance between groups was determined. All statistical comparisons were conducted with commercially available software at an $\alpha =$ (SPSS Inc., version 17.0, Chicago, IL, USA).

6.3 Results

6.3.1 Results of Implant Surface Analysis

Implant characterization prior to *in vivo* experimentation indicated that the designed cathodes had a similar Ra to the Zweymuller implant (1.115 µm vs. 1.640 µm, respectively) (Figures 42 and 43). During piloted impaction, the cathode did not liberate gold from the implant surface, as confirmed by spectral analysis (Figure 44). SEM indicated that the surfaces of the electrodes were composed of a heterogenous mixture of titanium, vanadium, aluminum and gold (Figure 45). However, XPS, which has higher sensitivity (0.005 - 0.01 µm) to that of BSE and SEM (0.5 - 5µm), indicated that the surface exterior of the electrodes consisted only of gold (Figure 46). A simplistic diagram of the electrode surface has been illustrated in Figure 47 using these techniques noted above.

6.3.2 Rabbit Experiment Results

Twenty-five rabbits underwent surgical implantation to evaluate the effectiveness of electrically induced osseointegration in the medullary canal; however, only 21 were included in the study. Four rabbits were excluded after clinical and radiographic evidence revealed a fractured femur, which required euthanizing the animal prior to the designated time period. Fractures appeared to be the consequence of misaligned reaming or drilling for the implant, combined with increased activity of the rabbits in open housing. Forty-two limbs from 21 rabbits were analyzed: 5 rabbits at time zero (5 limbs for Group I and 5 limbs for Group II) 6 rabbits at 3 weeks (4 limbs for Group I and 8 limbs for Group II), and 10 rabbits at 6 weeks (10 limbs for Group I and 10 limbs for Group II). No rabbits

were excluded due to electrical device failure, as the battery packs were fully functional before surgery and at the time of euthanasia.

A microscopic evaluation of the host bone and periprosthetic interface revealed viable tissue for all time periods and implant groups (UCI and ESI). Because the implants designed for this experiment were a cylindrical shape and had to accommodate the prominent anterior and lateral bows present in the rabbit femur, the implant proximity to the host bone varied. The periprosthetic bone at the cathode site appeared less mineralized than the midcortex of the bone and was most notably affected in the ESI group. Regions farthest from the endosteal wall consisted of bone and fibrous tissue which may have resulted from micromotion of the implant within the medullary canal or absence of proximity to the bone. Bone structure in the midcortex revealed larger vascular cavities in the ESI group compared to the UCI for quadrants D, E and F. In some instances, vascular cavities exceeded 10 times the size of time zero comparisons for the ESI group (Figure 48).

H&E stains of the tissue around the periphery of the anode sections demonstrated contrasts between the ESI and UCI groups for each time period. Observations for the 6-week UCIs noted a fibrous encapsulation around the circumference of the anode section with limited cellular and tissue organization within 100 μm of the implant borders. A more organized tissue structure was observed greater than 100 μm from the tissue-implant interface with distinct collagen patterns and fibroblastic activity (Figure 49). In contrast, the ESI at 6 weeks depicted obvious signs of electrode corrosion and brown staining of the tissue along the perimeter of the anode site (Figure 50). Within a 100 μm range from the implant, macrophages and monocytes were located throughout the host

tissue and consisted of a heterogeneous mixed population of inflammatory cells. Small particulate was identified around the anode which appeared to be liberated gold from the anode surface, but no histochemical analysis was performed to detect the particulate type in the tissue. The presence of metal particulate in the tissue undoubtedly increased the inflammatory response as these cells could not intracellulary digest metal particulate and would release potent cytokines and enzymes into the neighboring environment.[233] The noted difference in tissue integrity at 6 weeks may have resulted from hydrogen ion generation at the anode,[161] and may have contributed to the altered appearance of the tissue. Assessment of tissue structure at 3 weeks did not reveal as notable of a difference as was the case at 6 weeks (Figure 51). While early signs of corrosion were evident in the 3-week ESI, the tissue integrity at the anode site appeared less pathologic with more distinct fiber orientation around the periphery of the electrode.

ABI analysis performed from contact microradiographs demonstrated increased bone ongrowth for both implant groups (ESI and UCI) at each designated time period (t=3 weeks and t=6 weeks) compared to time zero implantation ($p<0.0001$). However, bone ongrowth between the ESI and UCI groups were not different (t=3 weeks, $p=0.878$; t=6 weeks, $p=0.436$) (Figure 52). A higher quantity of bone around the implant perimeter was noted for the ESI group when the implant was not in close apposition to the endosteal wall, but this observation was qualitative (Figure 53).

SEM images demonstrated similar skeletal fixation between the ESI and UCI groups when the implant and bone were in close apposition. However, in the cases where the bone-implant contact exceeded the 50 μm recommended by Bloebaum et al.,[234] only the ESI had stimulated bone ongrowth around the circumference of the intramedullary

implant (Figure 54). Qualitative results also demonstrated a greater periosteal response around the periphery of the cortical bones in the ESI group.

Porosity analysis collected using the SEM thresholding software concluded that the highest regional porosity occurred in quadrants D, E and F in the ESI group. It should be noted that these three regions were in the closest proximity to the anode site and indicated a spatial dependency on host bone porosity when using electrical stimulation. Qualitative observations of bone mineralization at the bone-implant construct demonstrated less mineralized bone for the ESI compared to the contralateral UCI. This phenomenon may in part explain the lower push-out forces required to displace the intramedulary implant for the ESI groups compared to the UCI groups with mechanical testing.

Porosity comparisons noted that the ESI and UCI groups were statistically higher than the time zero bones at each time period (t=3 week UCI, $p<0.0001$; t=3 week ESI, $p<0.0001$; t=6 week UCI; $p=0.032$, t=6 week ESI, $p<0.001$). This occurrence was likely the result of the host bone reestablishing a blood supply after implant insertion. However, global porosity comparisons between the 2 implant treatment groups (ESI and UCI) demonstrated no statistical difference at 3 weeks ($p=0.392$) and 6 weeks ($p=0.754$), thus reaffirming that the electrical stimulation effects were only regional (Figure 55). It is important to note that the host bone porosity at 6 weeks had still not returned to the time zero baseline, demonstrating continual remodeling of rabbit cortical bone even after 6 weeks postoperation.

MAR values calculated from fluorochrome labeling demonstrated higher bone formation along the endosteal and periosteal regions for both the ESI and UCI groups,

with the most prominent effect occurring with the ESI treatment group (Figure 56). The midcortex of both the ESI and UCI revealed a quiescent region with limited numbers of labeled osteons. The bone growth rates of the distal host bone, which were used for comparison against the treatment groups, were significantly lower compared to the periprosthetic bone at 3 and 6 weeks for the ESI and UCI groups ($p<0.0001$) (Figure 57). However, MAR calculations were similar for the ESI and UCI groups (t=3 weeks, p=0.752; t=6 weeks, p=0.993). Results from this investigation have indicated that rabbit host bone, in an undisturbed region in the diaphysis, remodels at approximately 1.4 μm/day compared to approximately 2.0 μm/day at 3 weeks and 1.7 μm/day at 6 weeks following implant insertion.

Biomechanical testing data indicated that the higher mechanical push-out forces were required to displace the intramedullary implant for the UCI group when compared to time zero implantation (t=3 week UCI, p=0.028; t=3 week ESI, p=0.934; t=6 week UCI, p=0.001; t=6 week ESI, p=0.378) (Figure 58). Comparisons between the ESI and UCI demonstrated a significantly higher push-out force for the UCI group at 6 weeks (p=0.032). Radiographic evidence confirmed some variability in implant placement as a higher percentage of UCI and were in apposition to cortical bone compared with the ESI group. This observation may have accounted for some of the discrepancy in implant push-out forces, but the percentage of cortical bone in contact with the UCI and ESI groups were not significant and were more likely attributed to levels of bone mineralization (cortical bone %: UCI = 61.8 ± 22.5%, ESI = 53.7 ± 23.6%; p = 0.514).

6.4 Discussion

Data from this model indicated that direct current did not expedite periprosthetic MAR rates or increase skeletal attachment at the bone-implant interface. While slightly higher ABI, bone porosity and MAR values were noted in the ESI group, the biomechanical data, high standard deviations and the lack of statistical significance have indicated no therapeutic benefit of electrical stimulation compared to the UCI group. To ensure accurate interpretation of the data collected in this experiment, post-hoc power analyses were conducted for the outcome measures of ABI and MAR. Statistical analyses concluded that the likelihood of achieving significant results between the treatment groups (ESI and UCI) would require several hundred animals, which would not be feasible and reaffirmed that *a prior*i power analyses were appropriate.

To avoid regional structural variability of cancellous bone, which has been reported to range in porosity from 50-95%,[90] and circumvent the known dissimilar surface area between cortical and cancellous bone, only cortical bone was analyzed in this investigation. Implants were placed in the metaphyseal region of the femur, which has been known to be the transition region between cancellous and cortical bone.[235] However, only regions distal to the third trochantor (in the area of the proximal diaphysis) were analyzed in Group I to reduce confounding variables associated with determining ABI, MAR and bone porosity. The reason for not initially selecting the middiaphysis regions for implantation was due to the prominent anterior and lateral bows present in the rabbit femur and the tendency of the bone to fracture with impaction in the canal. The diaphyseal shape precluded implant insertion at this site using the designed intramedullary device. Distal placement of the cylindrical cathode would have created

edge loading when the end of the device was forced against the endosteal wall of the cortical bone (which is only 1.5 mm in thickness) and would have subsequently increased the fracture rate in this investigation.

The osteoinductive abilities of electrical stimulation were qualitatively observed during ABI and SEM analyses (Figures 53 and 54). Cross sectional images of the intramedullary implant demonstrated 89% ABI in 6-week ESI implants, despite the implant not being in close apposition to the endosteal wall in some cases. This distinct occurrence in the ESI group demonstrated that DC electrical stimulation may be a useful means of improving implant attachment in long bones with suboptimal implant "fit and fill." The ability to facilitate osteoinduction, a process in which mesenchymal stem cells arrive at a cathode site and change phenotypes to the osteoblast lineage, may be important for enhancing skeletal attachment with a TOI.[90] In fact, altering mesenchymal stem cell function may be of utmost importance in the prevention and treatment for patients with pathological bone disorders (osteopenia and osteoporosis) who advocate for TOI procedures, since there is a naturally reduced healing capacity with age.[133]

SEM measurements indicated that a direct relationship existed between electrode positioning and bone porosity. In this investigation, the host bone sections which were closest to the intramuscular electrode (anode) had the highest bone porosity. The direct relationship between the anode and cathode placement and bone remodeling, although conceptually clear (since spatial position affects current density magnitudes), has been an area of frequent controversy in the peer-reviewed literature. Friedenberg et al. note that whether the anode was in close proximity or remote from the cathode, appeared not to affect the amount of bone formed.[158] However, it is important to note that Friedenberg's

study evaluated the percentage of bone that filled the medullary canal and SEM analysis was not conducted on cortical bone porosity. The increased porosity for quadrants D, E and F in the ESI group was likely the result of a lateral portion of the bone experiencing the largest voltage drop and being nearest to the anode site.

Altering bone porosity with electrical stimulation remains a biomechanical concern since an inverse relationship has been known to exist between bone porosity and mechanical stiffness. An increase in bone porosity will reduce the mechanical stiffness of the bone, while a decrease in bone porosity may restrict perfusion and the availability of nutrients for bone remodeling. Rosenbaum Chou et al. noted that a 3% increase in porosity reduced bone stiffness by 8-13%[236] and lessens the durability at the bone-implant construct. However, general increases in bone porosity have been a noted occurrence in fracture healing, as gradual increases in vascularity occur in the vicinity of a bone defect.[145] Data from this investigation supported this known phenomenon as time zero bone porosity was observed to be 4.7 ± 2.1% for rabbit cortical bone, but increased at the 3-week and 6-week time periods because the endosteum was reestablishing a blood supply (t=3 week UCI: 7.6 ± 4.6%; t=3 week ESI: 8.6 ± 3.9%; t=6 week UCI: 5.89 ± 3.5%; t=6 week ESI: 6.3 ± 4.3%). Data also indicated that quadrants D, E and F for the ESI group had the largest vascular cavities, but these observations were qualitative. Therefore, electrically induced TOI should remain cautionary for patients with osteopenia or osteoporosis, which may be an issue with amputation limbs. While electrically induced osseointegration may be useful in future after further electrical refinement, it may be necessary to wait until the host bone has been remodeled by strain-adaptive mechanical loading[12] prior to electrical stimulation implementation.

While ESI required significantly lower mechanical push-out forces, a higher abundance of less mineralized bone was noted with SEM at the bone-implant construct. This may be explained by the exponential curve that exists between bone mineral content and the modulus of elasticity of bone. As stated by Bloebaum et al., even a slight decrease in bone mineral content drastically reduces the mechanical stiffness of bone.[237] The reason for the higher abundance of unmineralized bone in the ESI group may have occurred because the mineralization process was altered in the periprosthetic bone with electrical stimulation. Bone is a highly organized, anisotropic tissue[87] composed of organic (proteins) and inorganic (hydroxyapatite) constituents.[90] During the process of secondary bone remodeling, osteoblasts secrete extracellular matrix components which includes osteocalcin, a potent stimulus for bone mineralization.[238] Calcification occurs as a two-phase process, which includes the release of matrix vesicles by osteoblasts and mesenchymal stem cells and the addition of circulating calcium and phosphate to the extracellular matrix.[239] Mineralization of bone is therefore regulated by an enzymatic process that involves recruitment of polyphosphates that sequester free calcium.[240,241] If the negatively charged polyphosphates cannot be deposited due to a negative charged cathode in the vicinity, then the inorganic component of bone may continue to be deposited further away from the electrode site where current densities are lower in the mid-cortex, but mineralization may be reduced closest to the bone-implant construct. MAR data confirmed this hypothesis as the bone growth rates collected from osteons suggested a slightly higher mineralization in the ESI group compared to contralateral UCI at both 3-week and 6-week time points, indicating that if mineralization was altered with electrical stimulation, this may be a regional phenomenon. Future use of electrically

induced osseointegration may require a pulsed or time-step configuration to determine if the negatively charged cathode results in less mineralized bone at the bone-implant construct using a DC configuration.

Assessment of fluorochrome double labeling indicated that rabbit bone remodels most significantly along the endosteal and periosteal walls with reduced osteon growth in the midcortex. SEM observations qualitatively supported this observation since osteocyte lacunae varied based on the region of examined bone. Regions around the endosteal and periosteal walls demonstrated an elliptical lacunae structure which is a sign of mature bone. However, lacunae in the midcortex of the UCI and ESI groups tended to be more disorganized with an abnormal geometry. The dissimilarity in lacunae geometry was apparent at 3 weeks for both implant groups (UCI and ESI), but was only observed for the ESI group at 6 weeks, thus indicating that bone maturation had not yet occurred. The discrepancy in lacunae morphology may be explained by D'Arcy Thompson who postulated that ostecytes were affected by differences in electrical gradients and pressure.[114] These cells extend their processes through canaliculi, which not only connect to adjacent bone cells and blood capillaries, but to the surfaces of the periosteum and endosteum.[242] Therefore, changes in the localized microenvironment from electrical stimulation, which notably occurred at the periosteal and endosteal surfaces in this experiment, may also alter bone cell response and the size and shape of lacunae. Osteon reconstruction has previously been reported to be affected by fluctuations in endosteal and periosteal activity, and more so with thin cortical bone-types as seen in rabbits.[242]

The investigational findings that rabbit bone remodels at 1.4 μm/day in normal host bone were lower than the 2.2 μm/day documented by Clark et al.[243] While MAR

rates increased to 2.0 μm/day at 3 weeks at the periprosthetic interface, these values never approached the rates previously reported in rabbit femora. However, it is important to note that the model developed by Clark et al., used to determine MAR, involved transcortical implantation which would undoubtedly increase localized remodeling given the disturbance to the periosteum. It has been well known that transcortical implants closely mimic the "classical fracture-healing model" which involves the advantages of the periosteal membrane that forms extensive bone when stimulated.[244] A transcortical insertion technique drastically differs from the surgical approach used in TOI procedures performed clinically and in this study.

Six weeks was selected as the terminal study duration for determining electrically induced osseointegration since previous reports have indicated that rabbit cortical bone remodels for that duration.[61,220] However, results from this investigation indicated that rabbit cortical bone continues to remodel greater than 6 weeks in the skeletally mature rabbit femora. Sennerby et al. and Slaets et al. previously defined 6 weeks as the terminal point of cortical bone remodeling in rabbits because these investigators used a transcortical model for their experiments.[61,220,245] Data from this experiment indicated that selecting 6 weeks as the end point did not provide sufficient time to determine if trajectories from biomechanical testing between the 2 implant groups would have eventually resulted in ESI, reaching or surpassing the mechanical push-out forces of the UCI group. A longer duration time period would be necessary to test this biological factor.

6.4.1 Experiment Limitations

The rabbit model designed for this experiment, while successful in determining the effect of electrically induced osseointegration in rabbit long bones, had some model imitations worth noting. The most obvious of these considerations was that the implants placed in the medullary canal were not transcutaneous, which is the true representative model for human procedures conducted currently in Europe and Australia for patients with limb loss.[52] While rabbits have been routinely used for investigating treatment of nonunions with electrical stimulation,[158,159,219] these animals have a much higher MAR than that of humans and extrapolating data from this model may be a translational disadvantage. Future studies using goats and/or sheep may be more appropriate since these animals have MAR more closely to that of humans[221] and these animals have been used for establishing TOI procedures.[41,56]

Selecting an intramedullary implant rather than a TOI for proof of concept of electrically induced osseointegration may have subsequently affected bone remodeling rates. Spadaro noted previously that optimal bone growth resulted from a combination of mechanical and endogenous electrical signals,[105] which subsequently control bone cell activity and macromolecular byproducts.[98] Mechanical loading at the bone-implant construct varies considerably with a TOI compared to a nontranscutaneous osseointegrated implant, since the implant (cathode) used for electrical stimulation is directly weight-bearing. While the cathode in this investigation was not directly load-bearing, the intramedullary implants may have been subject to microscopic deformations from contractual forces exerted by muscles[222] and would satisfy Spadaro's recommendation of electrical and mechanical stimuli.

The electrical system designed for this experimentation required that all components must be compact and completely subcutaneous to prevent disruption by the rabbit. While previous researchers have used externally applied electrical stimulation systems with percutaneous leads, these electrodes often fail due to mechanical breakage[147] and have associated infection risks.[86] Therefore, the battery packs designed for the rabbits in this investigation were simplified and consisted of only a battery and resistor. While researchers have cautioned the need for transistors to regulate electrical current,[157] it is important to note that electrical conduction in living bone demonstrates a linear relationship between voltage and current when maintained below 1 volt in the rabbit femur.[136] Because this experiment used 0.55 volts as the potential difference, polarization effects would not have occurred because the direct relationship between voltage and current would not have been violated in the tissue,[136] and localized field strengths should not have been significantly affected. However, once the potential difference in tissue has exceeded 1 volt, polarization effects may occur which surpass the ohmic threshold[136] and would require more advanced means such as FEA for accurate estimations. While quasi-static FEA provided insight into transient approximations of electric metrics for this experiment, it is important to note that this did not accurately represent chronic electrical stimulation usage which includes biological fluctuations (temperature, ion concentration) and fibrous tissue formation around the electrode sites.

Lastly, because external electrical anode bands could not be placed around the exterior of the rabbit limb, as would be the case in the desired TOI human system,[40,46] these electrodes had to be sutured to the interior muscle belly 1.5 cm from the periosteum of the bone. The anode, which consisted of titanium alloy and gold, demonstrated

corrosion in the tissue surrounding the electrode (an approximate 200 μm zone of corrosion) at 3 and 6 weeks for the ESI group. While modifying the surface of the titanium alloy implant with gold was necessary to improve the conductivity of the electrical system and to avoid problems with electrode polarization (since titanium alloy is not an optimal material for faradic current flow),[79,103,144] galvanic corrosion may have occurred. However, it is important to note that anodic corrosion is a common problem associated with electrical stimulation and may not have resulted from the dissimilar material surfaces.[157,158] Both Ti-6Al-4V and gold have been known to be very unreactive when placed in apposition to one another without electrical stimulation, but may have corroded *in vivo* due to the exchange of electrons which occurred when passing an electrical current through our electrolytic medium and volume conductor.

6.5 Conclusion

The use of controlled electrical stimulation, while studied for fracture healing, has not been investigated to accelerate the skeletal attachment of osseointegrated implants in long bone models. Data from this model indicated that DC did not expedite periprosthetic MAR rates or increase skeletal attachment at the bone-implant interface. Controlled electrical stimulation regionally increased bone porosity, demonstrating a spatial dependency between electrodes. ABI analyses were similar between implants groups (ESI and UCI), but qualitative observations noted that DC may hold promise for improving suboptimal implant "fit and fill." Therefore, future use of electrical stimulation for electrically enhanced TOI may require a pulsed or time-step electrical configuration, especially given the biomechanical testing and observed decreased mineralization at the

bone-implant interface for the ESI group. Longer time period animal studies or variations in the electrical stimulation modality may also be required before the utility of electrically induced osseointegration appears clinically feasible.

Figure 32: Anteroposterior (A) and lateral (B) radiographs demonstrating implant placement in the rabbit femora.

A: Battery Plug Adapters

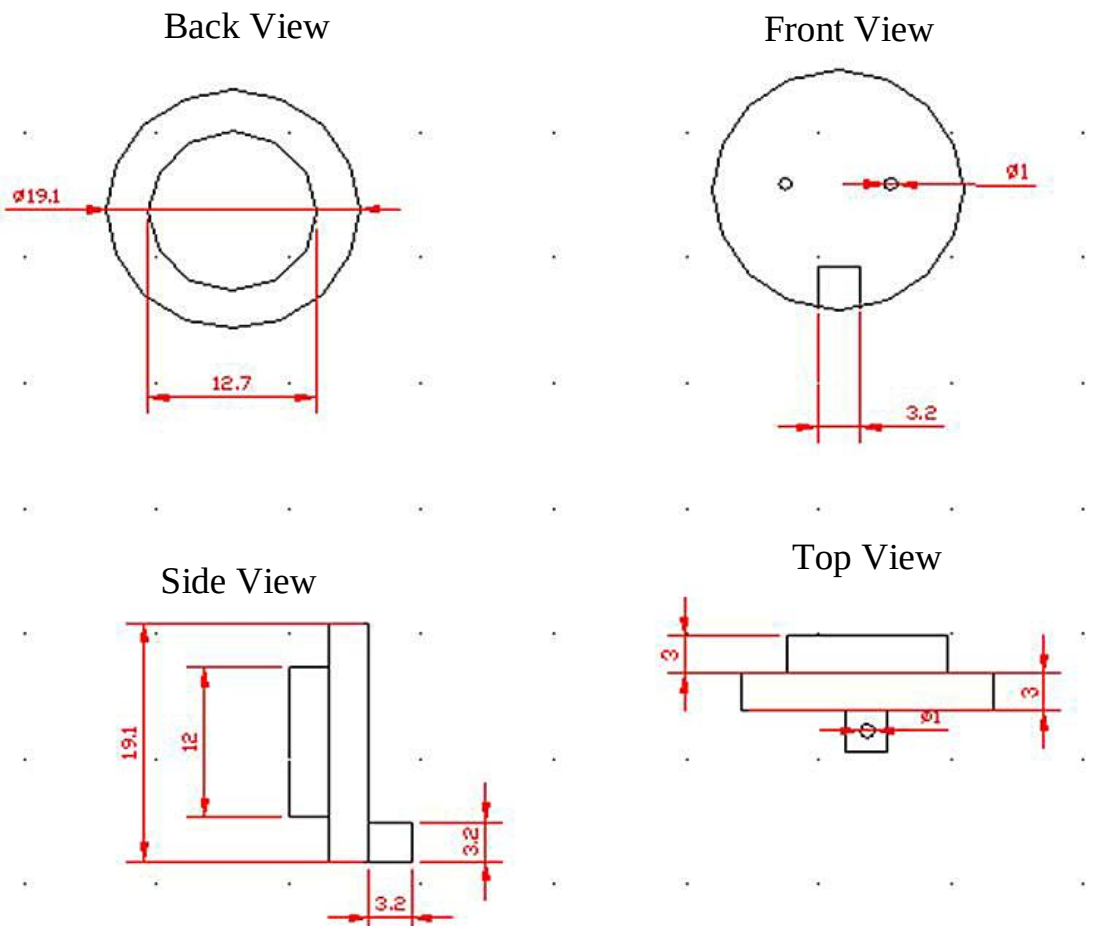

Figure 33: Two-dimensional schematics of the rabbit battery packs designed for electrically induced osseointegration.

B: Main Battery Pack

Front View

Side View

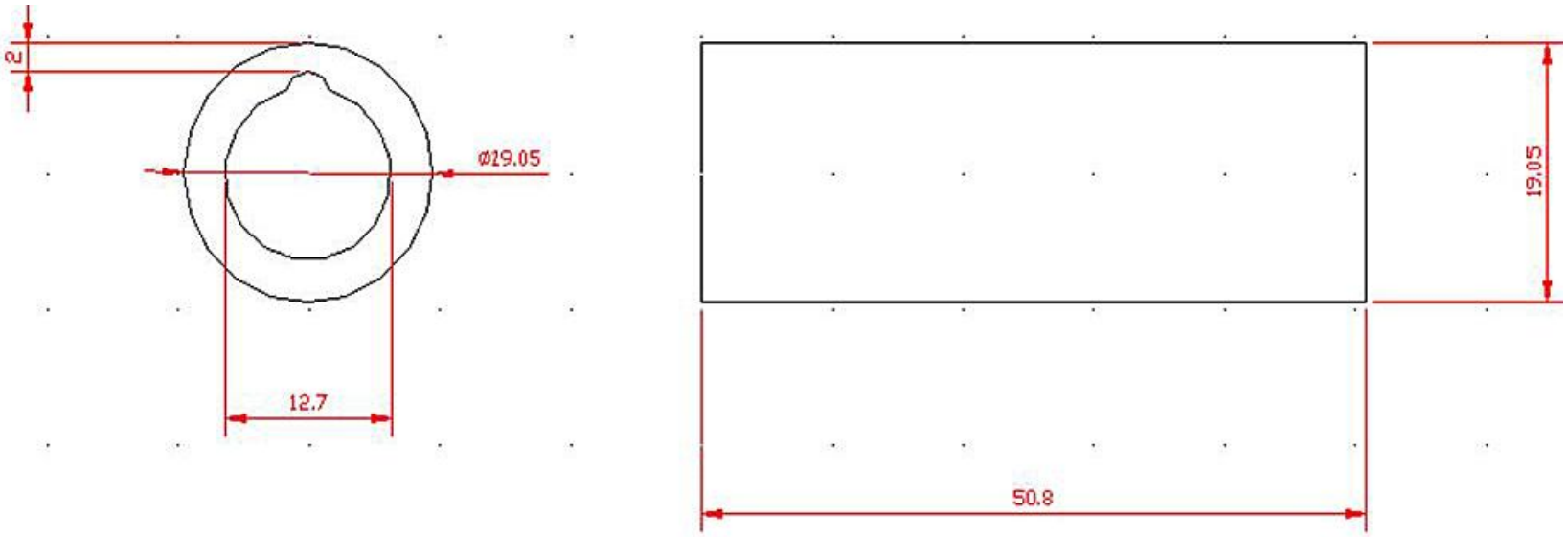

Figure 33: Continued

Figure 34: Three-dimensional models of the rabbit battery packs. Note the inclusion of end caps to prevent fluid penetration and corrosion of electrical equipment during experimentation.

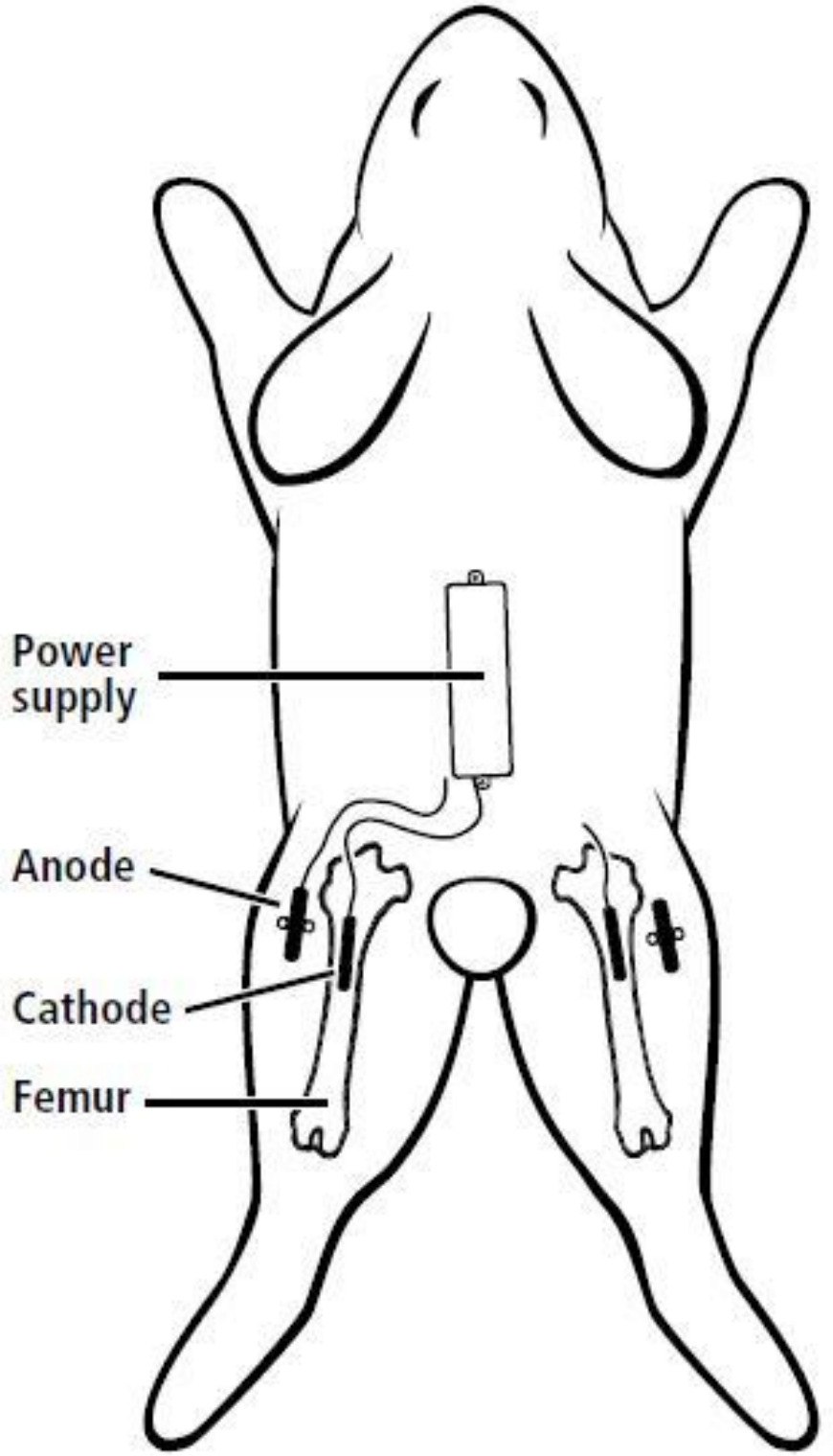

Figure 35: Schematic of the electrode placement in the rabbit model used for this investigation. Electrodes were placed in the right hind limb but were not attached to the battery pack and served as unstimulated control implants.

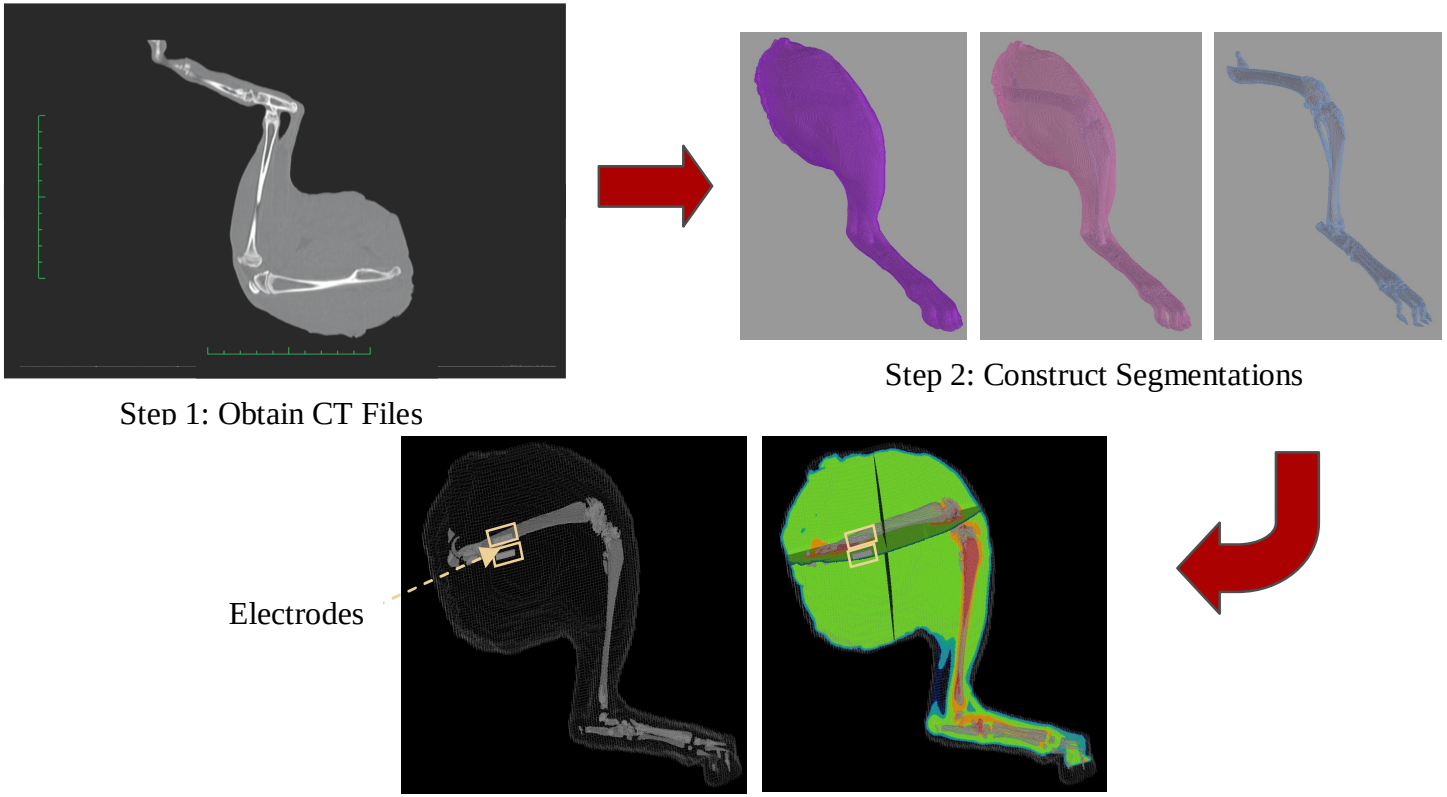

Figure 36: Stepwise demonstration of the rabbit model using FEA. Note the flow diagram is similar to the human model from Chapters 3 and 4 which required CTs, three-dimensional modeling and numerical approximations to determine the electric metrics.

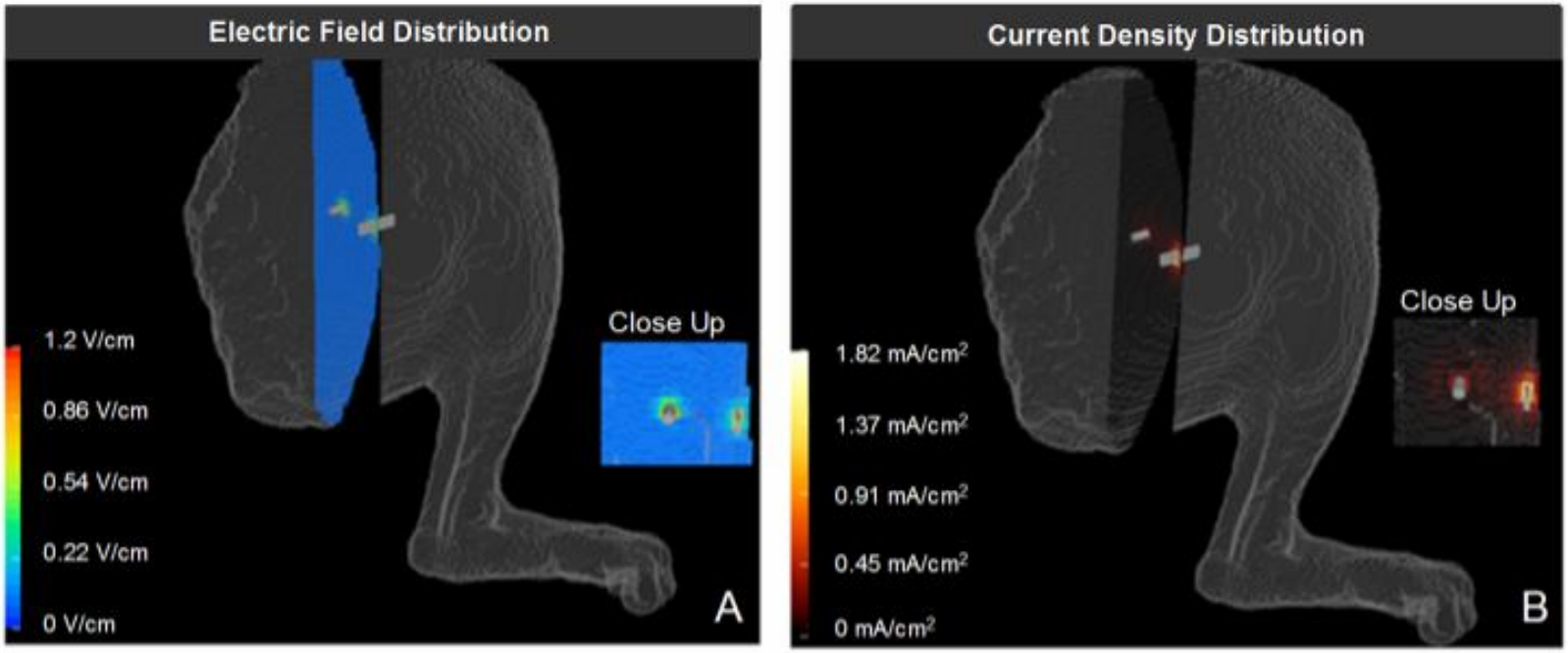

Figure 37: FEA was used to predict electric fields (A) and current densities (B) between the 2 electrodes prior to their implantation in the rabbit hind limb *in vivo*.

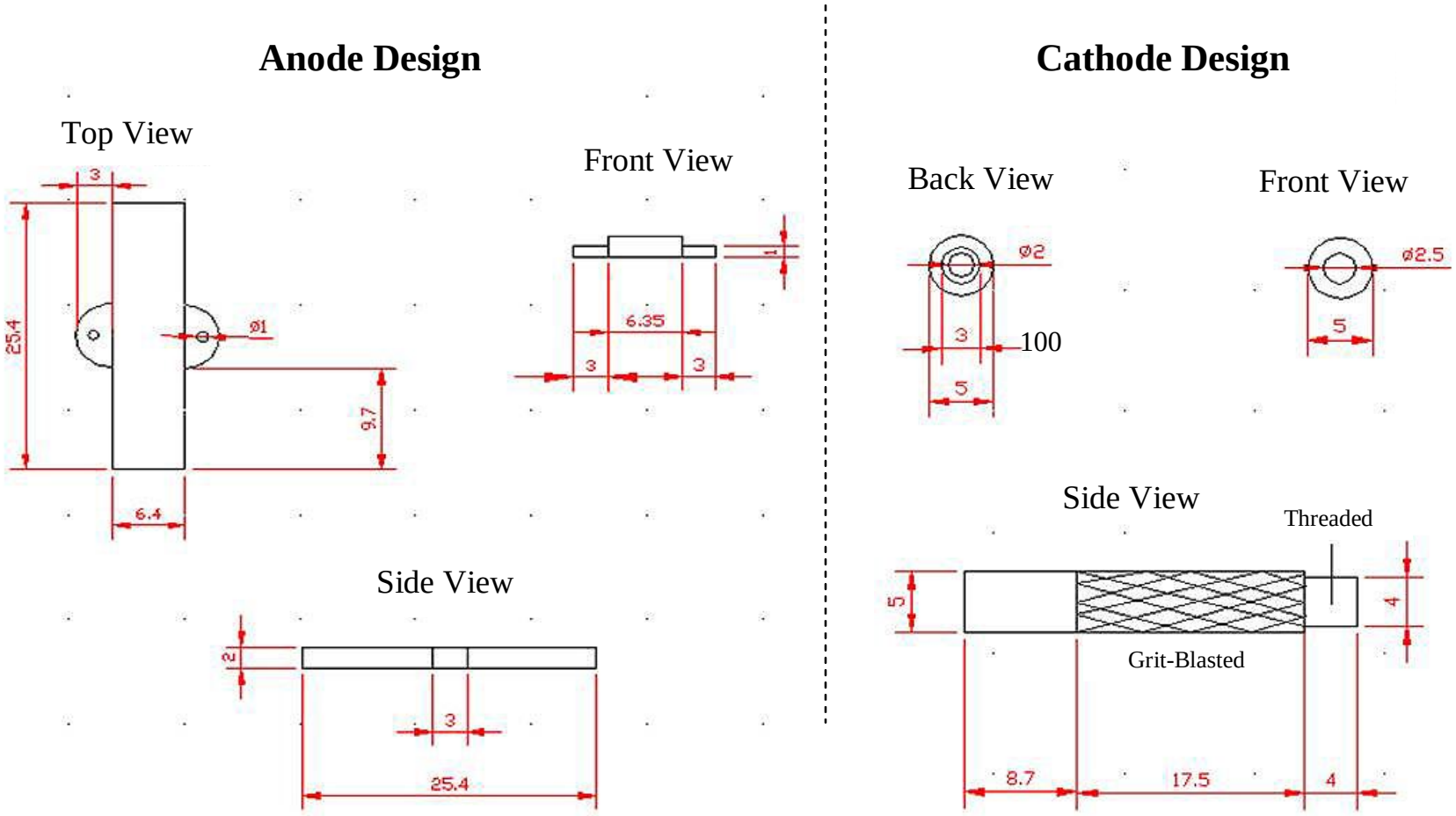

Figure 38: Computer aided drawing schematics of the designed implants for electrically induced osseointegration.

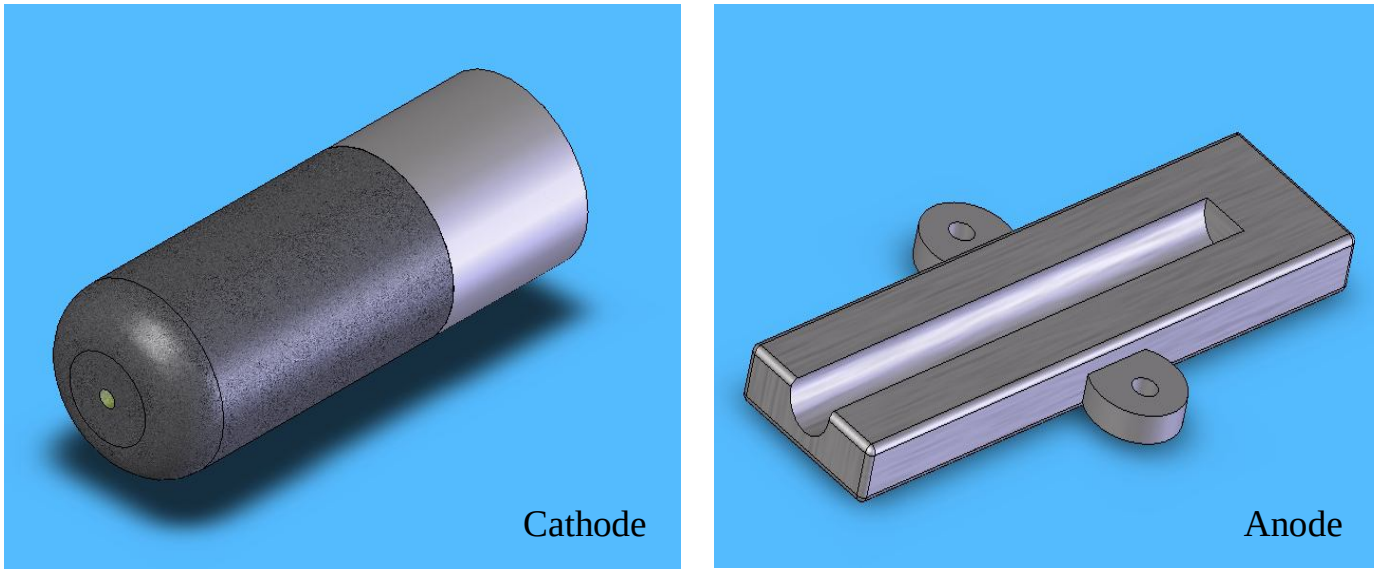

Figure 39: Three-dimensional models of the designed cathode and anode used for electrical stimulation. Note the grit-blasted region of the cathode (dark grey) which was performed to ensure skeletal attachment *in vivo*.

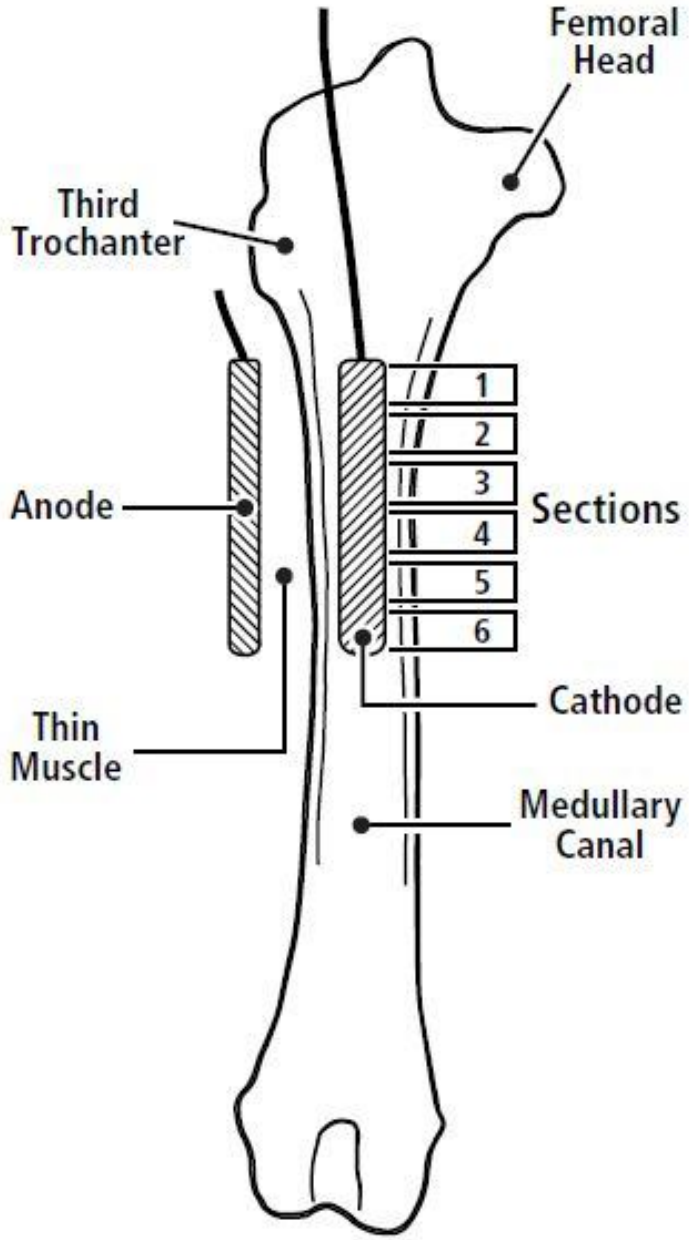

Figure 40: Implants were sectioned in 6 locations after PMMA embedment and were used for SEM analyses and BSE.

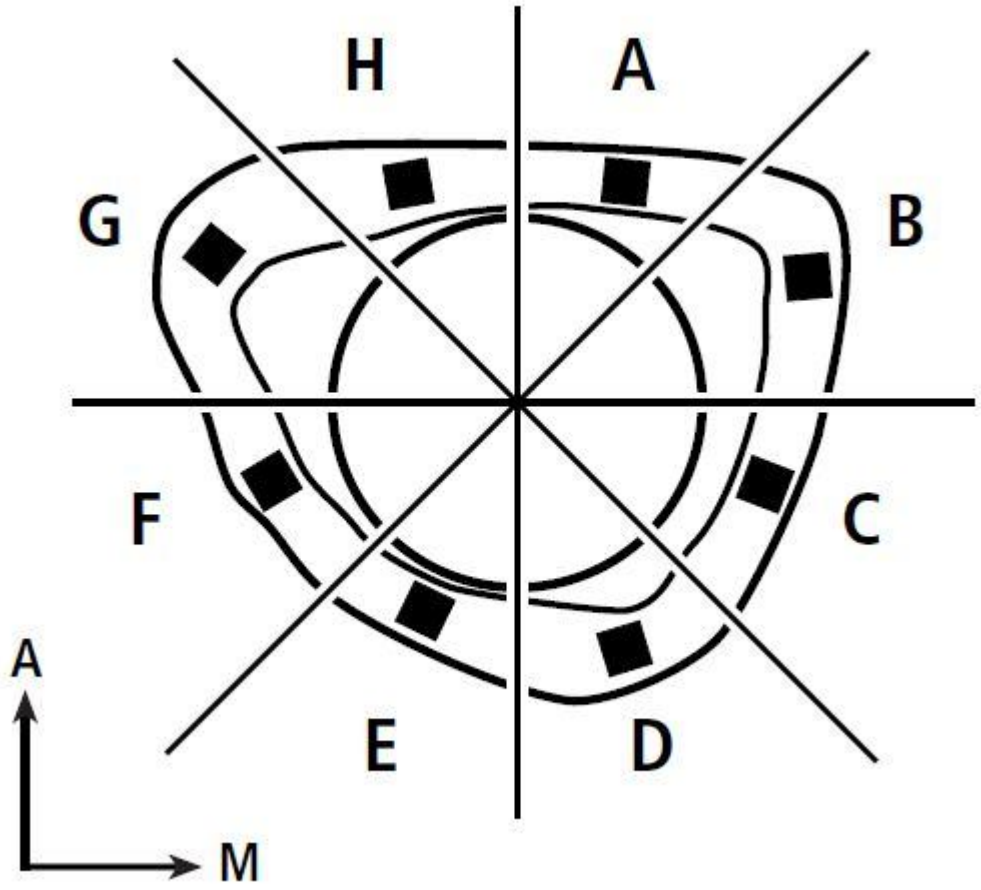

Figure 41: Eight quadrants were necessary to determine if cortical bone porosity was dependent on spatial positioning of the electrodes used to determine electrically induced osseintegration. The shaded regions above were designated as the focal areas for porosity evaluation. To ensure accurate comparisons, quadrants B and C were consistently directed medially (M), and quadrants A and H were positioned anteriorly (A) as noted in the picture orientation. The anode was positioned nearest to quadrants E and F and approximately 1.5 cm from the periosteum.

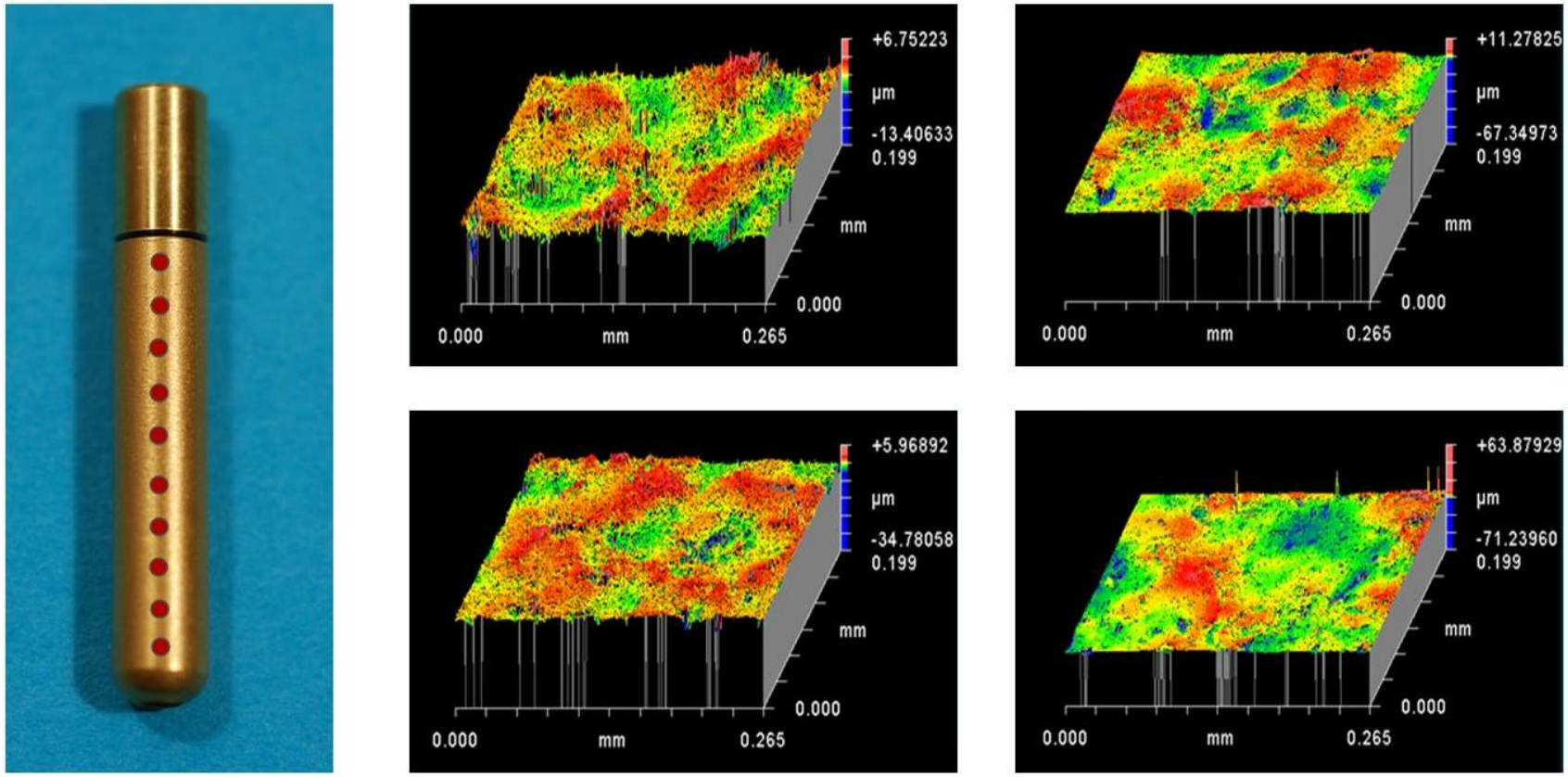

Figure 42: Optical profilometry was used to determine the Ra and topography of grit-blasted implants for the designed rabbit implant. The left image above indicates the 10 random data points sampled during analysis, while the figures to the right of the cathode demonstrates that 4 out of the 10 obtained surface profiles from the scanned surface.

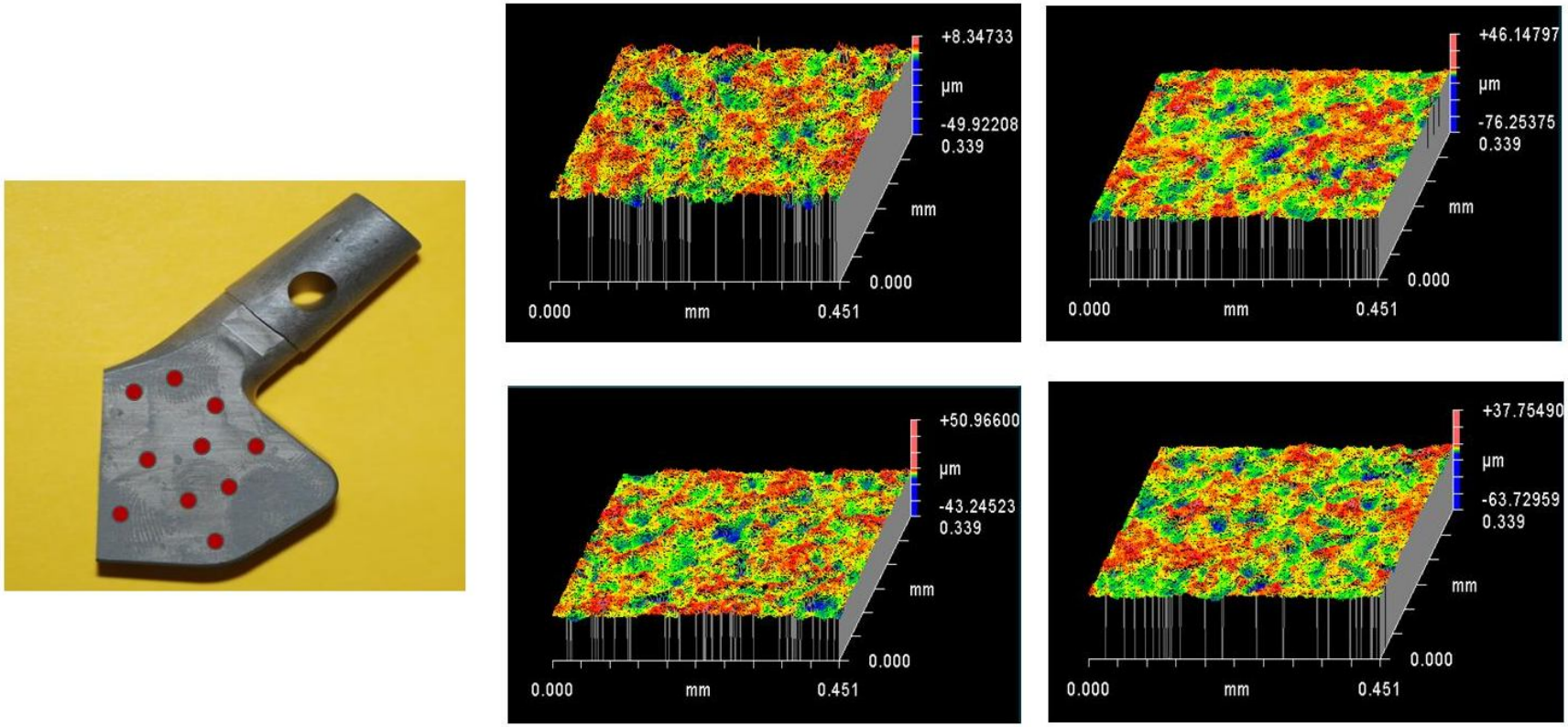

Figure 43: Optical profilometer measurements from the Zweymuller implant. Note the same protocol was used for this "gold standard" implant as the custom designed rabbit implant to ensure reproducibility.

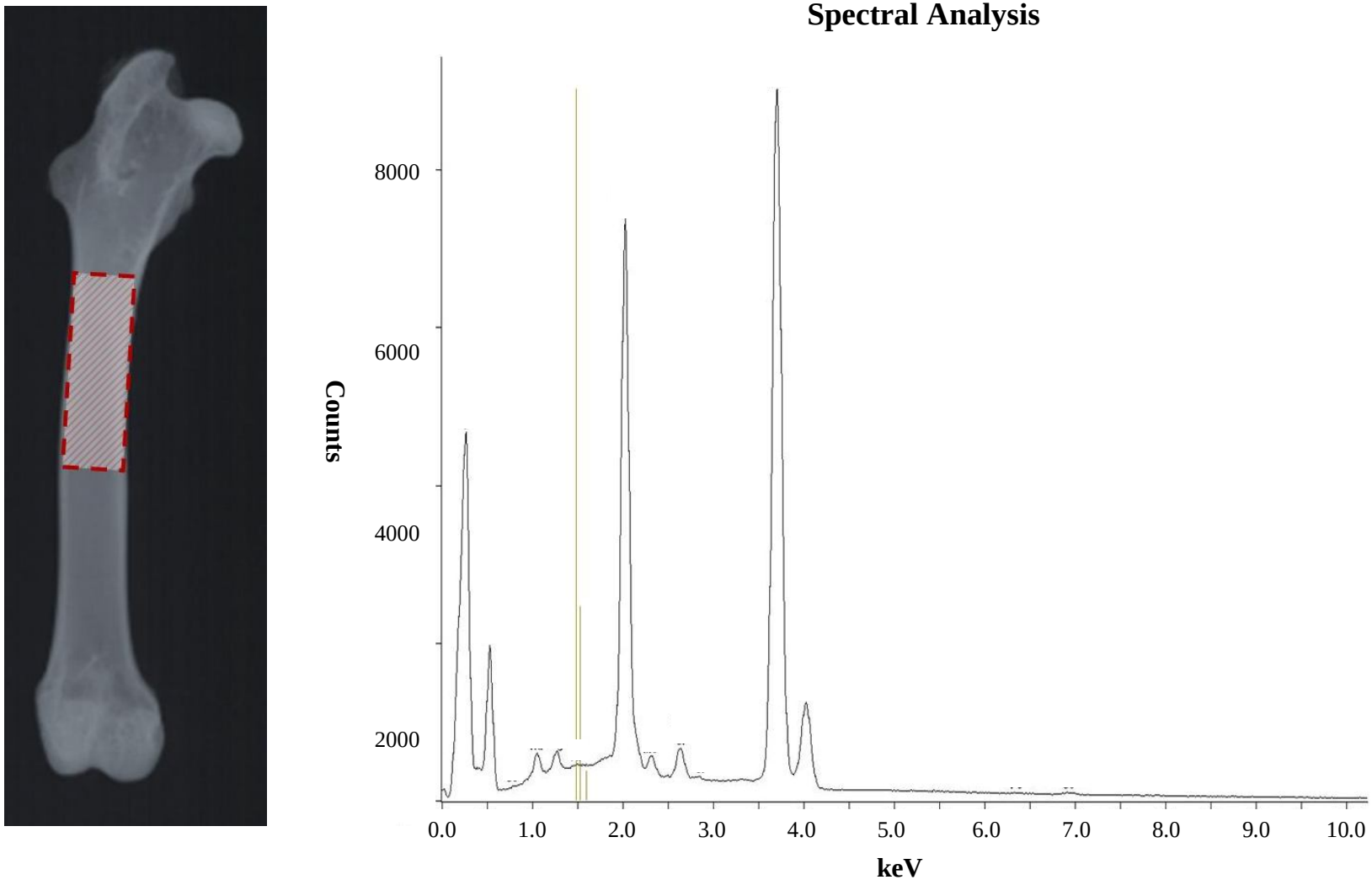

Figure 44: Spectral analysis performed on the host bone bed following implant impaction to determine the presence of liberated gold.

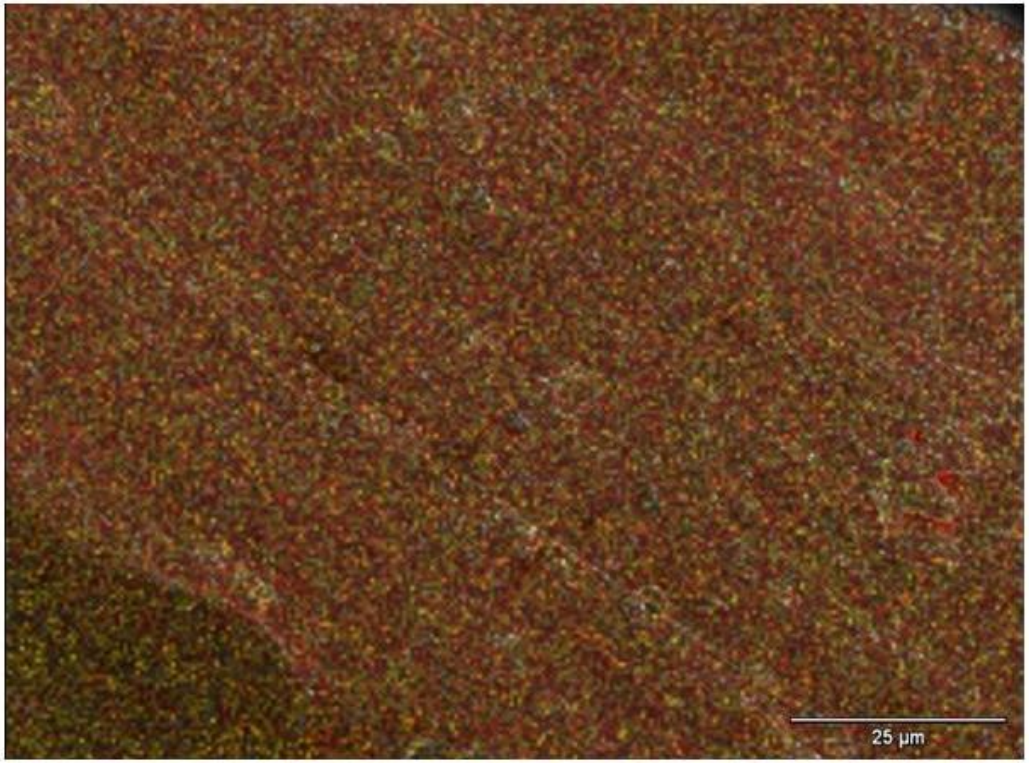

Figure 45: SEM spectral analysis confirmed that the surfaces of the electrodes were composed of a heterogenous mixture of gold, titanium, aluminum and vanadium.

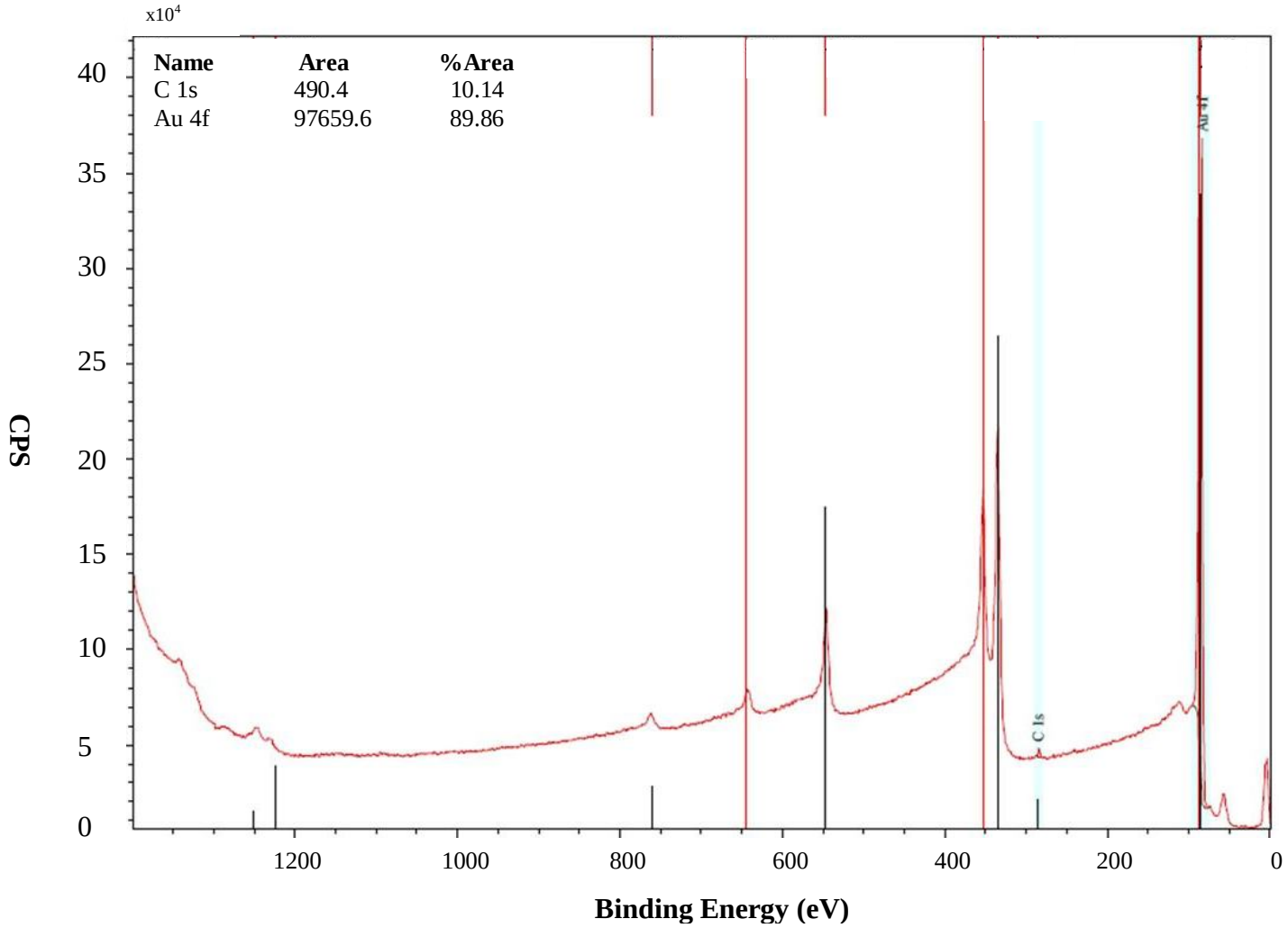

Figure 46: An XPS print graph indicated that the surface of the electrode consisted of only gold and carbon.

Figure 47: Representative diagram of the anode surface using the XPS and SEM analytical techniques. Note the XPS analytical tool demonstrated only gold on the surface of the electrodes, while the SEM determined the surface to be a combination of gold, titanium, vanadium and aluminum.

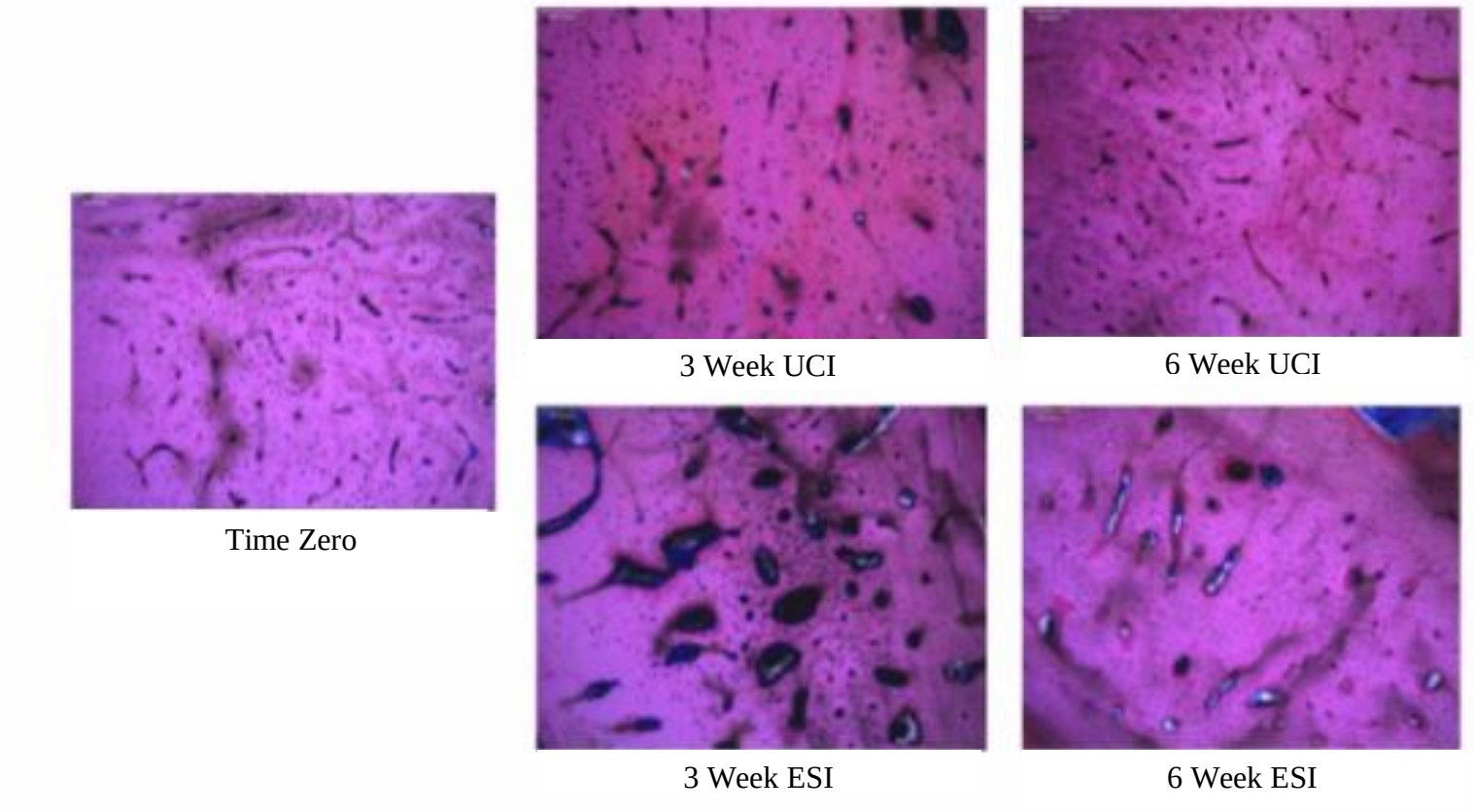

Figure 48: Discrepancies between the vascular cavities for each implant group were evident over the 3 designated time periods. The most prominent dissimilarity in vascular cavity size occurred within the ESI group in quadrants D, E and F as indicated with Sanderson's bone stain.

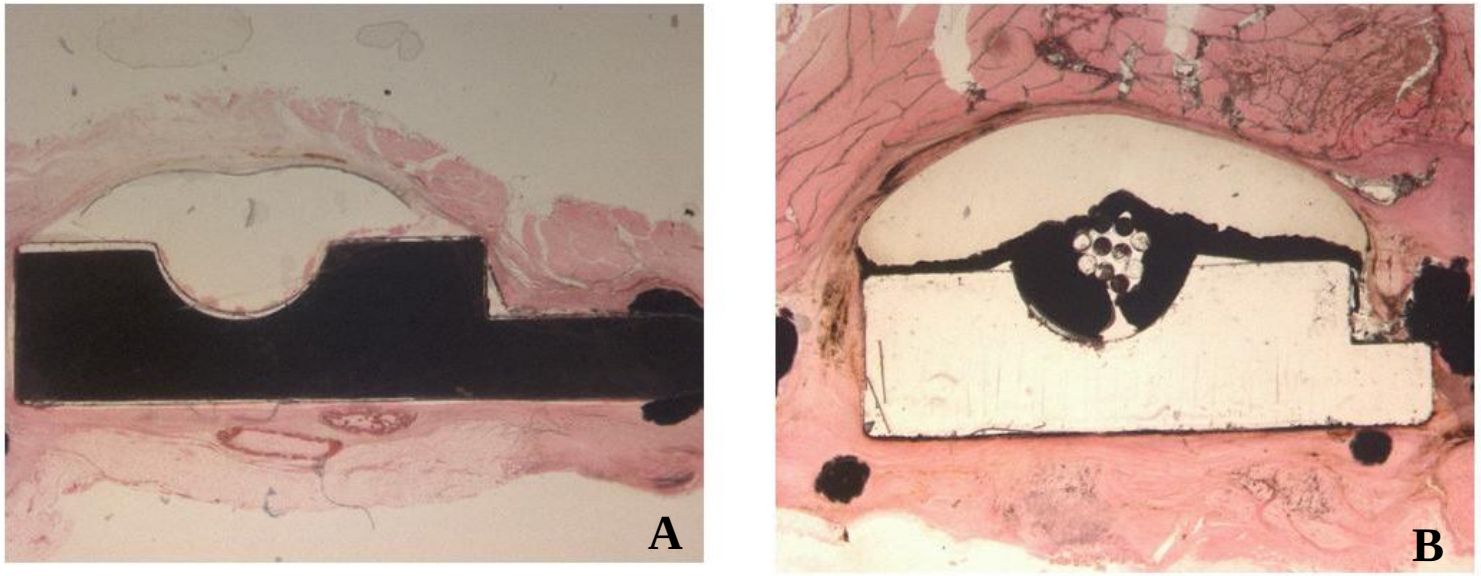

Figure 49: Cross section image of unstimulated control anode (A) and electrically stimulated anode (B) at 6 weeks. Note the apparent difference in corrosion which occurred in the ESI group due to localized electrochemical reactions as indicated by the H&E stain.

6 Week ESI Anode **6 Week UCI Anode**

Figure 50: Visible signs of electrode corrosion were noted on the surface of the electrically stimulated anode, which was not present on the control after 6 weeks *in vivo*.

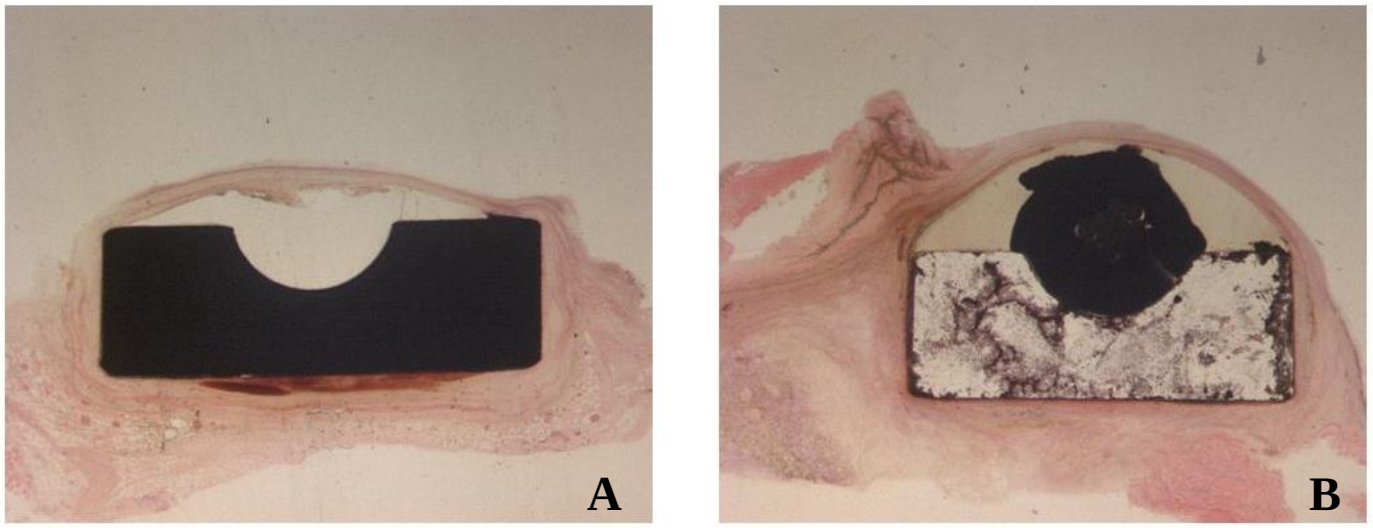

Figure 51: Cross section image of unstimulated control anode (A) and electrically stimulated anode (B) at 3 weeks. Note the presence of corrosion is minimal and not as prominent as the effect at 6 weeks.

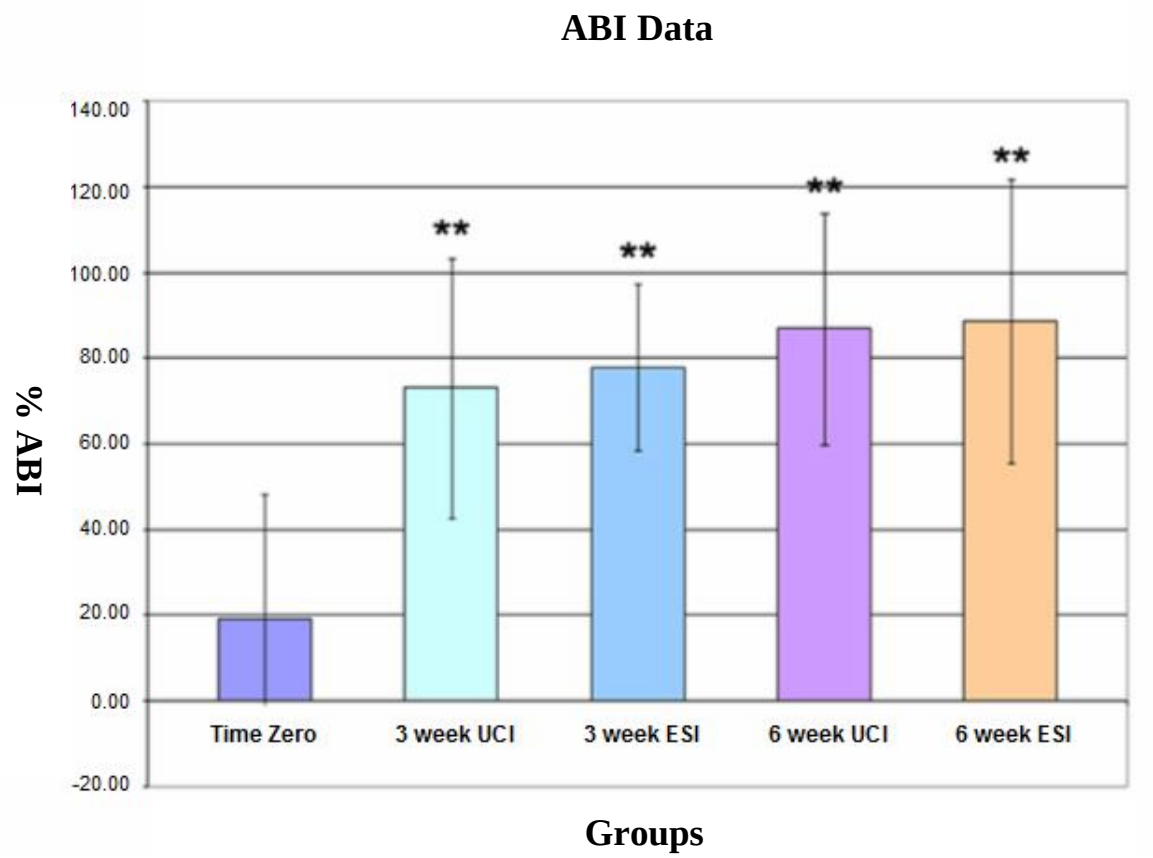

Figure 52: ABI percentages for each time period and group. Note the increase in bone-implant contact over time for each implant group but no difference between the ESI and UCI groups. (** represents $p<0.0001$ and error bars represent standard deviation)

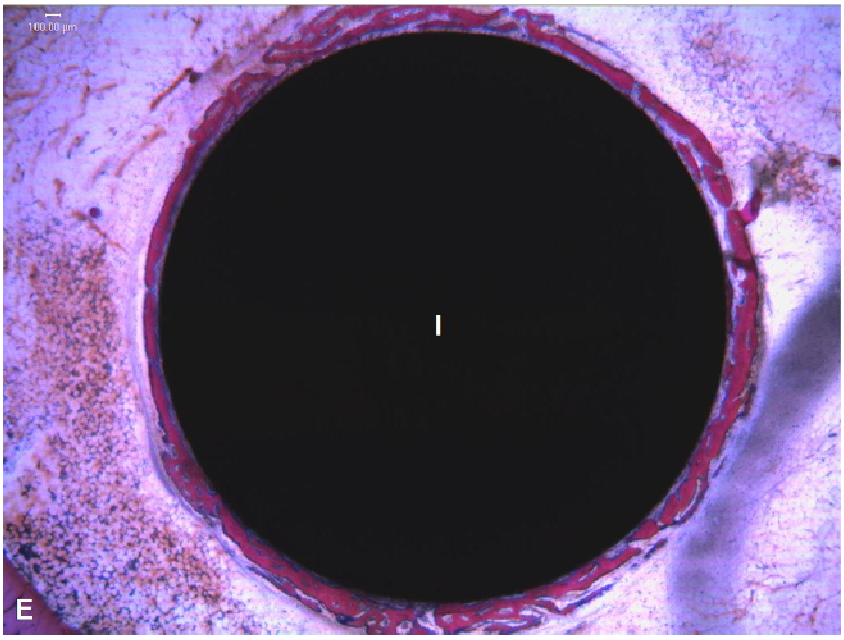

Figure 53: Qualitative image of bone ongrowth around the intramedullar implant (I) in the ESI group despite, in this case, being greater than 750 µm from the endosteal wall (E) as noted with Sanderson's bone stain.

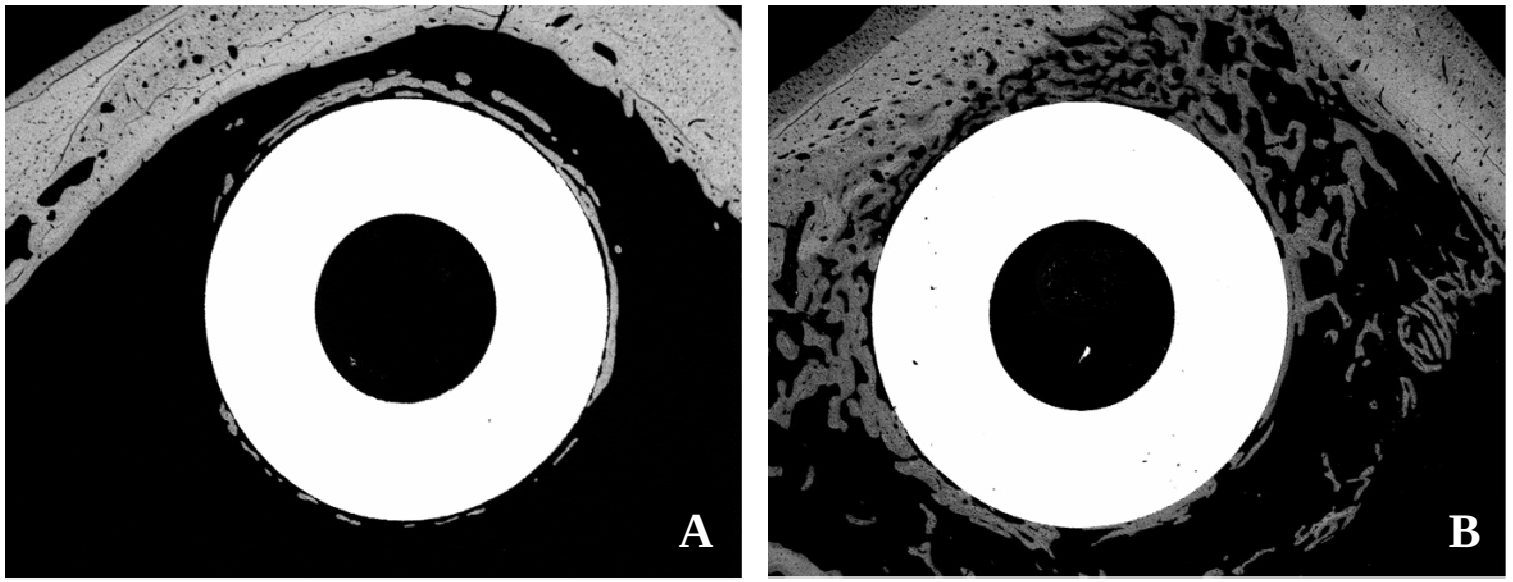

Figure 54: SEM images demonstrated reduced bone formation around the periphery of the UCI group (A) compared to the ESI group (B) for the same cross section in a 6-week animal.

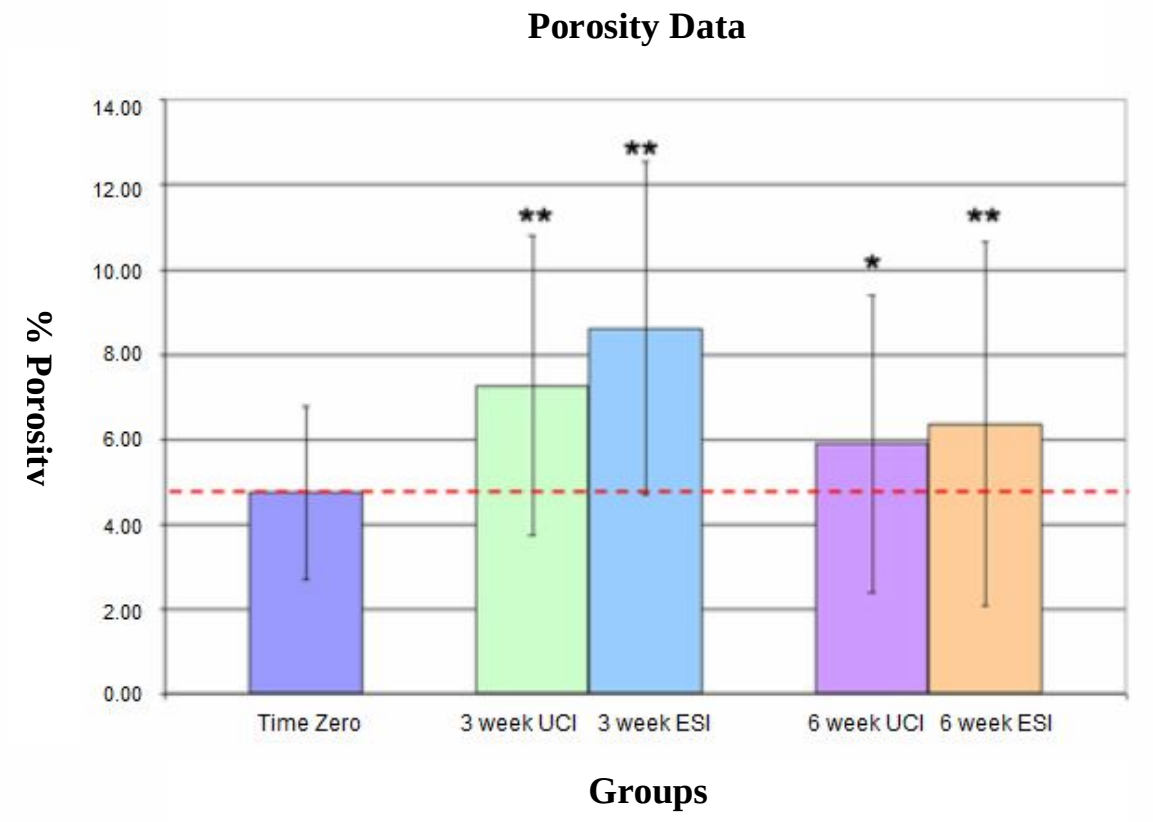

Figure 55: Overall porosity assessment for the 2 implant types (ESI and UCI) at each time period. Note the porosity at 6 weeks had not returned to baseline time zero values as indicated by the horizontal dashed line. (** represents $p<0.0001$, * represents $p<0.05$ and and error bars represent standard deviation)

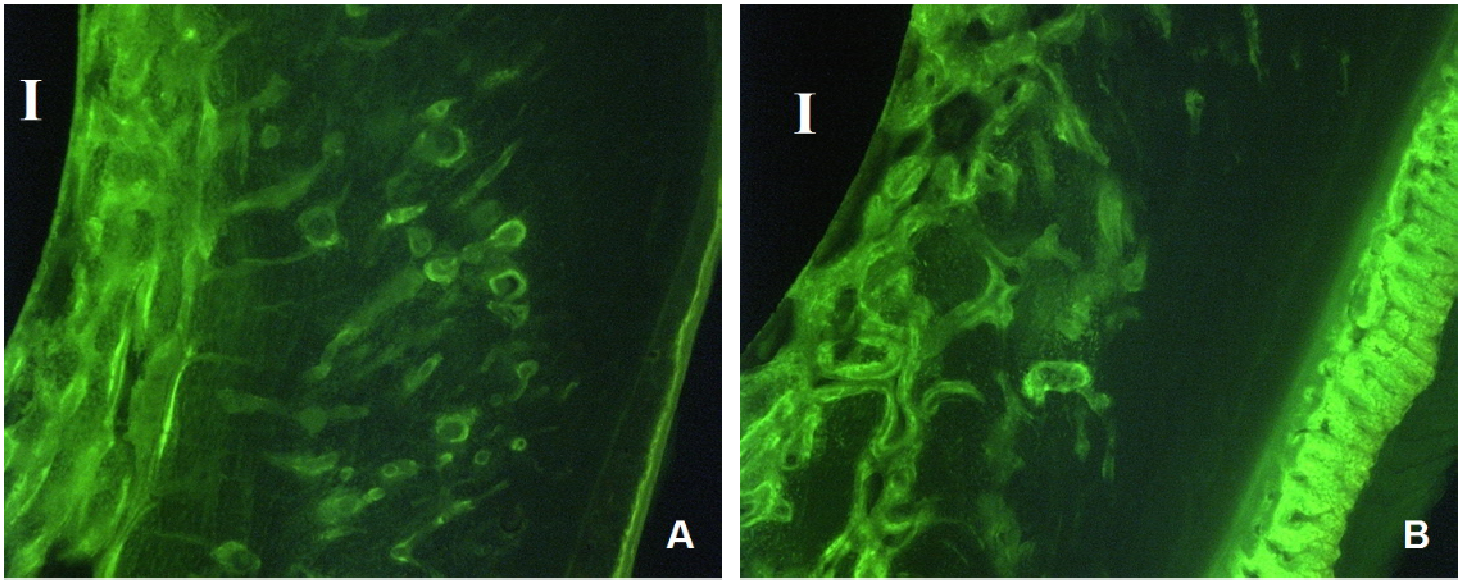

Figure 56: Flurochrome labeling demonstrated similar growth rates along the intramedullary implant (I) at 6 weeks, but a less pronounced periosteal effect in the UCI group (A) compared with the ESI group (B).

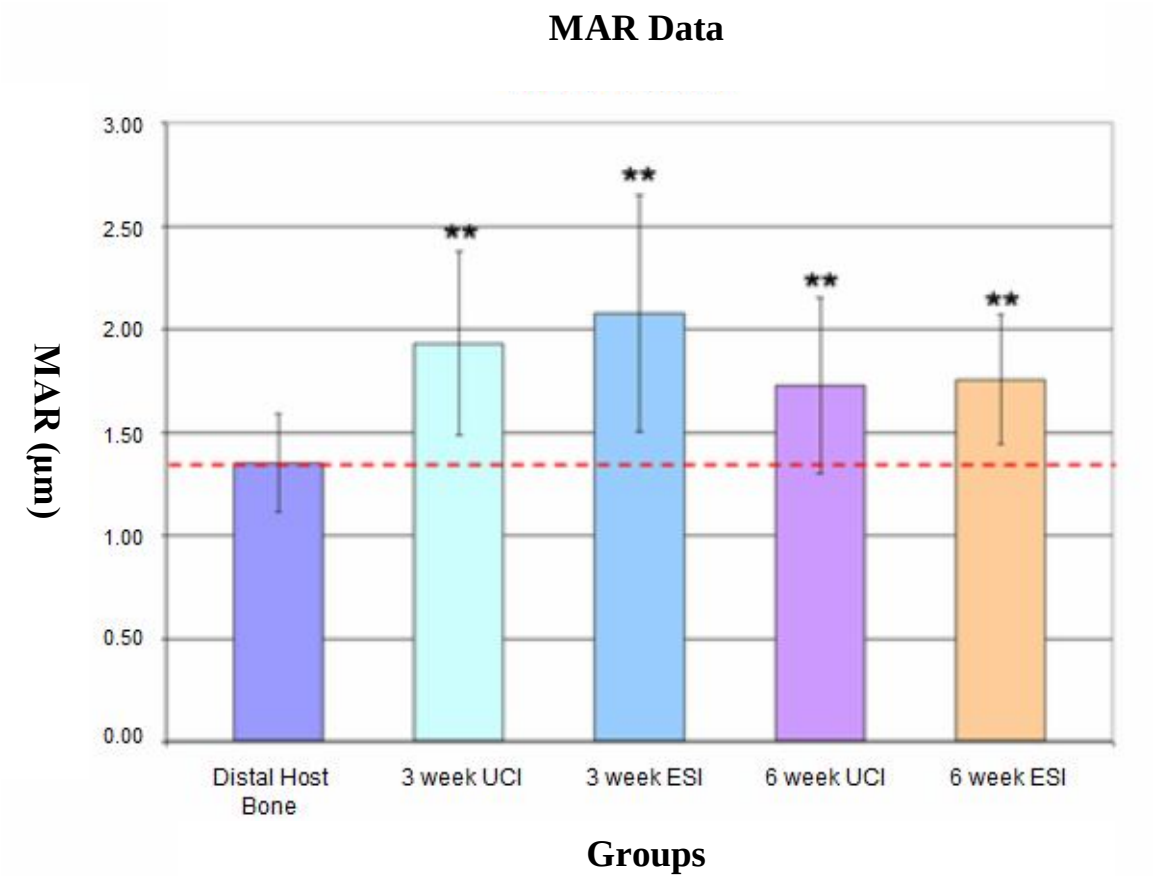

Figure 57: MAR in the distal host bone remote from the implantation site and periprosthetic cortical bone. Note that there were no differences between treatment groups (UCI and ESI). (** represents $p<0.0001$ and error bars represent standard deviation)

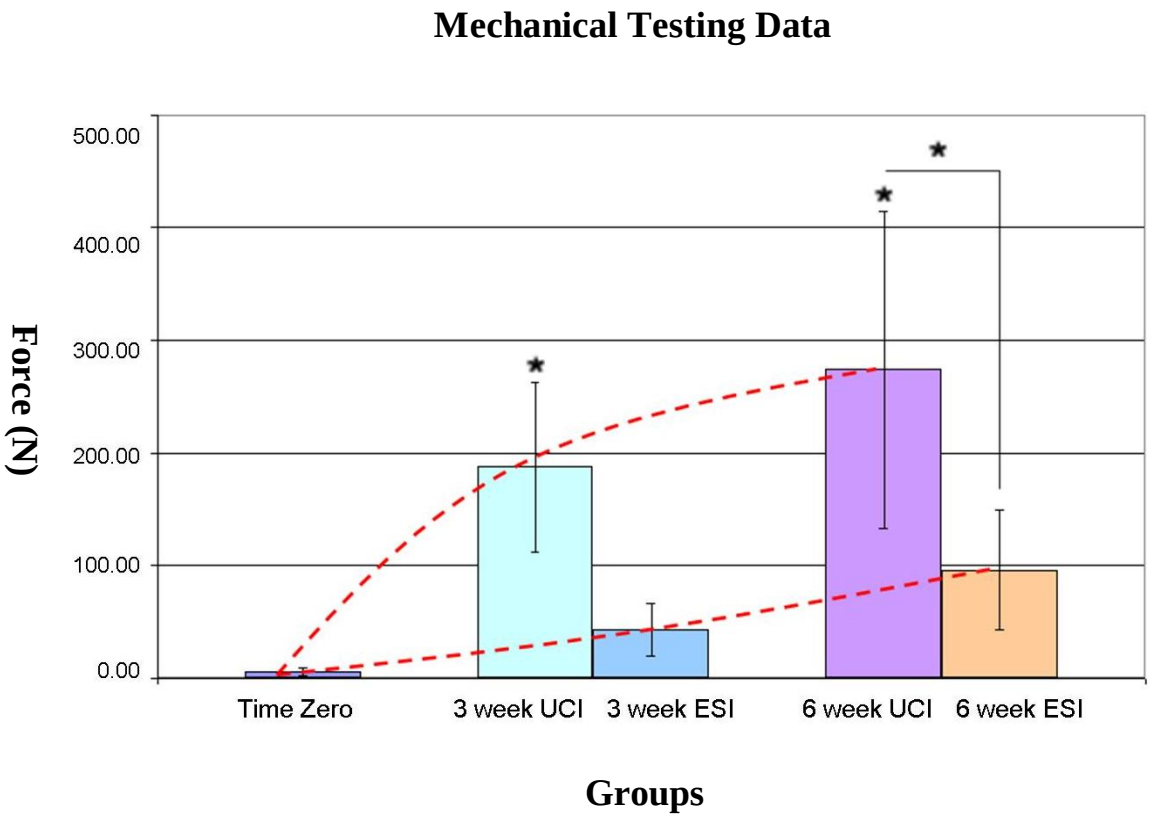

Figure 58: Mechanical push-out forces for the ESI and UCI groups. Note the exponential curve which has appeared to taper off in the UCI group but remains linear for the ESI group. (* represents $p<0.05$ and error bars represent standard deviation)

CHAPTER 7

CONCLUSIONS AND FUTURE RECOMMENDATIONS

7.1 Recommendations for Improving Model Predictability

Servicemen and women have been returning from combat with a higher percentage of amputations compared to other military conflicts[2] and require intensive follow-up care, extensive rehabilitation and expensive prosthetic services. The primary rehabilitation goal for these individuals has been to provide them with an expedited recovery and progressive reintroduction into the civilian or active duty population.[199] However, in order to continue to provide the best care for wounded service members, novel diagnostic tools and prosthetic devices must continue to be developed to address the many concerns and complications still present today.

Electrically based TOI offered a therapeutic alternative for accelerating rehabilitation regimens, as electrical stimulation has been well documented in the orthopaedic literature for repairing bony nonunions.[72] However, as demonstrated in fracture healing applications, variations in electrode size, placement, dosage and electric metric magnitudes (current density and electric field) have led to inconsistent success rates and have required a more predictive measure to ensure patient safety. Therefore, the

research in this dissertation utilized computer simulations and *in vitro* cell culturing as a transitional step to improve the likelihood of success prior to electrically induced TOI *in vivo*. Additionally, the idea of using an exoprosthetic attachment as a functional cathode to directly monitor electrical current at the bone-implant construct was a novel design principle which has not been investigated previously.

Critical assessment of the data collected from these experiments revealed that while electrical stimulation demonstrated efficacy using FEA and *in vitro* cell culturing, these initial observations did not improve osseointegration in the metaphyseal region of the rabbit femora. While electrical stimulation still appears to hold promise for improving suboptimal implant "fit and fill," the results from Chapter 6 demonstrated no distinct advantage when comparing the electrically stimulated implants to the untreated controls with respect to ABI, MAR and biomechanical testing. While these observations may initially appear discouraging, the discrepancy between the predicted and observed degree of osseointegration may have resulted from several factors which may be correctable in follow-up studies. Potential sources of error in this experiment may have occurred from (1) the hierarchical modes assembled for FEA, (2) the conductivities assigned to the thresholded tissues and (3) the electrode materials selected for *in vivo* use. Future adjustments with respect to these issues may improve the result of electrically induced TOI and each topic has been addressed in more detail below.

7.1.1 Hierarchal Thresholded Models

Three-dimensional hierarchical models were created using a thresholding software package for mesh generation and FEA. To ensure clear distinction between

tissue types and to make certain of proper tissue geometry and spatial position (Figure 11), CT scans were selected as the imaging modality.[246] However, the IRB-approved protocol used in Chapters 3 and 4 allowed only the inclusion of retrospective CTs. Therefore, the models developed for assessing the feasibility of electrically induced TOI in service member residual limbs was limited to a 6-layer segmentation, consisting of bone, bone marrow, musculature, adipose tissue, skin and internal organs. Similarly, the IACUC-approved protocol used in Chapter 6 allowed CT imagining from only post-mortem disarticulated rabbit limbs and provided a 4-layer model for experimentation consisting of bone, bone marrow, musculature and skin. Because CT scans were restricted to retrospective and postmortem review, both the human and animal studies could not be performed using contrast agents for illuminating arterial and venous pathways. Adding vascular networks in these model segmentations may have altered the localized electric field and current density magnitudes at the periprosthetic bone, and subsequently changed the voltage selected for this model since it has been well regarded that the hydrated fluid around bone is 80 times less resistive than bone itself.[140] Therefore, increasing the sensitivity of the segmented hierarchical models in future may reduce model error and improve the translation between FEA and the established rabbit model.

7.1.2 Tissue Conductivity

Model predictability may have also improved by altering the designated tissue conductivities selected prior to FEA. While each segmented tissue was assigned conductivity values based on recorded measurements in the peer-reviewed literature (Table 4), all tissue types were treated as piecewise, ohmic and isotropic for ease of

computation modeling. However, this assumption has been known to be both anatomically and bioelectrically incorrect, as bone, for example, has been reported as 100% more resistive in the circumferential direction compared to the longitudinal direction.[98]

As demonstrated in Chapter 3, the distal residual limb and myodesis and tenodesis procedures highly affected localized field strengths with electrically induced TOI. However, one limitation with using CTs for model reconstruction was that this technique did not provide tissue fiber orientation, so it was assumed that all musculature was in a longitudinal pattern and conductivity was set to be 0.25 S/m (Table 4). This assumption may have accounted for some of the error in model predictability, as a transverse muscle orientation may have been feasible and would have decreased tissue conductivity to 0.15 S/m. Preliminary computer modeling (unpublished data) was conducted after these experiments to determine the effect of changing the muscle fiber orientation in the distal residual limb from a longitudinal to a transverse pattern, and data indicated that the maximum electric field magnitude at the bone-implant interface would have been reduced from 4.1 V/cm to 3.2 V/cm and may have influenced the potential difference selected for clinic implementation of electrically induced TOI (Figure 59).

7.1.3 Electrode Materials

One final area for improving model predictability may have resulted from altering the electrodes selected for electrical stimulation in the rabbit experiment, as there was visible corrosion around the ESI anodes (Figures 49-51). When selecting a material for electrically induced osseointegration, Venugopalan and Ideker recommendations were

followed by considering (1) electrode geometry and surface area, (2) the quantity of charge and electrical current for the given application, (3) the environmental conditions where the electrodes will be implanted and (4) engineering of the electrodes (cost, strength and availability).[228] To ensure that the electrode material was conducive for cementless skeletal attachment, a titanium alloy-gold surface was used for electrically induced TOI. However, as noted in Chapter 6, electrically stimulated implants did not improve the quality or quantity of the host bone-implant interface unless the cathode was not within approximately 750 μm from the endosteal wall. Histological assessment from a pathologist, blinded to the specimen source, confirmed this observation and also indicated that tissue degradation around the anode site occurred, which may have been the result of hydrogen ion generation during the electrochemical reaction *in situ*.

It is important to note that while this specific experiment using FEA and *in vitro* cell culturing did not improve electrically induced TOI *in vivo*, alterations to electrode material and numerical approximations may be overcome in future studies. Modifications to the electrodes may improve biological acceptance of electrical stimulation. Traditional electrodes used for intracortical stimulation, intramuscular activation, neural prosthetics and cardiac pacemakers have been fabricated from platinum, platinum-iridium, stainless steel, nickel-cobalt, titanium and tantalum,[228] and may serve as alternative electrode types for electrically induced TOI. In order to provide clarity for the electrode materials available in future applications, a brief description of each material has been included in sections 7.1.3.1 to 7.1.3.3.

7.1.3.1 Platinum and Platinum-Iridium

Platinum has been reported as the most popular electrode material used for biomedical applications because it is a noble metal and is therefore stable, inert and very corrosion resistant when placed in the human body.[228] However, while platinum has optimal electrical characteristics, this metal has been known to be very costly for electrode fabrication and may be easily damaged due to the softness of the material.[228] Therefore, platinum has often been combined with iridium (approximately iridium 2-30%) to form platinum-iridium, a more cost-effective, stiffer electrode, suitable for intracortical stimulation. Fabricating the anode in the rabbit experiment (Chapter 6) from a platinum-iridium electrode would have undoubtedly improved corrosion resistance, since this material type has demonstrated surface stability up to 150 $\mu C/cm^2$.[228]

7.1.3.2 Stainless Steel and Nickel-Cobalt

Stainless steel and nickel-cobalt have been regarded as useful electrode materials for intramuscular activation, as these alloys have higher fatigue properties than that of platinum or platinum-iridium.[228] However, one limitation of stainless steel and nickel-cobalt electrodes is that these materials cannot inject higher than 40 $\mu C/cm^2$, otherwise corrosion has been noted to occur.[228] Therefore, utilizing these electrode materials for electrically induced TOI may be possible, but calculations would have to be performed to ensure that the size of the electrodes and electrical charge in the TOI system did not exceed manufacturing specifications.

7.1.3.3 Titanium and Tantalum

Titanium and tantalum have been used previously in neural prosthetic applications when capacitive electrodes have been required.[228] Capacitive electrodes have been known to function by injecting charge into a system without faradic reactions at the electrode-electrolyte interface. While titanium and tantalum have been regarded as excellent metals for orthopaedic applications due to the presence of an oxide layer and overall good biocompatibility,[183,184,247,248] this material did not allow for electrical current flow in an early pilot study using a carcass rabbit and would most likely not improve electrically induced TOI using this specific model.

7.2 Future Electrical Stimulation Applications for Older Veterans

While electrical stimulation was only experimented in young healthy service members with retrospective CTs (Chapters 3 and 4), it is well known that older veterans may advocate for a TOI, and with further refinement, require an electrical stimulation device to attach to their exoprosthetic to maintain healthy bone stock. Therefore, utilizing electrical stimulation for older amputees has remained a critical aspect which must be explored as well. Bone mass has been reported to be maximum a decade after skeletal growth ceases, but decreases significantly by the eighth and ninth decade.[115] As long bones change confirmation with age, the endosteal diameter tends to increase more rapidly than the periosteal diameter which may lead to TOI loosening.[94] This problem coupled with the reduction of strain on bones by weaker muscles may contribute to debilitating diseases such as osteoporosis and osteopenia,[94] and may require additional treatment options for older veterans. However, controlled electrical stimulation and

mechanical loading may act as a synergistic catalyst of bone ingrowth[105] and maintain host bone bed integrity with elderly patients using an osseointegrated electrical implant system.

To determine the influence of cortical aging on electrically induced TOI, a pilot study (unpublished data) was conducted using FEA. To simulate an older veteran who may advocate for osseointegration technology, bone conductivity was decreased from 0.02 S/m to 0.01 S/m, since both bone mineral density and hydration have been known to decrease with age while bone mineral content has been known to increase with age and would subsequently increase bone resistivity.[117] Results from this preliminary model indicated that a 14% ± 8.5% increase in the localized periprosthetic electric field may be expected with aging and require future investigations, especially since having a TOI would be a lifelong commitment (Figure 60).

7.3 Potential Options for Improving Electrical Stimulation

In order to advance the current state of the art in electrical stimulation, improved diagnostic tools will be necessary for accurately characterizing tissue conductivities. Experimental calculations have been known to provide a range of expected field strengths. However, current densities may only be "crudely estimated" without the use of FEA,[136] since the dielectric constant and conductivity of tissue has not been well characterized and accurately measuring field strengths inside living organisms *in vivo* has remained challenging.[173] Better understanding of electrical current pathways through biological tissue will undoubtedly improve volume conductor models and FEA simulations for future work with assisting our wounded service members. However, researchers must

ensure that current density and not electrical current has been accounted for on a patient-specific basis. While FEA cannot conclusively forecast the success of electrically induced osseointegration, the ability to monitor anticipated field strengths prior to *in vivo* use will help assure that current densities are sufficiently low to not cause patient complications.

Lastly, developing computer simulations which predict changes in electrical power due to age, activity level and fibrous encapsulation would provide tremendous insight into the bioelectric dynamics for future device development. FEA models currently generated for electrically enhanced osseointegration use a quasi-static approach which cannot predict field strengths over time. Creating more detailed FEA simulations, adhering to suggestions in section 7.1 and using implantable sensors will provide more accurate representations of the voltage gradients which occur at the periprosthetic interface to achieve successful electrically induced TOI in the future.

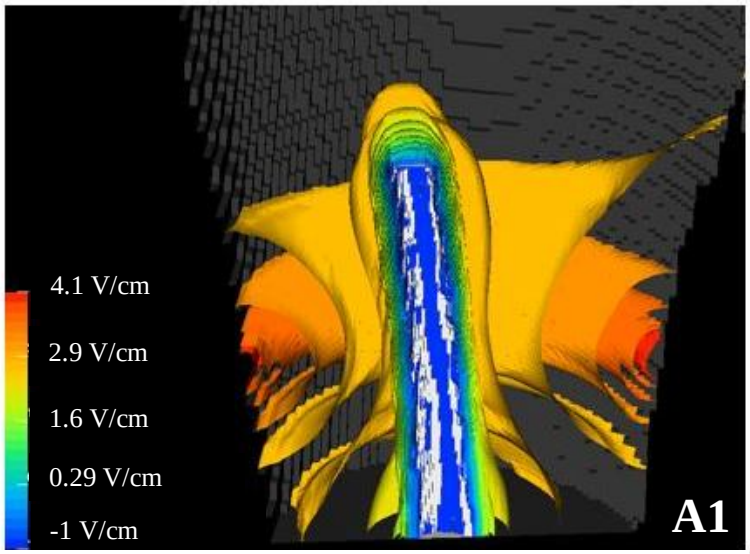

Electric Field 3D Representation:
Subject 1 Longitudinal Muscle

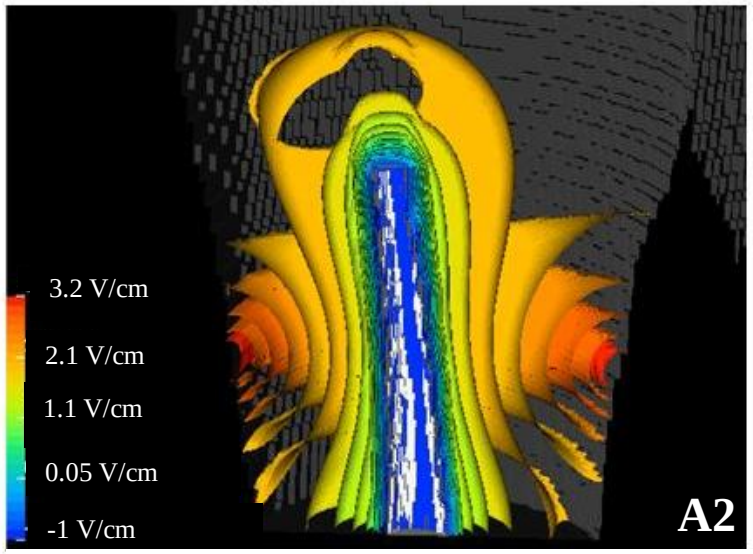

Electric Field 3D Representation:
Subject 1 Transverse Muscle

Figure 59: Comparative analysis of the electric field strengths (A1 and A2) and distributions (B1 and B2) based on the assumption that muscle pattern was longitudinal and not transverse in the distal residual limb during FEA.

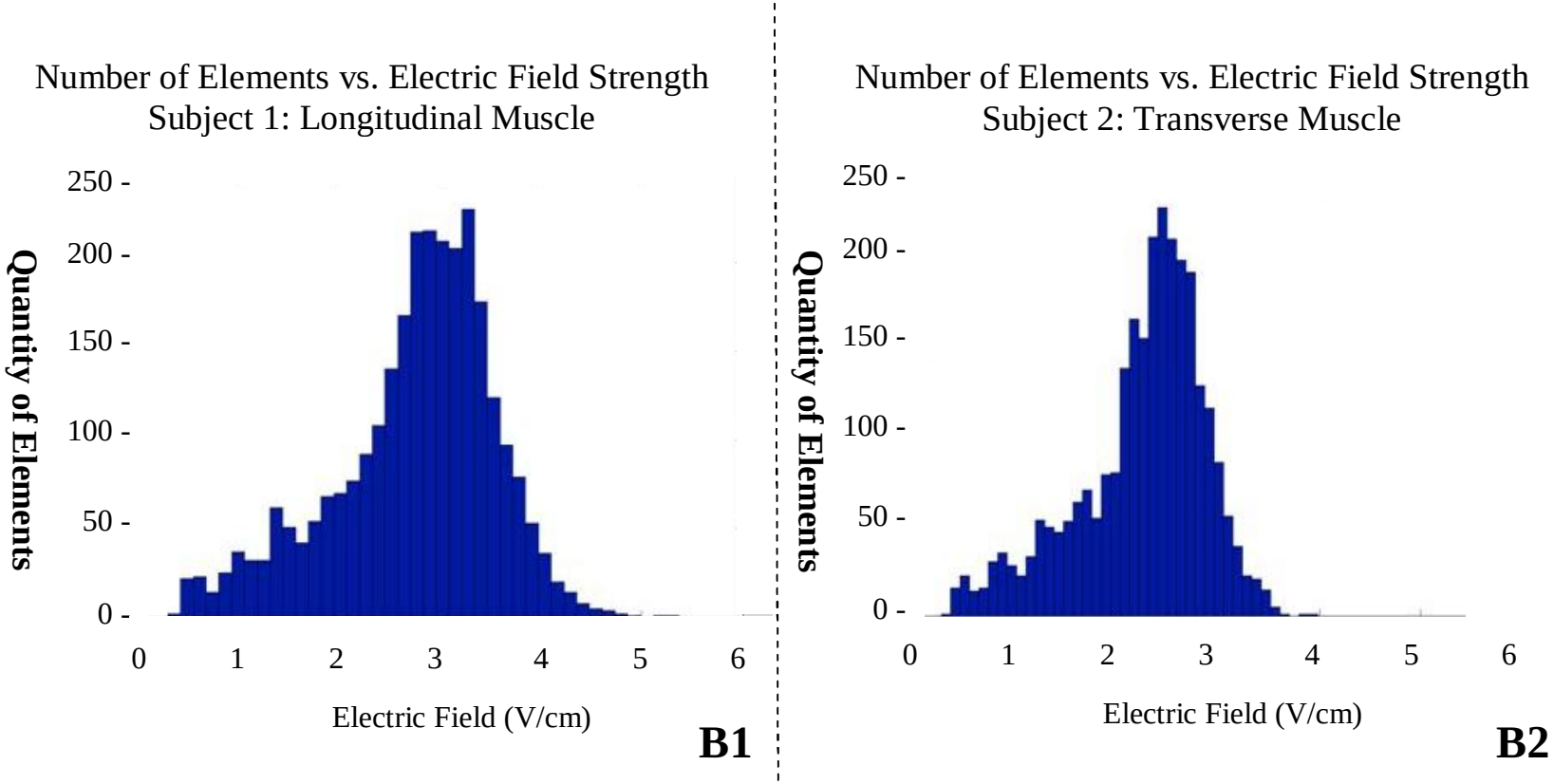

Figure 59: Continued

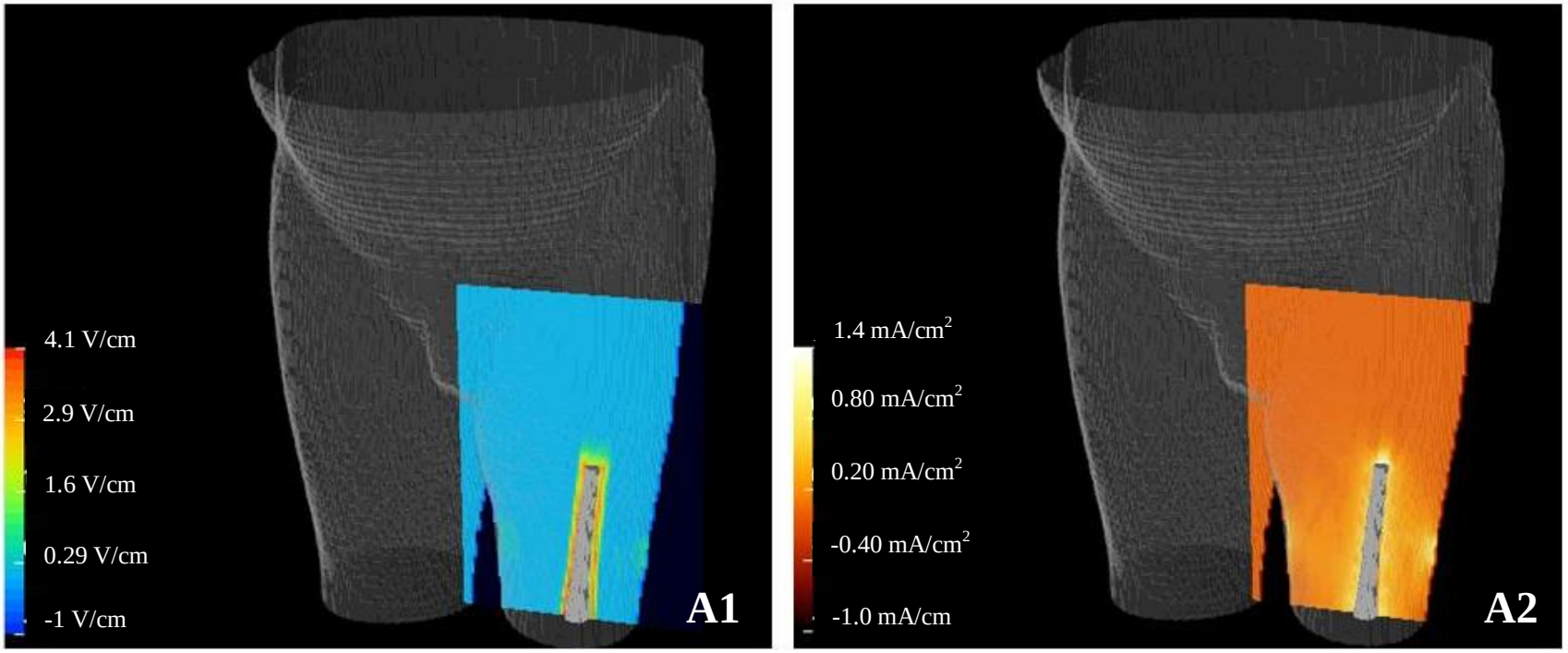

Figure 60: Comparison between a young (A1 and A2) and elderly (B1 and B2) amputee with electrically induced osseointegration. To represent the known cortical aging process, which involves an increase in bone mineral content and decrease in both bone mineral density and hydration, the conductivity of bone was decreased from 0.02 S/m to 0.01 S/m.

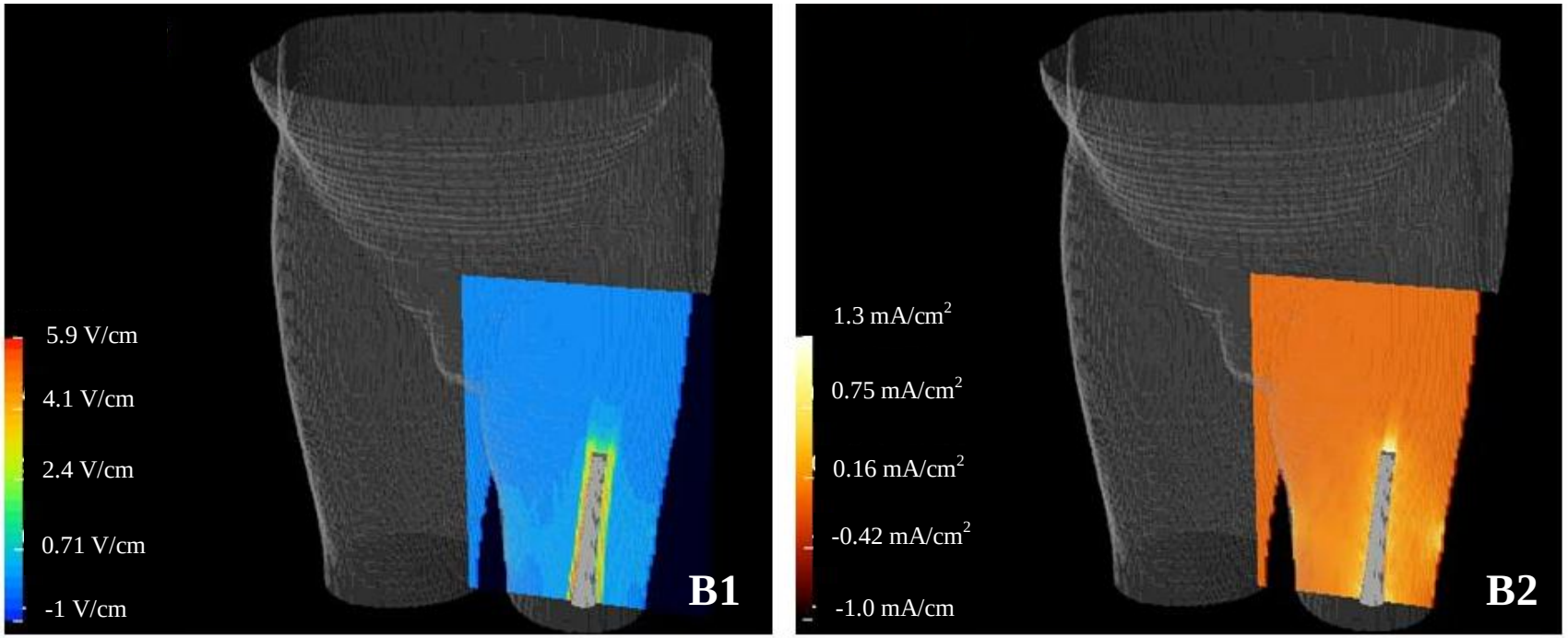

Figure 60: Continued

REFERENCES

1. Gajewski D, Granville R. The United States Armed Forces Amputee Patient Care Program. J Am Acad Orthop Surg 2006;14(10 Spec No.):S183-7.

2. Potter BK, Scoville CR. Amputation is not isolated: An overview of the US Army Amputee Patient Care Program and associated amputee injuries. J Am Acad Orthop Surg 2006;14(10 Spec No.):S188-90.

3. Pasquina PF, Tsao JW, Collins DM, Chan BL, Charrow A, Karmarkar AM, Cooper RA. Quality of medical care provided to service members with combat-related limb amputations: Report of patient satisfaction. J Rehabil Res Dev 2008;45(7):953-60.

4. Atesalp AS, Erler K, Gur E, Koseglu E, Kirdemir V, Demiralp B. Bilateral lower limb amputations as a result of landmine injuries. Prosthet Orthot Int 1999;23(1):50-4.

5. Pasquina PF. Optimizing care for combat amputees: Experiences at Walter Reed Army Medical Center. J Rehabil Res Dev 2004;41(3B):vii-xii.

6. Thurston AJ. Pare and prosthetics: The early history of artificial limbs. ANZ J Surg 2007;77(12):1114-9.

7. Marks LJ, Michael JW. Science, medicine, and the future: Artificial limbs. BMJ 2001;323(7315):732-5.

8. Esquenazi A. Amputation rehabilitation and prosthetic restoration. From surgery to community reintegration. Disabil Rehabil 2004;26(14-15):831-6.

9. Barber CG. The detailed changes characteristic of healing bone in amputation stumps. J Bone Joint Surg 1930;12:353-359.

10. Barber CG. Immediate and eventual features of healing in amputated bones. Ann Surg 1929;90(6):985-92.

11. Todd TW, Barber CG. The extent of skeletal change after amputation. J Bone Joint Surg Am 1934;16:53-64.

12. Frost H. Mechanical determinants of bone modelling. Metab. Bone Dis. Rel. Res. 1982;4:217-229.

13. Burke MJ, Roman V, Wright V. Bone and joint changes in lower limb amputees. Ann Rheum Dis 1978;37(3):252-4.

14. James U, Oberg K. Prosthetic gait pattern in unilateral above-knee amputees. Scand J Rehabil Med 1973;5(1):35-50.

15. Jaegers SM, Arendzen JH, de Jongh HJ. Changes in hip muscles after above-knee amputation. Clin Orthop Relat Res 1995;319:276-84.

16. Messier SP, Gutekunst DJ, Davis C, DeVita P. Weight loss reduces knee-joint loads in overweight and obese older adults with knee osteoarthritis. Arthritis Rheum 2005;52(7):2026-32.

17. Kulkarni J, Adams J, Thomas E, Silman A. Association between amputation, arthritis and osteopenia in British male war veterans with major lower limb amputations. Clin Rehabil 1998;12(4):348-53.

18. Jaegers SM, Arendzen JH, de Jongh HJ. Prosthetic gait of unilateral transfemoral amputees: A kinematic study. Arch Phys Med Rehabil 1995;76(8):736-43.

19. Dillingham TR, Pezzin LE, MacKenzie EJ, Burgess AR. Use and satisfaction with prosthetic devices among persons with trauma-related amputations: A long-term outcome study. AM J Phys Med Rehabil 2001;80(8):563-71.

20. Levy SW. Skin problems in the amputee. In: Smith DG, Michael JW, Bowker JH, editors. Atlas of Amputations and Limb Deficiencies. Rosemont, IL: American Academy of Orthopaedic Surgeons; 2004. p 701-710.

21. Pasquina PF, Bryant PR, Huang ME, Roberts TL, Nelson VS, Flood KM. Advances in amputee care. Arch Phys Med Rehabil 2006;87(3 Suppl 1):S34-43; quiz S44-5.

22. Sullivan J, Uden M, Robinson KP, Sooriakumaran S. Rehabilitation of the trans-femoral amputee with an osseointegrated prosthesis: The United Kingdom experience. Prosthet Orthot Int 2003;27(2):114-20.

23. Tortora GJ, Nielsen MT. Structure of the skin. In: Roesch B, Trost K, Wojcik L, Muriello L, Raccuia L, editors. Principles of Human Anatomy. Hoboken, NJ: John Wiley & Sons, Inc.; 2009. p 117.

24. Meulenbelt HE, Geertzen JH, Jonkman MF, Dijkstra PU. Determinants of skin problems of the stump in lower-limb amputees. Arch Phys Med Rehabil 2009;90(1):74-81.

25. Hagberg K, Branemark R. Consequences of non-vascular trans-femoral amputation: A survey of quality of life, prosthetic use and problems. Prosthet Orthot Int 2001;25(3):186-94.

26. Salawu A, Middleton C, Gilbertson A, Kodavali K, Neumann V. Stump ulcers and continued prosthetic limb use. Prosthet Orthot Int 2006;30(3):279-85.

27. Pierce RO, Jr., Kernek CB, Ambrose TA, 2nd. The plight of the traumatic amputee. Orthopedics 1993;16(7):793-7.

28. Persson BM, Liedberg E. A clinical standard of stump measurement and classification in lower limb amputees. Prosthet Orthot Int 1983;7(1):17-24.

29. Dudek NL, Marks MB, Marshall SC, Chardon JP. Dermatologic conditions associated with use of a lower-extremity prosthesis. Arch Phys Med Rehabil 2005;86(4):659-63.

30. Loeb GE. Taking control of prosthetic arms. JAMA 2009;301(6):670-1.

31. Moore TJ, Barron J, Hutchinson F, 3rd, Golden C, Ellis C, Humphries D. Prosthetic usage following major lower extremity amputation. Clin Orthop Relat Res 1989;238:219-24.

32. Mitka M. Advocates seek better insurance coverage for amputees needing limb prostheses. JAMA 2008;299(18):2138-2140.

33. Sanders J. Stump-Socket Interface Conditions. Pressure Ulcer Research; 2005. p 129-147.

34. Smith DG, Horn P, Malchow D, Boone DA, Reiber GE, Hansen ST, Jr. Prosthetic history, prosthetic charges, and functional outcome of the isolated, traumatic below-knee amputee. J Trauma 1995;38(1):44-7.

35. Lerner-Frankiel MB, Vargas S, Brown M, Krusell L, Schoneberger W. Functional community ambulation: What are your criteria? Clinical Management 1986;6(2):12-15.

36. MacKenzie EJ, Castillo RC, Jones AS, Bosse MJ, Kellam JF, Pollak AN, Webb LX, Swiontkowski MF, Smith DG, Sanders RW and others. Health-care costs associated with amputation or reconstruction of a limb-threatening injury. J Bone Joint Surg Am 2007;89(8):1685-1692.

37. Sherman RA. Utilization of prostheses among US veterans with traumatic amputation: a pilot survey. J Rehabil Res Dev 1999;36(2):100-8.

38. Branemark R, Branemark PI, Rydevik B, Myers RR. Osseointegration in skeletal reconstruction and rehabilitation: A review. J Rehabil Res Dev 2001;38(2):175-81.

39. Isaacson BM, Vance RE, Rosenbaum Chou TG, Bloebaum RD, Bachus KN, Webster JB. The effectiveness of resonance frequency in predicting orthopedic implant strength and stability in an in vitro osseointegration model. J Rehabil Res Dev 2009;46(9):1109-1120.

40. Isaacson BM, Stinstra JG, Macleod RS, Pasquina PF, Bloebaum RD. Developing a quantitative measurement system for assessing heterotopic ossification and monitoring the bioelectric metrics from electrically induced osseointegration in the residual limb of service members. Ann Biomed Eng 2010;38(9):2968-2978.

41. Pendegrass CJ, Goodship AE, Blunn GW. Development of a soft tissue seal around bone-anchored transcutaneous amputation prostheses. Biomaterials 2006;27(23):4183-91.

42. Pendegrass CJ, Goodship AE, Price JS, Blunn GW. Nature's answer to breaching the skin barrier: An innovative development for amputees. J Anat 2006;209(1):59-67.

43. Pendegrass CJ, Gordon D, Middleton CA, Sun SN, Blunn GW. Sealing the skin barrier around transcutaneous implants: *In vitro* study of keratinocyte proliferation and adhesion in response to surface modifications of titanium alloy. J Bone Joint Surg Br 2008;90(1):114-21.

44. Jacobs R, Van Steenberghe D. From osseoperception to implant-mediated sensory-motor interactions and related clinical implications. J Oral Rehabil 2006;33(4):282-92.

45. Ysander M, Branemark R, Olmarker K, Myers RR. Intramedullary osseointegration: Development of a rodent model and study of histology and neuropeptide changes around titanium implants. J Rehabil Res Dev 2001;38(2):183-90.

46. Isaacson BM, Stinstra JG, MacLeod RS, Webster JB, Beck JP, Bloebaum RD. Bioelectric analyses of an osseointegrated intelligent implant design system for amputees. J Vis Exp 2009(29):1-6.

47. Lee WCC, Frossard LA, Hagberg K, Haggstrom E, Brånemark R, Evans JH, Pearcy MJ. Kinetics of transfemoral amputees with osseointegrated fixation performing common activities of daily living. Clinical Biomechanics 2007;22(6):665-673.

48. Lee WCC, Frossard LA, Hagberg K, Haggstrom E, Gow DL, Gray S, Brånemark R. Magnitude and variability of loading on the osseointegrated implant of transfemoral amputees during walking. Medical Engineering & Physics 2008;30(7):825-833.

49. Hagberg K, Häggström E, Jönsson S, Rydevik B, Brånemark R. Osseoperception and Osseointegrated Prosthetic Limbs. Psychoprosthetics; 2008. p 131-140.

50. Hagberg K, Branemark R. One hundred patients treated with osseointegrated transfemoral amputation prostheses--rehabilitation perspective. J Rehabil Res Dev 2009;46(3):331-44.

51. Ward DA, Robinson KP. Osseointegration for the skeletal fixation of limb prostheses in amputations at the trans-femoral level. In: Brånemark P-I, Chien S, Gröndahl H-G, Robinson K, editors. The Osseointegration Book. From Calvarium to Calcaneus. Berlin, Germany: Quintessenz Verlags-GmbH; 2005. p 463-476.

52. Hagberg K, Branemark R, Gunterberg B, Rydevik B. Osseointegrated trans-femoral amputation prostheses: Prospective results of general and condition-specific quality of life in 18 patients at 2-year follow-up. Prosthet Orthot Int 2008;32(1):29-41.

53. Aschoff HH, Clausen A, Hoffmeister T. The endo-exo femur prosthesis - A new concept of bone-guided, prosthetic rehabilitation following above-knee amputation. Zeitschrift Fur Orthopadie Und Unfallchirurgie 2009;147(5):610-615.

54. Blunn G, Cobb J, Goodship A, Unwin P; University College London, assignee. Transcutaneous prosthesis patent US 07014661. 2006 Mar 21 2006.

55. Beck JP, Bachus KN, Jeyapalina S, Epperson RT, Bloebaum RD. Bone response to load bearing percutaneous osseointegrated implants for amputees: A sheep amputation model. 2010 Mar 6-9; New Orleans, LA. p 2085.

56. Bloebaum RD, Beck JP, Olsen R, Norlund L, Bachus KN. Development of a single stage surgical model for percutaneous osseointegrated implants for amputees. 2009 Feb 22-25; Las Vegas, NV. p 2255.

57. Shelton TJ, Bloebaum RD, Bachus KN. Percutaneous, osseointegrated implants: A 12 month study of limb compensation in an amputated ovine model. 2010 Mar 6-9; New Orleans, LA. p 1869.

58. Albrektsson T, Branemark I-I, Hansson H-A, Lindstrom J. Osseointegrated titanium implants. Acta Orthop Scand 1981;52:155-170.

59. Meyer U, Joos U, Mythili J, Stamm T, Hohoff A, Fillies T, Stratmann U, Wiesmann HP. Ultrastructural characterization of the implant/bone interface of immediately loaded dental implants. Biomaterials 2004;25(10):1959-67.

60. Hofmann AA, Bloebaum RD, Bachus KN. Progression of human bone ingrowth into porous-coated implants. Acta Orthop. Scand. 1997;68(2):161-166.

61. Slaets E, Naert I, Carmeliet G, Duyck J. Early cortical bone healing around loaded titanium implants: A histological study in the rabbit. Clin Oral Implants Res 2009;20(2):126-34.

62. Duyck J, Vandamme K, Geris L, Van Oosterwyck H, De Cooman M, Vandersloten J, Puers R, Naert I. The influence of micro-motion on the tissue differentiation around immediately loaded cylindrical turned titanium implants. Arch Oral Biol 2006;51(1):1-9.

63. Szmukler-Moncler S, Salama H, Reingewirtz Y, Dubruille JH. Timing of loading and effect of micromotion on bone-dental implant interface: Review of experimental literature. J Biomed Mater Res 1998;43(2):192-203.

64. Glauser R, Sennerby L, Meredith N, Ree A, Lundgren A, Gottlow J, Hammerle CH. Resonance frequency analysis of implants subjected to immediate or early functional occlusal loading. Successful vs. failing implants. Clin Oral Implants Res 2004;15(4):428-34.

65. Meredith N, Alleyne D, Cawley P. Quantitative determination of the stability of the implant-tissue interface using resonance frequency analysis. Clin Oral Implants Res 1996;7(3):261-7.

66. Roser K, Johansson CB, Donath K, Albrektsson T. A new approach to demonstrate cellular activity in bone formation adjacent to implants. J Biomed Mater Res 2000;51(2):280-91.

67. Nkenke E, Lehner B, Weinzierl K, Thams U, Neugebauer J, Steveling H, Radespiel-Troger M, Neukam FW. Bone contact, growth, and density around immediately loaded implants in the mandible of mini pigs. Clin Oral Implants Res 2003;14(3):312-21.

68. Slaets E, Carmeliet G, Naert I, Duyck J. Early trabecular bone healing around titanium implants: A histologic study in rabbits. J Periodontol 2007;78(3):510-7.

69. Piattelli A, Corigliano M, Scarano A, Costigliola G, Paolantonio M. Immediate loading of titanium plasma-sprayed implants: A histologic analysis in monkeys. J Periodontol 1998;69(3):321-7.

70. Vandamme K, Naert I, Vander Sloten J, Puers R, Duyck J. Effect of implant surface roughness and loading on peri-implant bone formation. J Periodontol 2008;79(1):150-7.

71. Penarrocha M, Boronat A, Garcia B. Immediate loading of immediate mandibular implants with a full-arch fixed prosthesis: A preliminary study. J Oral Maxillofac Surg 2009;67(6):1286-93.

72. Mercola JM, Kirsch DL. The basis of microcurrent electrical therapy in conventional medical practice. Journal of Advancement in Medicine 1995;8(2):107-120.

73. Colella SM, Miller AG, Stang RG, Stoebe TG, Spengler DM. Fixation of porous titanium implants in cortical bone enhanced by electrical stimulation. J Biomed Mater Res 1981;15(1):37-46.

74. Caldwell CW, Reswick JB. A percutaneous wire electrode for chronic research use. IEEE Trans Biomed Eng 1975;22(5):429-32.

75. Isaacson BM, Bloebaum RD. Bone Bioelectricity: What have we learned in the past 160 years? J Biomed Mater Res A 2010;95A:1270-1279.

76. Martonosi AN. Animal electricity, Ca2+ and muscle contraction. A brief history of muscle research. Acta Biochim Pol 2000;47(3):493-516.

77. Burr HS, Northrop FS. Evidence for the existence of an electro-dynamic field in living organisms. Proc Natl Acad Sci U S A 1939;25(6):284-8.

78. Levin M. Bioelectromagnetics in morphogenesis. Bioelectromagnetics 2003;24(5):295-315.

79. Burr HS, Lane CT. Electrical characteristics of living systems. Yale Journal of Biology and Medicine 1935:32-35.

80. Chao PH, Roy R, Mauck RL, Liu W, Valhmu WB, Hung CT. Chondrocyte translocation response to direct current electric fields. J Biomech Eng 2000;122(3):261-7.

81. Robinson KR. The responses of cells to electrical fields: A review. J Cell Biol 1985;101(6):2023-7.

82. Borgens RB, Vanable JW, Jr., Jaffe LF. Bioelectricity and regeneration: Large currents leave the stumps of regenerating newt limbs. Proc Natl Acad Sci U S A 1977;74(10):4528-32.

83. Mycielska ME, Djamgoz MB. Cellular mechanisms of direct-current electric field effects: Galvanotaxis and metastatic disease. J Cell Sci 2004;117(Pt 9):1631-9.

84. Ferrier J, Ross SM, Kanehisa J, Aubin JE. Osteoclasts and osteoblasts migrate in opposite directions in response to a constant electrical field. J Cell Physiol 1986;129(3):283-8.

85. Ross SM. Morphological responses of cells to exogenous ionic currents. Annual International Conference of IEEE Engineering in Medicine and Biology. Volume 12; 1990. p 1570-1571.

86. Haddad JB, Obolensky AG, Shinnick P. The biologic effects and the therapeutic mechanism of action of electric and electromagnetic field stimulation on bone and cartilage: New findings and a review of earlier work. J Altern Complement Med 2007;13(5):485-90.

87. Reilly DT, Burstein AH. The mechanical properties of cortical bone. J. Bone Joint Surg. [Am.] 1974;56-A(5):1001-1022.

88. Rodan GA. Introduction to bone biology. Bone 1992;13 Suppl 1:S3-6.

89. Sela J, Gross UM, Kohavi D, Shani J, Dean DD, Boyan BD, Schwartz Z. Primary mineralization at the surfaces of implants. Crit Rev Oral Biol Med 2000;11(4):423-36.

90. Behari J. Elements of Bone Biophysics Biophysical Bone Behaviour: Principles and Applications. Singapore: John Wiley & Sons; 2009. p 1-52.

91. Ross FP, Christiano AM. Nothing but skin and bone. J Clin Invest 2006;116(5):1140-9.

92. Currey JD. Changes in the impact energy absorption of bone with age. J. Biomech. 1979;12:459-469.

93. Rosenbaum TG, Bloebaum RD, Ashrafi S, Lester DK. Ambulatory activities maintain cortical bone after total hip arthroplasty. Clin Orthop Relat Res 2006;450:129-37.

94. Lane JM, Vigorita VJ. Osteoporosis. J Bone Joint Surg Am 1983;65(2):274-8.

95. Shea KG, Ford T, Bloebaum RD, D'Astous J, King H. A comparison of the microarchitectural bone adaptations of the concave and convex thoracic spinal facets in idiopathic scoliosis. J Bone Joint Surg Am 2004;86A(5):1000-1006.

96. Skedros JG, Baucom SL. Mathematical analysis of trabecular 'trajectories' in apparent trajectorial structures: The unfortunate historical emphasis on the human proximal femur. J Theor Biol 2007;244(1):15-45.

97. Currey JD. The mechanical properties of bone. Clin. Orthop. 1970;73:210-232.

98. Singh S, Saha S. Electrical properties of bone. A review. Clin Orthop Relat Res 1984(186):249-71.

99. Chakkalakal DA, Johnson MW. Electrical properties of compact bone. Clin Orthop Relat Res 1981(161):133-45.

100. Yasuda I. Electrical callus and callus formation by electret. Clin Orthop Relat Res 1977;124:53-6.

101. Brighton CT. Bioelectrical fffects on bone and cartilage. Clin Orthop Relat Res 1977;124:2-4.

102. Yasuda I. The classic fundamental aspects of fracture treatment. Clin Orthop Relat Res 1977;124:5-8.

103. Friedenberg ZB, Brighton CT. Bioelectric potentials in bone. J Bone Joint Surg Am 1966;48(5):915-23.

104. Victoria G, Petrisor B, Drew B, Dick D. Bone stimulation for fracture healing: What's all the fuss? Indian J Orthop 2009;43(2):117-120.

105. Spadaro JA. Mechanical and electrical interactions in bone remodeling. Bioelectromagnetics 1997;18(3):193-202.

106. Rubinacci A, Tessari L. A correlation analysis between bone formation rate and bioelectric potentials in rabbit tibia. Calcif Tissue Int 1983;35(6):728-31.

107. Fukada E, Yasuda I. On the Piezoelectric effect of bone. J Physical Soc Japan 1957;12(10):1158-1162.

108. Fukada E, Yasuda I. Piezoelectric effects in collagen. Japanese J Applied Physics 1964;3(2):117-21.

109. Lavine LS, Grodzinsky AJ. Electrical stimulation of repair of bone. J Bone Joint Surg Am 1987;69(4):626-30.

110. Currey J. Comparative mechanical properties and histology of bone. Am. Zool. 1984;24:5-12.

111. Bassett CA. Electrical effects in bone. Sci Am 1965;213(4):18-25.

112. Williams WS, Breger L. Piezoelectricity in tendon and bone. J Biomech 1975;8(6):407-13.

113. Bassett CA, Becker RO. Generation of electric potentials by bone in response to mechanical stress. Science 1962;137:1063-4.

114. Bassett CAL. Biologic significance of piezoelectricity. Calcif. Tissue. Res. 1968;1:252-272.

115. Buckwalter JA, Glimcher MJ, Cooper RR, Recker R. Bone biology. J Bone Joint Surg Am 1995;77(2):1276-1289.

116. Marino AA. Electrical stimulation in orthopaedics: Past, present and future. Journal of Bioelectricity 1984;3(1&2):235-244.

117. Nyman JS, Roy A, Shen X, Acuna RL, Tyler JH, Wang X. The influence of water removal on the strength and toughness of cortical bone. J Biomech 2006;39(5):931-8.

118. Anderson JC, Eriksson C. Piezoelectric properties of dry and wet bone. Nature 1970;227(5257):491-2.

119. Lente FD. Cases of un-united fracture treated by electricity. Transactions of the Medical Society of the State of New York. 1850:317-319.

120. Hartshorne E. On the causes of treatment of pseudoarthrosis and especially that form of it sometimes called supernumerary joint. The American Journal of the Medical Sciences 1841;1(1):121-156.

121. Lavine LS, Lustrin I, Shamos MH, Moss ML. The influence of electric current on bone regeneration in vivo. Acta Orthop Scand 1971;42(4):305-14.

122. Adey WR. 862 - The sequence and energetics of cell membrane transductive coupling to intracellular enzyme systems. Bioelectrochemistry Bioenergetics 1986;15:447-456.

123. Rodan GA, Rodan SB. Expression of the osteoblast phenotype. In: Peck WA, editor. Bone and Mineral Research. Amsterdam: Elsevier Science Publishers B. V.; 1983. p 244-262.

124. Matsunaga S. Histological and histochemical investigations of constant direct current stimulated intramedullary callus. J. Jpn. Orthop. Ass. 1986;60(12):1293-303.

125. Korenstein R, Somjen D, Fischler H, Binderman I. Capacitative pulsed electric stimulation of bone cells. Induction of cyclic-AMP changes and DNA synthesis. Biochim Biophys Acta 1984;803(4):302-7.

126. Braidman IP, Anderson DC, Weiss JB. Evidence for a local interaction between osteoclasts and osteoblasts in culture. Calcif Tissue Int 1982;34(Suppl 1):S3.

127. Norton LA, Rodan GA, Bourret LA. Epiphyseal cartilage cAMP changes produced by electrical and mechanical perturbations. Clin Orthop Relat Res 1977(124):59-68.

128. Bourret LA, Rodan GA. The role of calcium in the inhibition of cAMP accumulation in epiphyseal cartilage cells exposed to physiological pressure. J Cell Physiol 1976;88(3):353-61.

129. McLeod KJ, Porres L, Donahue HJ. Electric field induced changes in calcium ion activity response in osteoblastic cells: Frequency and duration dependence. 1994 Oct 13. p 4.

130. Brighton CT, Wang W, Seldes R, Zhang G, Pollack SR. Signal transduction in electrically stimulated bone cells. J Bone Joint Surg Am 2001;83-A(10):1514-23.

131. Soong HK, Parkinson WC, Bafna S, Sulik GL, Huang SC. Movements of cultured corneal epithelial cells and stromal fibroblasts in electric fields. Invest Ophthalmol Vis Sci 1990;31(11):2278-82.

132. Albrektsson T, Johansson C. Osteoinduction, osteoconduction and osseointegration. Eur Spine J 2001;10 Suppl 2:S96-101.

133. Pearce D, Bonnet D. Ageing within the hematopoietic stem cell compartment. Mech Ageing Dev 2009;130(1-2):54-7.

134. Kooistra BW, Jain A, Hanson BP. Electrical stimulation: Nonunions. Indian J Orthop 2009;43(2):149-55.

135. Friedenberg ZB, Harlow MC, Brighton CT. Healing of nonunion of the medial malleolus by means of direct current: A case report. J Trauma 1971;11(10):883-5.

136. Liboff AR, Rinaldi RA, Lavine LS, Shamos MH. On electrical condution in living bone. Clin Orthop Relat Res 1975(106):330-5.

137. Geddes LA, Baker LE. The specific resistance of biological material--a compendium of data for the biomedical engineer and physiologist. Med Biol Eng 1967;5(3):271-93.

138. Beddoe AH. Measurements of the microscopic structure of cortical bone. Phys Med Biol 1977;22(2):298-308.

139. Martin RB, Pickett JC, Zinaich S. Studies of skeletal remodeling in aging men. Clin Orthop Relat Res 1980(149):268-82.

140. Hassler CR, Rybicki EF, Diegle RB, Clark LC. Studies of enhanced bone healing via electrical stimuli. Comparative effectiveness of various parameters. Clin Orthop Relat Res 1977(124):9-19.

141. Ryaby JT. Clinical effects of electromagnetic and electric fields on fracture healing. Clin Orthop Relat Res 1998(355 Suppl):S205-15.

142. Renooij W, Janssen LW, Akkermans LM, Lagey CL, Wittebol P. Electrode-oxygen consumption and its effects on tissue-oxygen tension. A study by mass spectrometry. Clin Orthop Relat Res 1983(173):239-44.

143. Treharne RW, Brighton CT, Korostoff E, Pollack SR. An in vitro study of electrical osteogenesis using direct and pulsating currents. Clin Orthop Relat Res 1979(145):300-6.

144. Robblee LS, Rose TL. Electrochemical guidelines for selection of protocols and electrode materials for neural stimulation. In: Agnew WF, McCreery DB, editors. Neural Prostheses: Fundamental Studies. Englewood Cliffs Prentice Hall; 1990. p 25-66.

145. Heppenstall RB, Grislis G, Hunt TK. Tissue gas tensions and oxygen consumption in healing bone defects. Clin Orthop Relat Res 1975(106):357-65.

146. Brighton CT, Adler S, Black J, Itada N, Friedenberg ZB. Cathodic oxygen consumption and electrically induced osteogenesis. Clin Orthop Relat Res 1975(107):277-82.

147. Akers JM, Peckham PH, Keith MW, Merritt K. Tissue response to chronically stimulated implanted epimysial and intramuscular electrodes. IEEE Trans Rehabil Eng 1997;5(2):207-20.

148. Grill WM, Mortimer JT. Electrical properties of implant encapsulation tissue. Ann Biomed Eng 1994;22(1):23-33.

149. Einhorn TA. Clinically applied models of bone regeneration in tissue engineering research. Clin Orthop Relat Res 1999(367 Suppl):S59-67.

150. Einhorn TA. Enhancement of fracture-healing. J Bone Joint Surg [Am] 1995;77-A(6):940-56.

151. Cieszynski T. Studies on the regeneration of ossal yissue. Ii. Treatment of bone fractures in experimental animals with electric energy. Arch Immunol Ther Exp (Warsz) 1963;11:199-217.

152. Poolman RW. Adjunctive non-invasive ways of healing bone fractures. BMJ 2009;338:b11.

153. Akai M, Hayashi K. Effect of electrical stimulation on musculoskeletal systems; a meta-analysis of controlled clinical trials. Bioelectromagnetics 2002;23(2):132-43.

154. Carter DR, Blenman PR, Beaupre GS. Correlations between mechanical stress history and tissue differentiation in initial fracture healing. J Orthop Res 1988;6(5):736-48.

155. Kooijman CM, Dijkstra PU, Geertzen JH, Elzinga A, van der Schans CP. Phantom pain and phantom sensations in upper limb amputees: An epidemiological study. Pain 2000;87(1):33-41.

156. Brighton CT, Black J, Friedenberg ZB, Esterhai JL, Day LJ, Connolly JF. A multicenter study of the treatment of non-union with constant direct current. J Bone Joint Surg Am 1981;63(1):2-13.

157. Brighton CT. The treatment of non-unions with electricity. J Bone Joint Surg Am 1981;63(5):847-51.

158. Friedenberg ZB, Zemsky LM, Pollis RP, Brighton CT. The response of non-traumatized bone to direct current. J Bone Joint Surg Am 1974;56(5):1023-30.

159. Friedenberg ZB, Roberts PG, Jr., Didizian NH, Brighton CT. Stimulation of fracture healing by direct current in the rabbit fibula. J Bone Joint Surg Am 1971;53(7):1400-8.

160. Brighton CT, Friedenberg ZB, Zemsky LM, Pollis PR. Direct-current stimulation of non-union and congenital pseudarthrosis. Exploration of its clinical application. J Bone Joint Surg Am 1975;57(3):368-77.

161. Baranowski TJ, Jr., Black J, Brighton CT, Friedenberg ZB. Electrical osteogenesis by low direct current. J Orthop Res 1983;1(2):120-8.

162. Mortimer JT, Kaufman D, Roessman U. Intramuscular electrical stimulation: Tissue damage. Ann Biomed Eng 1980;8(3):235-44.

163. O'Connor BT, Charlton HM, Currey JD, Kirby DR, Woods C. Effects of electric current on bone in vivo. Nature 1969;222(5189):162-3.

164. Friedenberg ZB, Andrews ET, Smolenski BI, Pearl BW, Brighton CT. Bone reaction to varying amounts of direct current. Surg Gynecol Obstet 1970;131(5):894-9.

165. Ishida M, Fujioka M, Takahashi KA, Arai Y, Kubo T. Electromagnetic fields: A novel prophylaxis for steroid-induced osteonecrosis. Clin Orthop Relat Res 2008;466(5):1068-73.

166. Jorgensen TE. Electrical stimulation of human fracture healing by means of a slow pulsating, asymmetrical direct current. Clin Orthop Relat Res 1977;124:124-7.

167. Minkin C, Poulton BR, Hoover WH. The effect of direct current on bone. Clin Orthop Relat Res 1968;57:303-9.

168. Leitgeb N, Cech R, Schrottner J. Electromagnetic field spectral evaluation problems in exposure assessment. Radiat Prot Dosimetry 2007;124(2):124-9.

169. Day L. Electrical stimulation in the treatment of ununited fractures. . Clin Orthop Relat Res 1981;161 54-57.

170. Hopper RA, VerHalen JP, Tepper O, Mehrara BJ, Detch R, Chang EI, Baharestani S, Simon BJ, Gurtner GC. Osteoblasts stimulated with pulsed electromagnetic fields increase HUVEC proliferation via a VEGF-A independent mechanism. Bioelectromagnetics 2009;30(3):189-97.

171. Brighton CT, Friedenberg ZB, Mitchell EI, Booth RE. Treatment of nonunion with constant direct current. Clin Orthop Relat Res 1977(124):106-23.

172. Shayesteh YS, Eslami B, Dehghan MM, Vaziri H, Alikhassi M, Mangoli A, Khojasteh A. The effect of a constant electrical field on osseointegration after immediate implantation in dog mandibles: A preliminary study. J Prosthodont 2007;16(5):337-42.

173. Marino AA, Cullen JM, Reichmanis M, Becker RO, Hart FX. Sensitivity to change in electrical environment: A new bioelectric effect. Am J Physiol 1980;239(5):R424-7.

174. Crile GW, Hosmer HR, Rowland AF. The electrical conductivity of animal tissues under normal and pathological conditions. The American journal of Physiology 1921;60:59-106.

175. Patterson D. Treatment of nonunion with a constant direct current: A totally implantable system. Orthop Clin North Am 1984;15:47-59.

176. Brighton CT, Pollack SR. Treatment of recalcitrant non-union with a capacitively coupled electrical field. A preliminary report. J Bone Joint Surg Am 1985;67(4):577-85.

177. Supronowicz PR, Ajayan PM, Ullmann KR, Arulanandam BP, Metzger DW, Bizios R. Novel current-conducting composite substrates for exposing osteoblasts to alternating current stimulation. J Biomed Mater Res 2002;59(3):499-506.

178. Heckman JD, Ingram AJ, Loyd RD, Luck JV, Jr., Mayer PW. Nonunion treatment with pulsed electromagnetic fields. Clin Orthop Relat Res 1981(161):58-66.

179. Bassett CA, Mitchell SN, Gaston SR. Treatment of ununited tibial diaphyseal fractures with pulsing electromagnetic fields. J Bone Joint Surg Am 1981;63(4):511-23.

180. Shawen SB, Doukas WC, Shrout JA, Ficke JR, Potter BK, Hayda RA, Keeling JJ, Granville RR, Smith DC. General surgical principles for the combat casualty with limb loss. In: Pasquina PF, Cooper RA, editors. Care of the Combat Amputee: TMM; 2009. p 117-153.

181. Hofmann AA, Bachus KN, Bloebaum RD. Comparative study of human cancellous bone remodeling to titanium and hydroxyapatite coated implants. J. Arthroplasty 1993;8(2):157-166.

182. Black J. Methods for Stimulating Tissues. Electrical stimulation: Its Role in Growth, Repair and Remodeling of the Musculoskeletal System. Westport: Greenwood Press; 1986. p 92-97.

183. Agins HJ, Alcock NW, Bansal M, Salvati EA, Wilson PD, Pellicei PM, Bullogh PG. Metallic wear in failed titanium-alloy total hip replacements. J. Bone Joint Surg. [Am.] 1988;70-A(3):347-356.

184. Beder OE, Eade G. An investigation of tissue tolerance to titanium metal implants in dogs. Surgery 1956;39(3):470-3.

185. Emneus H, Gudmundsson G. Final report on clinical testing of titanium. Acta Orthop Scand 1967:372-3.

186. Noda M, Sato A. Appearance of osteoclasts and osteoblasts in electrically stimulated bones cultured on chorioallantoic membranes. Clin Orthop Relat Res 1985(193):288-98.

187. Potter BK, Burns TC, Lacap AP, Granville RR, Gajewski DA. Heterotopic ossification following traumatic and combat-related amputations. Prevalence, risk factors, and preliminary results of excision. J Bone Joint Surg Am 2007;89(3):476-86.

188. Ahrengart L. Periarticular heterotopic ossification after total hip arthroplasty. Risk factors and consequences. Clin Orthop Relat Res 1991(263):49-58.

189. Potter BK, Burns TC, Lacap AP, Granville RR, Gajewski D. Heterotopic ossification in the residual limbs of traumatic and combat-related amputees. J Am Acad Orthop Surg 2006;14(10 Suppl):S191-7.

190. Errico TJ, Fetto JF, Waugh TR. Heterotopic ossification. Incidence and relation to trochanteric osteotomy in 100 total hip arthroplasties. Clin Orthop Relat Res 1984(190):138-41.

191. Garland DE, Hanscom DA, Keenan MA, Smith C, Moore T. Resection of heterotopic ossification in the adult with head trauma. J Bone Joint Surg Am 1985;67(8):1261-9.

192. Furman R, Nicholas JJ, Jivoff L. Elevation of the serum alkaline phosphatase coincident with ectopic-bone formation in paraplegic patients. J Bone Joint Surg Am 1970;52(6):1131-7.

193. Goldman J. Heterotopic ossification in spinal cord injuries. Physiotherapy 1980;66(7):219-20.

194. Kircher J, Martinek V, Mittelmeier W. Heterotopic ossification after minimally invasive rotator cuff repair. Arthroscopy 2007;23(12):1359 e1-3.

195. Gaur A, Sinclair M, Caruso E, Peretti G, Zaleske D. Heterotopic ossification around the elbow following burns in children: Results after excision. J Bone Joint Surg Am 2003;85-A(8):1538-43.

196. Bayley SJ. Funnybones: A review of the problem of heterotopic bone formation. Orthopaedic Review 1979;8(1):113-120.

197. Wharton GW. Heterotopic ossification. Clin Orthop Relat Res 1975(112):142-9.

198. Dudek NL, DeHaan MN, Marks MB. Bone overgrowth in the adult traumatic amputee. Am J Phys Med Rehabil 2003;82(11):897-900.

199. Andersen R, Davis S, Scoville C. Rehabilitation of military amputees: From injury to independence. Orthopedics 2008;31(10).

200. Hsu JD, Sakimura I, Stauffer ES. Heterotopic ossification around the hip joint in spinal cord injured patients. Clin Orthop Relat Res 1975(112):165-9.

201. Riegler HF, Harris CM. Heterotopic bone formation after total hip arthroplasty. Clin Orthop Relat Res 1976(117):209-16.

202. Kolbl O, Knelles D, Barthel T, Kraus U, Flentje M, Eulert J. Randomized trial comparing early postoperative irradiation vs. the use of nonsteroidal antiinflammatory drugs for prevention of heterotopic ossification following prosthetic total hip replacement. Int J Radiat Oncol Biol Phys 1997;39(5):961-6.

203. Quarto R, Thomas D, Liang CT. Bone progenitor cell deficits and the age-associated decline in bone repair capacity. Calcif Tissue Int 1995;56(2):123-9.

204. Doll BA, Tegtmeier F, Koch H, Acarturk O, Hollinger JO. Evidence for a cellular and molecular decline in bone healing with age. Operative Techniques in Orthopaedics 2002;12(2):72-77.

205. Brumback RJ, Wells JD, Lakatos R, Poka A, Bathon GH, Burgess AR. Heterotopic ossification about the hip after intramedullary nailing for fractures of the femur. J Bone Joint Surg Am 1990;72(7):1067-73.

206. Garland DE, Blum CE, Waters RL. Periarticular heterotopic ossification in head-injured adults. Incidence and location. J Bone Joint Surg Am 1980;62(7):1143-6.

207. Garland DE, Miller G. Fractures and dislocations about the hip in head-injured adults. Clin Orthop Relat Res 1984(186):154-8.

208. Karp FB, Bernotski NA, Valdes TI, Böhringer KF, Ratner BD. Foreign body response investigated with an implanted biosensor by in situ electrical impedance spectroscopy. IEEE Sensors 2008;8(1):104-112.

209. Mahaisavariya B, Sitthiseripratip K, Oris P, Chaichanasiri E, Suwanprateeb J. Fit-and-fill analysis of trochanteric gamma nail for the Thai proximal femur: A virtual simulation study. J Med Assoc Thai 2004;87(11):1315-20.

210. Jackson WM, Aragon AB, Bulken-Hoover JD, Nesti LJ, Tuan RS. Putative heterotopic ossification progenitor cells derived from traumatized muscle. J Orthop Res 2009:1-7.

211. Hierton C, Blomgren G, Lindgren U. Factors associated with heterotopic bone formation in cemented total hip prostheses. Acta Orthop Scand 1983;54(5):698-702.

212. Hirata K, Mizuno A, Yamaguchi A. Transplantation of skin fibroblasts expressing BMP-2 contributes to the healing of critical-sized bone defects. J Bone Miner Metab 2007;25(1):6-11.

213. Wiesmann H, Luttenberg B, Meyer U. Tissue engineering of bone In: Epple M, Bauerlein E, editors. Handbook of Biomineralization: Medical and Clinical Aspects Wiley-VCH; 2007. p 150-151.

214. Chang-Liu CM, Woloschak GE. Effect of passage number on cellular response to DNA-damaging agents: Cell survival and gene expression. Cancer Lett 1997;113(1-2):77-86.

215. Phelan M. Basic Techniques for Mammalian Cell Tissue Culture. Current Protocols in Cell Biology: John Wiley & Sons. ; 1998. p 1-10.

216. Lu JC, Chen F, Xu HR, Huang YF, Lu NQ. Comparison of three sperm-counting methods for the determination of sperm concentration in human semen and sperm suspensions. LabMedicine 2007;38(4):232-236.

217. Prathalingam NS, Holt WW, Revell SG, Jones S, Watson PF. The precision and accuracy of six different methods to determine sperm concentration. J Androl 2006;27(2):257-62.

218. Fedoroff S, Richardson A. Quantification of cells in culture. In: Fedoroff S, Richardson A, editors. Protocols for Neural Cell Culture. Totowa, NJ: Humana Press, Inc.; 2001. p 1-7.

219. Brighton CT, Friedenberg ZB, Black J, Esterhai JL, Jr., Mitchell JE, Montique F, Jr. Electrically induced osteogenesis: Relationship between charge, current density, and the amount of bone formed: Introduction of a new cathode concept. Clin Orthop Relat Res 1981(161):122-32.

220. Sennerby L, Thomsen P, Ericson E. Early tissue response to titanium implants inserted in rabbit cortical bone. J Mater Sci: Mater Med 1993;4(5):240-250.

221. Willie B, Bloebaum R, Bireley W, Bachus K, Hofmann A. Determining relevance of a weight-bearing ovine model for bone ingrowth assessment. J Biomed Mater Res Part A 2004;69A(3):567-576.

222. Ling RS. Observations on the fixation of implants to the bony skeleton. Clin Orthop Relat Res 1986(210):80-96.

223. Eriksson AR, Albrektsson T. Temperature threshold levels for heat-induced bone tissue injury: A vital-microscopic study in the rabbit. J. Prosthet. Dent. 1983;50(1):101-107.

224. Mahan J, Seligson D, Henry SL, Hynes P, Dobbins J. Factors in pin tract infections. Orthopedics 1991;14(3):305-8.

225. Feighan JE, Goldberg VM, Davy D, Parr JA, Stevenson S. The influence of surface-blasting on the incorporation of titanium-alloy implants in a rabbit intramedullary model. J. Bone Joint Surg. [Am.] 1995;77-A(9):1380-1395.

226. Vervest TM, Anderson PG, Van Hout F, Wapstra FH, Louwerse RT, Koetsier JW. Ten to twelve-year results with the Zweymuller cementless total hip prosthesis. J Arthroplasty 2005;20(3):362-8.

227. Jemt T. Failures and complications in 391 consecutively inserted fixed prostheses supported by Branemark implants in edentulous jaws: A study of treatment from the time of prosthesis placement to the first annual checkup. Int J Oral Maxillofac Implants 1991;6(3):270-6.

228. Venugopalan R, Ideker R. Bioelectrodes. In: Ratner BD, Hoffman AS, Schoen FJ, Lemons JE, editors. Biomaterials Science: An Introduction to Materials in Medicine London: Elsevier Academic Press 2004. p 648-656.

229. Bloebaum RD, Rhodes DM, Rubman MH, Hofmann AA. Bilateral tibial components of different cementless designs and materials: Microradiographic, backscattered imaging, and histologic analysis. Clin Orthop Relat Res 1991;268:179-187.

230. Bloebaum RD, Rubman MH, Hofmann AA. Bone ingrowth into porous-coated tibial components implanted with autograft bone chips: Analysis of ten consecutively retrieved implants. J. Arthroplasty 1992;7(4):483-493.

231. Bloebaum RD, Merrell M, Gustke K, Simmons M. Retrieval analysis of a hydroxyapatite-coated hip prosthesis. Clin. Orthop. 1991;267:97-102.

232. Dimitriou R, Babis GC. Biomaterial osseointegration enhancement with biophysical stimulation. J Musculoskelet Neuronal Interact 2007;7(3):253-65.

233. Bloebaum RD, Beeks D, Dorr LD, Savory CG, DuPont JA, Hofmann AA. Complications with hydroxyapatite particulate separation in total hip arthroplasty. Clin Orthop Relat Res 1994(298):19-26.

234. Bloebaum RD, Bachus KN, Momberger NG, Hofmann AA. Mineral apposition rates of human cancellous bone at the interface of porous coated implants. J Biomed Mater Res 1994;28(5):537-544.

235. Hecker AT, Shea M, Hayhurst JO, Myers ER, Meeks LW, Hayes WC. Pull-out strength of suture anchors for rotator cuff and Bankart lesion repairs. Am J Sports Med 1993;21(6):874-9.

236. Rosenbaum Chou TG, Child JR, Naughtin RJ, Rigdon RR, Schumann C, Bloebaum RD. The relationship between femoral periprosthetic cortical bone geometry and porosity after total hip arthroplasty. J Biomed Mater Res A 2008;87(1):107-15.

237. Bloebaum RD, Lundeen GA, Shea JE, Whitaker EL. Age-related mineralization heterogeneity changes in trabecular bone of the proximal femur. Anat Rec 2004;281A(2):1296-302.

238. Mizuno M, Kuboki Y. Osteoblast-related gene expression of bone marrow cells during the osteoblastic differentiation induced by type I collagen. J Biochem 2001;129(1):133-8.

239. Sela J, Gross UM, Kohavi D, Shani J, Dean DD, Boyan BD, Schwartz Z. Primary mineralization at the surfaces of implants. Critical Reviews in Oral Biology and Medicine 2000;11(4):423-436.

240. Fleisch H, Neuman W. The role of phosphatase and polyphosphates in calcification of collagen. Helv Physiol Pharmacol Acta 1961;19:C17-8.

241. Omelon S, Georgiou J, Henneman ZJ, Wise LM, Sukhu B, Hunt T, Wynnyckyj C, Holmyard D, Bielecki R, Grynpas MD. Control of vertebrate skeletal mineralization by polyphosphates. PLoS One 2009;4(5):e5634.

242. Wai-Hong Y. Repair in mammalian long bone fracture -- a review of the cellular and electrical factors influencing the reparative processes. The Bulletin of the Hong Kong Medical Association 1982;34:137-167.

243. Clark PA, Rodriguez A, Sumner DR, Hussain MA, Mao JJ. Modulation of bone ingrowth of rabbit femur titanium implants by in vivo axial micromechanical loading. J Appl Physiol 2005;98(5):1922-9.

244. Bloebaum RD, Willie BM, Mitchell BS, Hofmann AA. Relationship between bone ingrowth, mineral apposition rate, and osteoblast activity. J Biomed Mater Res A 2007;81A(2):505-514.

245. Slaets E, Carmeliet G, Naert I, Duyck J. Early cellular responses in cortical bone healing around unloaded titanium implants: An animal study. J Periodontol 2006;77(6):1015-24.

246. Ziskin MC. Applications of ultrasound in medicine - comparison with other modalities. Ultrasound: Medical applications, biological effects, and hazard potential 1987:49-59.

247. Takatsuka K, Yamamuro T, Nakamura T, Kokubo T. Bone-bonding behavior of titanium alloy evaluated mechanically with detaching failure load. J Biomed Mater Res 1995;29(2):157-63.

248. Tummler H-P, Thull R, Schaldach M. The mechanism of repassivation and the concentration of corrosion products shown on TIALV. 1982 Sep 5-11; Congress Centrum Hamburg, Germany. p 3.11.